AN HSP90 PHYSICAL INTERACTOME

BY

JANHAVI ATIT KOLHE

DISSERTATION

Submitted in partial fulfillment of the requirements
for the degree of Doctor of Philosophy in Cell and Developmental Biology
in the Graduate College of the
University of Illinois Urbana-Champaign, 2022

Urbana, Illinois

Doctoral Committee:

Professor Brian C. Freeman, Chair and Director of Research
Professor William M. Brieher
Associate Professor Lori T. Raetzman
Assistant Professor Xin Li

ABSTRACT

Hsp90 is a critical eukaryotic molecular chaperone, ubiquitously expressed in all organisms. It is a highly abundant protein (~2% of a cell's protein mass) and is involved in numerous processes including protein trafficking, chromatin remodeling, and signal transduction. To govern a broad variety of biological pathways Hsp90 exploits two different modes of interactions with clients and/or co-chaperones - a stable association such as when maintaining a metastable client in a soluble state and a transient binding such as when driving the dynamics of proteins working in transcription, chromatin remodeling, or DNA repair. Despite the numerous and extensive studies on Hsp90, the complete clientele of Hsp90 is unknown. Likely, the transient interactions between Hsp90 and many of its clients make their identification through traditional techniques difficult. To gain a better understanding of the factors interacting with Hsp90, I exploited the non-natural amino acid p-Benzoyl-L-Phenylalanine (Bpa) to generate an *in vivo* kinetic trap to capture Hsp90 interactions. In conjunction with mass spectrometry, I have identified 1114 physical interactors of Hsp90. Nearly half of the hits were novel for Hsp90-association and included pathways such as translation initiation and genome organization. My studies provide mechanistic insights into Hsp90 as a molecular chaperone as well as its functional role in different cellular processes.

ACKNOWLEDGMENTS

First and foremost, I am extremely grateful to my advisor, Dr. Brian Freeman, for his support and guidance throughout my Ph.D. Brian encouraged me to pursue all the opportunities I desired, scientific and extra-curricular and was always available for advice, whether it was for an experiment, or on how to build a table from scratch. He has taken an active interest in my personal and professional development, making me the scientist I am today.

I would like to thank my labmates – Audrey, Neethu and Anna, who made the atmosphere at work collaborative, lively and supportive.

I would like to thank Lindsey and Colby Behrens. I truly do not know if I would have made it through my Ph.D. and gotten to this point without both of you. You have been available for stress relieving game nights and dinner, have brought me pints of ice cream at my absolute lows and have made my life so much better. I will be eternally grateful to the universe for bringing you both into my life.

The person who has picked me up from my lows (sometimes quite literally) and cheered me on relentlessly to this finish line has been Sam. I cannot begin to describe how much your trust and faith in me motivates me and encourages me every day to do more and be more. I love you.

Most importantly, I would like to thank my family – my parents and my sister – for their unending love and support. My sister Shivani is my role model on how to live life and I am forever in awe of her. Regardless of where I am or what time of the day it is, I can always be certain that if I need help, my family will be there for me and that they will move heaven and earth to help me figure things out.

I would like to dedicate this thesis to my Mom and Dad.

TABLE OF CONTENTS

CHAPTER 1: INTRODUCTION

Protein homeostasis, or proteostasis, is the maintenance of a healthy cellular proteome. It involves the dynamic regulation of each protein within the cell from its biogenesis to its degradation, including the diverse conformational and functional aspects of the protein (Powers *et. al.* 2009). It is obvious then, that proteostasis is essential to the survival of the cell, especially when considering the constantly changing environmental conditions experienced by the cell that can drastically affect the proteome. Breakdown in the proteostasis network is a common feature of aging and several diseases such as neurodegeneration, heart failure and type II diabetes (Labbadia and Morimoto, 2015). Cancer cells facing a highly stressful hypoxic, nutrient deprived environment with an increasing burden of mutation laden proteins are heavily dependent on the proteostasis network to maintain a functional proteome (Mercier and LaPointe, 2022).

Molecular chaperones are key regulators of proteostasis (Jayaraj *et. al.* 2019). Initially discovered due to their specific, elevated expression during the heat shock response (Ritossa 1996), these proteins have been shown to be important for various cellular processes under physiological conditions such as protein folding (Frydman *et.al.* 1994), macromolecular complex assembly (Cuéllar *et. al.* 2019), maintenance of metastable proteins (Brugge 1981; Joab *et. al.* 1984) and the surveillance and targeting of misfolded proteins for degradation (Parsell *et. al.* 1994). The eukaryotic molecular chaperone network comprises of three major chaperones systems – TriC/CCT system (Lopez *et. al.* 2015), Hsp70 system (Rosenzweig *et. al.* 2019) and the Hsp90 system (Schopf *et. al.* 2017). Each system is centered around an essential molecular chaperone (CCT, Hsp70 and Hsp90) with its multiple different binding partners or co-chaperones.

The chaperonin CCT is a large oligomer forming a double ring structure of eight paralogous subunits (Rommelaere *et. al.* 1993). Each subunit has an ATP binding domain and a potential substrate binding domain, and the entire oligomeric structure itself has a hydrophobic core thought to be the site for chaperone-client interactions (Joachimiak *et. al.* 2014). In spite of its size and complexity, several CCT clients and CCT-client interaction sites (Spiess *et.al.* 2006; Gestaut *et. al.* 2019) as well as the functional outcome of CCT-client interaction – such as protein folding, and prevention of aggregation (Balchin *et. al.* 2018) have been determined. Similarly, the molecular chaperone Hsp70 is almost synonymous with the protein folding process (Rosenweig *et. al.* 2019). With well-defined ATP binding (Flaherty *et. al.* 1990) and substrate binding domains (Zhu *et. al.* 1996), it associates with the translating ribosome at the nascent chain exit tunnel, using the hydrophobic surface generated by the substrate binding domain to interact with the emerging polypeptide, surveying for and preventing protein misfolding and aggregation (Lee *et. al.* 2021).

Despite extensive study, the complete clientele, determining features of chaperone-client interaction, and the function of the Hsp90 molecular chaperone remain largely unknown. While Hsp90 has been associated with metastable proteins (Brugge, 1981; Joab *et. al.* 1984) and can refold misfolded proteins (Weich *et. al.* 1992; Freeman *et. al.* 1996), previous studies have demonstrated a functional role for Hsp90 with native proteins (Fig. 1), i.e., completely folded proteins that do not necessarily depend on Hsp90 for folding but rather for function (Freeman and Yamamoto, 2002; Toogun *et. al.* 2008, DeZwaan *et. al.* 2009, Echtenkamp *et. al.* 2016, Wang *et. al.* 2020). This deviation of Hsp90 from the chaperone norm, along with the complexities associated with the determination of Hsp90 interactors led to the following study

wherein I designed a novel high throughput crosslinking approach to not only identify Hsp90 clients, but also further the understanding of Hsp90 specificity and function.

1.1 PHYSIOLOGICAL RELEVANCE OF HSP90

Hsp90 is associated with many neurodegenerative disorders such as Huntington's, Alzheimer's, amyotrophic lateral sclerosis, and Parkinson's (Brehme *et. al.* 2014; Lackie *et. al.* 2017). Hsp90 has been shown to inhibit the aggregation of aberrant amyloid β (Aβ) and tau protein *in vitro* (Evans *et. al.* 2006). However, the story is significantly more complex *in vivo*, where Hsp90 inhibition has been shown to have both protective and aggregation-promoting roles (Sittler *et. al.* 2001; Falsone *et. al.* 2009; Putcha *et. al.* 2010*;* Daturpalli *et. al.* 2013).

The ability of Hsp90 to stabilize different conformations of client proteins suggests a potential for evolutionary buffering wherein Hsp90 suppresses deleterious effects of spontaneous mutations on protein stability. This has been tested in *Drosophila melanogaster* (Rutherford and Lindquist, 1998), *Arabidopsis thaliana* (Queitsch *et. al.* 2002), yeasts (Jarosz and Lindquist, 2010) and cavefish (Rohner *et. al.* 2013) and it has been demonstrated that inhibition or deletion of Hsp90 reveals phenotypes that a suppressed by Hsp90 under physiological conditions.

The buffering effect of Hsp90 extends to cancer where the stabilization of mutant proteins can promote genetic variation promoting cancer progression, and potentially counteracting protein inhibitors (Rutherford and Lindquist, 1998). Hsp90 also modulates several oncoproteins such as v-Src (Brugge 1981), human epidermal growth factor receptor (Shimamura *et. al.* 2005), telomerase (DeZwaan *et. al.* 2009), hypoxia-inducible factor 1 (Minet *et. al.* 1999), and p53 (Rudiger *et. al.* 2002). These results have driven several Hsp90 inhibitor clinical trials.

However, a heat shock response (HSR) triggered by Hsp90 inhibition compensates for its loss, resulting in failure of these trials (Whitesell *et. al.* 2003).

1.2 HSP90: DISCOVERY AND EARLY INSIGHTS

As with several other heat shoch proteins, heat shock protein 90 (Hsp90) was also originally discovered in the salivary glands of *Drosophila melanogaster* as a protein upregulated in response to heat stress (Tissières *et. al.* 1974). However, a series of publications in the 1980s identified a 90 kDa protein as being in complex with metastable proteins such as steroid hormone receptors and kinases in physiological conditions (Brugge 1981; Oppermann *et. al.* 1981, Joab *et. al.* 1984; Catelli *et. al.* 1985; Sanchez *et. al.* 1985). Functional studies in the field of hormone receptor signaling demonstrated that Hsp90 associated with the 8-9S non-transformed forms of the progesterone (PR) and glucocorticoid receptor (GR) to facilitate high affinity hormone binding (Picard *et. al*. 1990; Pratt and Toft, 1997). In fact, disassociation of unliganded steroid hormone receptors from Hsp90 led to a collapse of the receptor into a DNA-binding deficient misfolded state. It was only upon binding to a ligand, did functional receptor dissociate from Hsp90 and bind DNA (Czar *et. al.* 1997; Pratt and Toft, 1997). Hsp90 was also shown to bind with newly synthesized src kinase until the kinase was able to associate with the plasma membrane (Courtneidge and Bishop 1982; Brugge *et. al.* 1983). This association of Hsp90 with metastable proteins drove the idea of Hsp90 serving as a "stability factor", a typical chaperoning role.

While Hsp90 is essential in eukaryotes and is expressed up to 2% of the protein mass within the cell, reducing the levels of Hsp90 to $1/10^{th}$ the normal level of the protein has no effect on yeast cells at the physiologically relevant temperature of 25°C (Borkovich *et. al.* 1989).

This reduction of Hsp90 protein level only affected the thermotolerance of the cells. Furthermore, the reduction in Hsp90 levels did not result in misfolding or aggregation of other cellular proteins (Borkovich *et. al.* 1982). Unlike bacteria, yeast and humans have two iso forms of Hsp90 – Hsc82 and Hsp82 in *Saccharomyces cerevisiae* and HSP90α and HSP90β in *Homo sapiens* (Chen *et. al.* 2006). Hsc82 and HSP90β are constitutively expressed, and Hsp82 and HSP90α are induced upon heat stress, further increasing the levels of Hsp90 with temperature (Borkovich *et. al.* 1989; Shen *et. al.* 1997; Zhang *et. al.* 1999). The fact that a small portion of the available Hsp90 pool is seemingly sufficient as a stabilizing factor for metastable proteins, raises the question why Hsp90 is expressed to such a high level and what roles of Hsp90 remain to be found.

1.3 HSP90 CONFORMATION CYCLE AND CO-CHAPERONES

Hsp90 consists of three highly conserved domains – the amino-terminal domain (N), which binds to ATP (Prodromou *et. al.* 1997), the middle domain (M) which enables ATP hydrolysis and is thought to be the primary domain for client binding (Harris *et. al.* 2004), and the carboxy-terminal domain (C), which is involved in Hsp90 dimerization (Wayne and Bolon, 2007). Other important structural characteristics of Hsp90 include a C-terminal Met-Glu-Glu-Val-Asp (MEEVD) motif that can be bound by tetraticopeptide repeat (TPR) domains (Buchner 1999) present on several Hsp90 co-chaperones such as Sti1 (Johnson *et. al.* 1999), Cpr6 (Zuehlke *et. al.* 2013), Cpr7 (Zuehlke *et. al.* 2012), and Cns1 (Marsh *et. al.* 1998) as well as a long, flexible, charged linker connecting the N and M domains, regulating Hsp90 function (Hainzl *et. al.* 2009; Jahn *et. al.* 2014). Functionally, Hsp90 is a homodimer, as dimerization is essential for its function *in vivo* (Wayne and Bolon, 2007).

When not bound to ATP, Hsp90 exist in an open 'V-shaped' conformation (Shiau *et. al.* 2006; Dollins *et. al.* 2007). The binding of the N domain to ATP results in large conformational changes that rearranges the two N domains into a second point of dimerization, creating the 'closed' conformation (Hellenkamp *et. al.* 2017). The conformational cycle is completed upon ATP hydrolysis which requires N and M domain interactions modulated through the charged linker connecting the two domains (Meyer *et. al.* 2003; Cunningham *et. al.* 2008). As an ATPase, Hsp90 has a very low enzymatic activity and hydrolyses only 0.1 ATP min^{-1} in humans and 1 ATP min^{-1} in yeast (Prodromou *et. al.* 1997; Scheibel *et. al.* 1997; McLaughlin *et. al.* 2002). However, this ATPase activity has been reported to be essential *in vivo* (Obermann *et. al.* 1998; Panaretou *et. al.* 1998; Mishra and Bolon, 2014). The regulation of the Hsp90 ATPase conformation cycle is thought to be one of the two primary roles of its co-chaperones, the other being serving as an adaptor protein for client binding. Co-chaperones such as Sti1 carry out both functions, acting as an adaptor for client transfer between Hsp70 and Hsp90 (Johnson *et. al.* 1998; Wegele *et. al.* 2006) as well as inhibiting the ATPases activity of Hsp90 (Prodromou *et. al.* 1999; Richter *et. al.* 2003), maintaining it in the open conformation. In contrast, Aha1 is a strong activator of Hsp90 ATPase activity (Panaretou *et. al.* 2002), driving the Hsp90 conformation cycle forward by displacing Sti1 and interfering with client binding (Li *et. al.* 2013; Koulov *et. al.* 2010). While Sti1 inhibits the ATPase activity of Hsp90, locking it in the open conformation, Sba1 is a co-chaperone that stabilizes the closed conformation of Hsp90 by preventing ATP hydrolysis (Johnson and Toft, 1994; Richeter *et. al.* 2004; Ali *et. al.* 2006). To do so, Sba1 competes with Aha1 for Hsp90 binding. Thus, the binding of certain co-chaperones requires sequential association and dissociation, creating a co-chaperone cycle within the Hsp90 conformational cycle (Li *et. al.* 2011).

While some co-chaperones modulate the Hsp90 conformation cycle through direct binding, others such as Ppt1, which is also a TPR containing co-chaperone, dephosphorylates Hsp90 and its co-chaperone Cdc37 (Wandinger *et. al.* 2006; Vaughan *et. al.* 2008), affects both Hsp90 conformational dynamics and the maturation of clients (Soroka *et. al.* 2012). Cdc37 is a client specific Hsp90 co-chaperone, involved in the maturation of kinases (Siligardi *et. al.* 2002; Roe *et. al.* 2004). Other co-chaperones such as Sgt1 do not affect the ATPase activity of Hsp90 and only serve as client adaptor proteins (Catlett and Kaplan, 2006), and the role of yet others such as Cns1 is yet to be fully understood (Schopf *et. al.* 2019).

1.4 NOVEL FUNCTION OF HSP90 WITH NATIVE PROTEINS

While originally thought to only serve metastable proteins such as hormone receptors and kinases that need to be maintained in a functional yet quiescent state until activated (Pratt and Toft, 1997), our group has highlighted Hsp90 dependent modulation of several native proteins (Freeman and Yamamoto, 2002; Toogun *et. al.* 2008, DeZwaan *et. al.* 2009, Echtenkamp *et. al.* 2016, Gvozdenov *et. al.* 2019; Wang *et. al.* 2020). The very metastable hormone receptors that are bound by Hsp90 and maintained in a ligand inducible form are released from their cognate DNA post-ligand binding by Hsp90 (Fig. 1A). In fact, Hsp90 serves as a regulator of protein-DNA interactions for several different transcription factors (Gvozdenov *et. al.* 2019) and DNA binding proteins (Echtenkamp *et. al.* 2016) ensuring a highly dynamic nuclear environment capable of rapid response to external stimuli. In the context of telomere extension, Hsp90 acts as a molecular switch, releasing the capping complex from the telomere end to enable binding and extension by the telomere holoenzyme (Fig. 1B) (DeZwaan *et. al.* 2009). Finally, Hsp90 ensures that even within the crowded milieu of the nucleus, the dynamics of protein-protein and protein-

DNA interactions are maintained (Fig. 1C) (Echtenkamp *et. al* 2016). Hsp90 regulation of native proteins is often through transient interactions, evidenced by the inconsistent or complete lack of capture of these interactors in high throughput screens probing the clientele of Hsp90. The transient and dynamic nature of Hsp90-client interactions also makes crystallization of the Hsp90-client complexes difficult. A significant question for the field thus becomes, “How does one capture the transient interactions between a molecular chaperone and its seemingly native clients?”

1.5 FIGURE

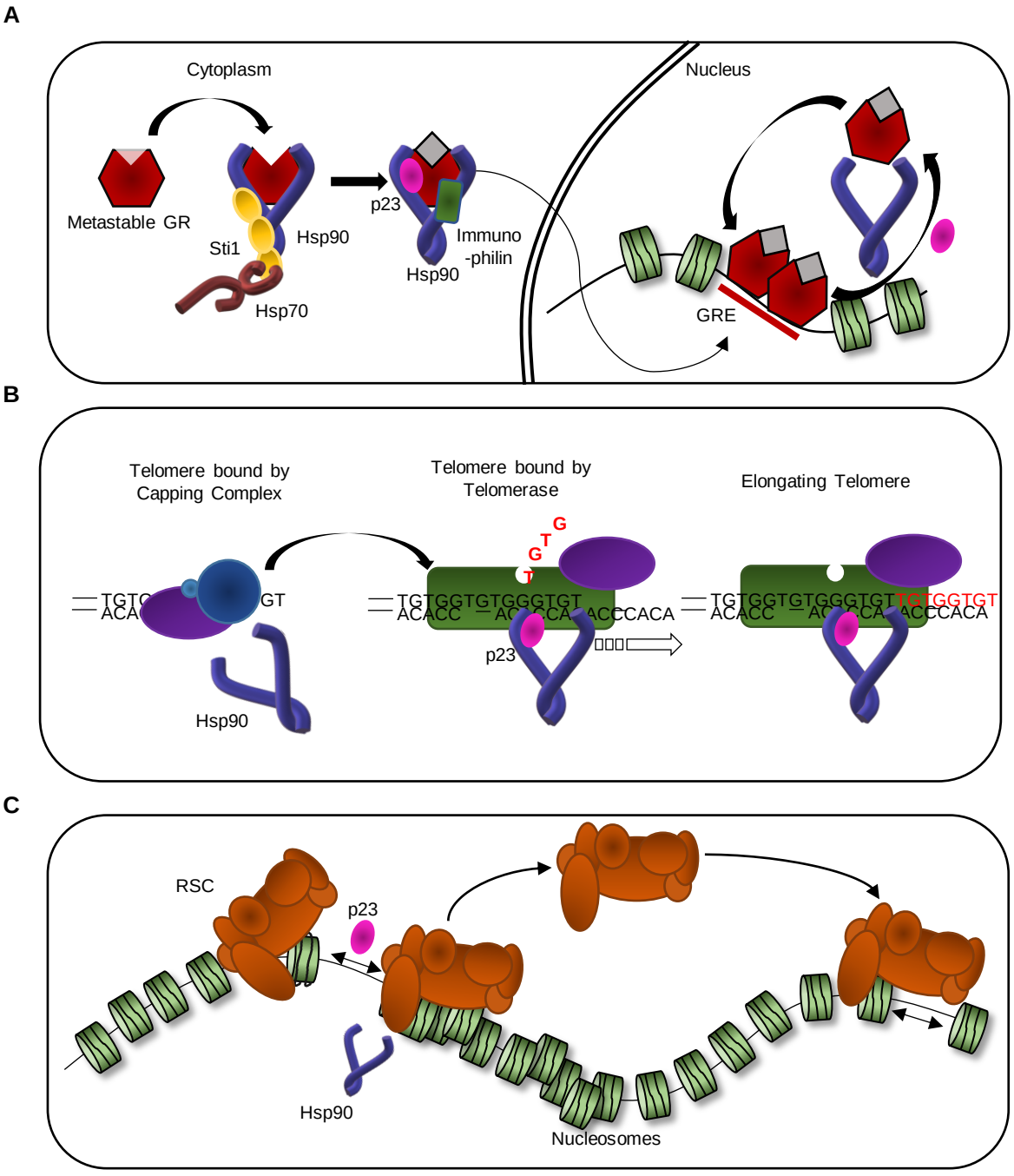

Figure 1. Transient and stable Hsp90-client interactions. (A) Hsp90 stably interacts with metastable steroid hormones receptors, maintaining them in a functional, ligand inducible form. Upon binding to the ligand (hormone), the receptor translocates to the nucleus for gene activation. Hsp90 transiently interacts with ligand bound-receptor to release it from the DNA. **(B)** Hsp90 transiently interacts with the Telomere capping complex, enabling the transition from capping to telomere elongation. Stable Est1-Hsp90 interaction is necessary for telomerase processivity. **(C)** Hsp90 transiently interacts with the RSC chromatin remodelling complex, releasing it from bound nucleosomes, ensuring a free pool of RSC is always available within the nucleus.

CHAPTER 2: ESTABLISHING A PHYSICAL HSP90 INTERACTOME

2.1 INTRODUCTION

Hsp90 is an essential eukaryotic molecular chaperone, ubiquitously expressed in all organisms. It comprises of up to 2% of the protein content of a cell and is involved in a plethora of processes such as protein folding (Weich *et. al.* 1992), chromatin remodeling (Echtenkamp *et. al.* 2016), and chromosome motion (Wang *et. al.* 2020). To carry out these diverse activities, Hsp90 interacts with various clients through a complex binding cleft modulated by numerous co-chaperones (Biebl *et. al.* 2019). Metastable clients require stable interactions with Hsp90 while transient interactions are carried out with native proteins involved in complex and dynamic macromolecular structures. Despite the extensive studies into Hsp90 function, the complete clientele and co-chaperone interaction network of Hsp90 is unknown.

The very first attempt at generating an Hsp90 interactome in yeast using the yeast two hybrid technique resulted in the identification of 5 interactors – 3 known co-chaperones and 2 novel hits of unknown function (Fig 2A; Millson *et. al.* 2004). Only upon using an Hsp90 mutant – E33A – that is thought to stabilize Hsp0-client interactions by inhibiting the final step of the Hsp90 ATPase reaction, was a functional two hybrid interaction screen yielding 126 potential Hsp90 interactors (Fig 2A; Millson *et. al.* 2005). Several high-throughput screens using different techniques to identify Hsp90's interactors have yielded in numerous hits (when combined), but the overlap between these datasets was less than 5%. In fact, in yeast, nearly 80% of the interactors were only found through synthetic genetic or synthetic chemical screens – typically not considered to indicate physical interaction between the tested proteins (Fig 2A; McClellan *et. al.* 2007). Screens in mammalian systems using affinity purification have also been unsuccessful

in capturing the complete range of Hsp90 clientele, with each screen resulting in only ~40-100 interactors and very little overlap (Fig 2B; Falsone *et. al.* 2005; Tsaytler *et. al.* 2009). A novel quantitative assay combining luciferase activity with an enzyme-linked immunosorbent assay (ELISA) in mammalian cells was able to capture 60% of mammalian kinases as Hsp90 clients, an expected result considering kinases were one of the first few proteins to be discovered to be associated with Hsp90 that rely on stable binding to Hsp90 for their activity. Surprisingly, less than 7% of the human transcription factors were detected in the very same screen despite a known role for Hsp90 in transcription factor-DNA binding regulation (Fig 2C; Taipale *et. al.* 2012). This difficulty and inconsistency in detecting most Hsp90 interactors is attributed to the transient nature of Hsp90-client binding.

Transient associations also hinder the study of the specific selection of clients by Hsp90. Hsp90 has three domains – amino-terminal (N), middle (M), and carboxyl-terminal (C) – and binding of clients and co-chaperones is facilitated through hydrophobic patches on all three (Bieble *et. al.* 2019). Different co-chaperones of Hsp90 are believed to be involved in specific client selection; however, the Hsp90 determinants of this specificity have not been elucidated. Furthermore, client features that enable specific Hsp90 interaction are poorly understood (Taipale *et. al.* 2010).

The expanded genetic code is a promising approach to establish new methods for the capture of protein-protein interactions. Using an orthogonal suppressor tRNA and amino-acyl tRNA synthetase pair, one can incorporate different non-canonical amino acids with novel and unique properties into proteins in a site specific manner (Liu and Schultz, 2010). One such non-canonical amino acid is p-Benzoyl-L-phenylalanine (Bpa) – a benzophenone derivative of the natural amino acid phenylalanine (Chin *et. al.* 2002; Krishnamurthy *et. al.* 2011). Upon UV

exposure, photolysis of the keto group within the benzophenone is induced that reacts with C-H bonds (Fig 3A; Dormán and Prestwich, 1994).

In this study, I created a high throughput screen utilising a p-Benzoyl-L-Phenylalanine (Bpa) dependent *in vivo* kinetic trap for Hsp90-protein interactions (Fig. 3B, 6). By incorporating Bpa in a site-specific manner within Hsp90, I was able to identify 1114 yeast proteins as Hsp90 interactors (Fig. 8; Table 1). Due to the selection of Bpa sites across the three domains of Hsp90, I was also able to gain insights into the utilisation of the N, M and C domains in Hsp90-client/co-chaperone interaction (Fig. 11, 12, Table 2). By analysing the client and co-chaperone peptides captured by the incorporated Bpa, I have discovered a specific feature required for the functional regulation of clients by Hsp90 (Fig. 14, Table 3). Finally, I was able to elucidate a novel role for Hsp90 and Hsp90 interactors in two different pathways – that of Chromosome Motion (Fig. 16) and Translation (Fig 17-19). The implications of Hsp90's role in translation have direct physiological relevance in cancer clinical trials.

2.2 RESULTS

2.2.1 Creating an *in vivo* kinetic trap for Hsp90-protein interactions

To capture the transient interactions between Hsp90 and its co-chaperones and clients, I chose *Saccharomyces cerevisiae* (budding yeast) as my model system. Yeast is an effective model for Hsp90 studies as it is genetically tractable, and many fundamental processes have been shown to be conserved from yeast to humans. Yeast, like humans, has two isofroms of Hso90 – Hsc82 and Hsp82 (Borkovich *et. al.* 1989). Hsc82 is the constitutively expressed form of Hsp90 while Hsp82 is the heat inducible isoform. However, in the absence of one isoform, the

other has been shown to compensate for its loss, which was thought to indicate that most functions between Hsc82 and Hsp82 are conserved (Borkovich *et. al.* 1989).

For the purpose of this study, I used the yeast strain JJ117 (*hsc82::kanr hsp82::kanr trp1 leu2 his3 ura3 met2 lys2 ade2/Yep24-HSP82* kindly provided by Dr. Jill Johnson, University of Idaho). The endogenous loci for both Hsp82 and Hsc82 have been completely disrupted with a Kanamyscin selection marker in this strain. Since *HSP90* is an essential gene in eukaryotes, the strain is supported by plasmid borne Hsp82 also carrying the *URA3* gene. The *URA3* gene on the plasmid allows for its counter-selection on 5-Fluoroacetic acid (5-FOA), and thus, plasmid shuffle can be used to replace Hsp82 with any variant form of Hsp82 or Hsc82, ensuring that the mutant form is the only source of Hsp90 in the yeast. For the purpose on incorporating Bpa in a site specific manner in the sequence of Hsp90, I used the plasmid pRS313 *GPD* His-*Hsc82* which provides a plasmid borne 6xHistidine-tagged Hsc82 under the control of a *GPD* promoter to generate Amber (UAG) stop codon derivatives of Hsc82 at the desired sites of Bpa incorporation. These Amber stop codon variants along with the plasmid pSNR Bpa, which carries the Bpa specific tRNA synthetase as well as the Amber Stop suppressor Bpa-tRNA enable the creation of Hsp90-Bpa variants within the yeast. This 6xHistidine-tag on the Hsc82 allows antibody detection of Hsc82 as well as Cobalt/Nickel affinity purification of the Hsc82 following crosslinking (Fig. 3B, 6).

Generation of Hsp90-Bpa variants required careful consideration and selection of sites for Bpa incorporation. The crystal structures for hsp90 with a few co-chaperones (Aha1, Cdc37, Sgt1, Sba1) and clients (Cdk4) have been solved (Meyer *et. al* 2004; Ali *et. al.* 2006; Zhang *et. al.* 2008; Verba *et. al.* 2016). I used the available crystal structures to create interfaces for Hsp90-cochaperone and Hsp90-client interactions (Fig. 4). This interaction interface map and a

hydrophobicity plot of Hsp90 served as a guide for the selection of sites for Bpa incorporation. Specifically, I chose sites such that they were structurally proximal to the interaction interfaces with the expectation that minimally, these known co-chaperones would be crosslinked to the proximal Bpa and serve as a positive control for crosslinking. I also used client and co-chaperone crystal structure data to ensure that the sites chosen were not directly involved in known Hsp90 interactions. To address the domain specificity of Hsp90-protein interaction, I chose two sites from each domain. Furthermore, since Bpa is a phenylalanine derivative, I considered phenylalanine sites within the Hsp90 sequence for mutagenesis wherever possible. In cases where phenylalanine was not structurally proximal to the binding regions, I first queried other amino acids in a structure prediction software (Site Directed Mutator) that uses a statistical potential energy function to predict the effect of single amino acid changes on the stability of proteins. Due to Bpa being a non-natural amino acid, the queries were carried out using mutation of the chosen amino acid to phenylalanine. I selected amino acids that were unlikely to significantly affect the structure of Hsp90 upon mutation to phenylalanine. The selected amino acid sites for mutagenesis were – Y24 and F120 for the N domain, F325 and E427 in the middle domain, and F579 and E656 in the C domain. The amino acid Y24 has been previously shown to be phosphorylated and is required for Hsp90 function (Mollapour *et.al* 2010). However, with the N-domain undergoing extensive conformation changes and binding ATP, other surface amino acids were unavailable for mutation. I selected Y24 to serve as a negative control for Hsp90-Bpa function, i.e., since Y24 is required for Hsp90 function, incorporation of Bpa in place of Y24 should result in non-functional Hsp90. The Hsp90 variants generated using the above-described amino acids are referred to as Hsp90-Y24Bpa, Hsp90-F120Bpa, Hsp90-F325Bpa, Hsp90-E427Bpa, Hsp90-F579Bpa and Hsp90-E656Bpa for all future experiments. Wild type His-Hsc82

was also introduced in JJ117 and taken through the plasmid shuffling process to generate a control strain referred to as WT for future experiments.

The system of JJ117, transformed with Hsp90-Bpa variant plasmids and the tRNA suppressor system, provides a quick functionality test for the Hsp90-Bpa variants. Since Hsp90 is essential in eukaryotes and the Hsp90-Bpa variants would be the only source of Hsp90 in the JJ117 strain after plasmid shuffling, replacing amino acids essential for Hsp90 function with Bpa would result in non-functional Hsp90 and the yeast would not survive the plasmid shuffling. In addition to that, in the absence of Bpa in the growth media, the suppressor tRNA system would not be able to incorporate Bpa at the Amber stop codons, resulting in premature termination of Hsp90 translation and the production of truncated versions of Hsp90 which would also be non-functional. Thus, Bpa incorporation can be indirectly tested by growth in the presence and absence of Bpa. Bpa incorporation can also directly be tested by immunoblot analysis of full length Hsp90 production in the cells in the presence and absence of Bpa.

I tested the Hsp90 for functionality using a standard yeast spot test assay (Fig. 5A). As expected, Hsp90-Y24Bpa showed a growth defect even in the presence of Bpa when compared to WT, due to the requirement of Y24 as a phosphorylation site for Hsp90 function. In the absence of Bpa, Hsp90-Y24Bpa was dead. The other 5 Hsp90-Bpa variants grew comparable to WT in the presence of Bpa at both 30°C and a heat stress temperature of 37°C indicating functional Hsp90 despite incorporation of Bpa at the specific sites. Hsp90-F120Bpa, Hsp90-F325Bpa and Hsp90-E427Bpa showed a growth defect as expected in the absence of Bpa, however at 30°C, Hsp90-F579Bpa and Hsp90-E656Bpa did not show a growth defect in the absence of Bpa. It is possible that the truncation of Hsp90 in yeast up to amino acid 579 still renders a viable Hsp90, sufficient for survival of the yeast (Louvion *et. al.* 1996). Increasing the

temperature to 37°C resulted in a growth defect even in Hsp90-F579Bpa and Hsp90-E656Bpa indicating that the truncated forms of Hsp90 in these two strains were not fully functional.

The production of full length Hsp90 was tested by immunoblot analysis, using an anti-His antibody to visualise the Hsp90 in all 5 Hsp90-Bpa variant strains with WT as a control (Hsp90-Y24Bpa was discarded at this stage). As expected, full length Hsp90 is produced in the presence of Bpa (Fig. 5B) in all the Hsp90-Bpa variant strains. In the absence of Bpa, all the Hsp90-Bpa variants except Hsp90-F120Bpa are unable to produce detectable full length Hsp90. A small amount of full length Hsp90 is seen in the case of Hsp90-F120Bpa in the absence of Bpa in the medium, likely due to stop codon read through.

Thus, all 5 Hsp90-Bpa variants produce a full length Hsp90 in the presence of Bpa that supports life in a manner comparable to WT.

2.2.2 Crosslinking Hsp90 to interacting proteins

Previously published Bpa crosslinking studies frequently tested the crosslinking between two specific proteins of interest, and thus, established protocols for crosslinking were not suitable for a high throughput screening of protein-protein interactions. This includes both the method of keeping the cells cool under an intense heat generating source as well as the duration of UV exposure to achieve maximal possible crosslinking of Hsp90 to its interacting proteins.

Typical crosslinking studies carry out UV exposure for less than an hour (Ting *et. al.* 2017) and can use a single freezer pack under the cell suspension petri plate to ensure the temperature of the cells remains at ~4°C despite the heat from the UV bulbs. Having tested this method along with an hour UV exposure that did not lead to successful crosslinking, I devised an alternative set up to maintain the temperature of the cell suspension during crosslinking. Using

multiple freezer packs or changing the freezer packs was not practical for the number of petri dishes being used for crosslinking at the same time. Packing the bottom third of a Styrofoam box with dry ice, and then densely packing the remaining volume with ice ensured that the ice did not melt significantly within the crosslinker. This was an important consideration as the cell suspension containing petri plates would be placed on top of the ice and melting of the ice would lower the plates away from the bulbs, significantly reducing the efficiency of crosslinking (efficiency is inversely proportional to d^6, where d is distance from the bulbs). Increasing the dry ice results in the ice and the cell suspension freezing, while reducing the dry ice results in the ice melting and the crosslinking being unsuccessful. To keep the cell suspension petri plates level for the entire duration of crosslinking, I place a metal plate on top of the ice (Fig. 6B).

I determined Hsp90 crosslinking empirically by modulating the time of the UV exposure followed by analysis of the whole cell extracts (WCE) or affinity purified eluants (Fig. 6, 7). Successful crosslinking can be classified into two different categories – appearance of one or more higher molecular weight bands in the affinity purified eluants or upon immunoblot analysis of the whole cell extracts that are absent in the WT control, along with a reduction in the Hsp90 levels corresponding to its standard molecular weight of 90 kDa (Fig. 6B) or reduction of Hsp90 levels without the appearance of higher molecular weight bands (indicating that the crosslinked Hsp90 has shifter higher on the gel but is below the detection limit of Coomassie stain or immunoblot analysis). Preliminary crosslinking validation carried out using WCE and immunoblot analysis with an anti-His antibody used for visualisation of Hsp90 showed the presence of a higher molecular weight band for Hsp90-F120Bpa after 1 hour of UV exposure. No crosslinking could be seen in the other variants with just 1 hour of UV exposure (data not

shown) but increasing the duration to 3 and 4 hours resulted in a reduction of the Hsp90 levels in the Hsp90-F325Bpa and Hsp90-E427Bpa variants.

To further validate the crosslinking, I analyzed the crosslinked samples of the Hsp90-F120Bpa and Hsp90-F325Bpa variants by immune-blotting for the Hsp90 co-chaperone Sti1. . Since Sti1 is a "strong" interactor of and is co-purified upon affinity purification of Hsp90, as seen by the presence of a band at ~75 kDa. Sti1 is thought to interact with the middle domain of Hsp90 and my expectation was that if Sti1 is crosslinked to Hsp90, the Sti1 antibody would detect a higher molecular weight species in the crosslinked samples due to the combined weight of Hsp90 and Sti1 being much higher than that of Sti1. Affinity purified crosslinked samples were resolved by SDS polyacrylamide gel electrophoresis (SDS PAGE) and gels were either stained with Coomassie stain or analyzed further by immunoblotting with an anti-Sti1 antibody (Fig 7A, B). Higher molecular weight bands were seen in the affinity purified crosslinked samples by Coomassie staining in both Hsp90-F120Bpa and Hsp90-F325Bpa that were absent in the WT purifications. Surprisingly, the Sti1 antibody showed the presence of a higher molecular weight band even in the Hsp90-F120Bpa variant crosslinked sample, in addition to the Hsp90-F325Bpa variant crosslinked sample (Fig. 7A, B right panels). Thus, the Hsp90-F120Bpa variant reveals a novel Sti1-Hsp90 N-domain interaction.

Crosslinking of all 5 Hsp90-Bpa variants was detectable upon affinity purification by Coomassie staining of affinity purified crosslinked samples resolved by SDS PAGE. In the case of Hsp90-F120Bpa, Hsp90-F325Bpa and Hsp90-E427Bpa, higher molecular weight bands could be seen in the crosslinked samples that were absent in both the non-crosslinked samples as well as the WT crosslinked/non-crosslinked samples. For Hsp90-F579Bpa and Hsp90-E656Bpa, the crosslinking was only seen as a significant (more than half) reduction in the Hsp90 levels when

compared to the non-crosslinked controls for the respective variants (Fig. 7C). By using the Hsp90-Bpa variants along with a WT control for mass spectrometry of the affinity purified crosslinked products I expect to identify Bpa-dependent or transient interactors. A second control of W303 yeast supported by an untagged Hsp90 would then provide a general control for background that would also enable determination of stable proteins identified with the WT His-Hsp90 affinity purification.

2.2.3 An Hsp90-Bpa Physical Interactome

Analysis of the mass spectrometry results identified 1114 proteins or ~20% of the yeast proteome as Hsp90 interactors with 629 being Bpa-dependent, i.e., hits that were enriched with the Hsp90-Bpa variants by at least 1.5 fold when compared to WT or found only with the Hsp90-Bpa variants (Fig. 8A; Table 1). Gene ontology (GO) mapping of the hits indicated a distribution of Hsp90 interacting partners across diverse cellular processes with a bias towards processes canonically associated with Hsp90 such as protein folding, protein targeting, and response to heat (Fig. 8B, C). My dataset highlights Hsp90 as a central hub of the eukaryotic chaperone network with several chaperones including Hsp70s, Hsp40s, CCT, Hsp104 as well as the majority of known Hsp90 cochaperones (11 out of 14) being identified as direct physical interactors.

A significant problem with previous high throughput screens identifying Hsp90 interactors was the minimal overlap between different screens. This has been attributed to the transient nature of Hsp90-protein interactions, making consistent identification of interactions difficult. My Hsp90 physical interactome shows high overlap with previously generated physical and genetic interactomes (Fig. 9A, B). The overlap between the first two physical interactomes

generated from the Piper and Houry groups was ~12% (Millson *et. al.* 2005; Zhou *et. al.* 2005). A more recent physical interactome from the Buchner group (Girstmair *et. al.* 2019) utilising a non-specific crosslinker increased the overlap to ~17% with both the Piper and Houry interactomes. In comparison, the Hsp90-Bpa interactome showed ~25% overlap with the Piper and Houry interactome, and 38% overlap with the Buchner interactome (Fig. 9C).

The Buchner interactome can be divided into two categories – a non-Heat Shock (HS) interactome identifying Hsp90 partners under normal physiological conditions, and an HS interactome detecting Hsp90 interactors upon heat stress. Interestingly, the Hsp90-Bpa interactome showed considerable overlap (~35%) with the HS overlap (Fig. 9C). It is possible that when using a non-specific crosslinker, some transient interactors are missed, which are captured upon stabilization of the interactions during heat stress. These same transient interactors can be captured in the Hsp90-Bpa interactome without the induction of a heat shock response, highlighting the success of the method in capturing transient interactors.

Comparison to the known Hsp90 physical and genetic interactors as determined by the Saccharomyces Genome Database showed overlaps of ~30% for each as well, providing validity to the identified hits. As expected, attempts to validate the physical interactome using canonical techniques such as yeast two hybrid remained futile (Fig. 10A). Sti1, a “strong” Hsp90 interactor, denoted as such due to its capture with Hsp90 in every single physical interactome generated, results in only a ~2.5 fold activation of β-galactosidase transcription in an Hsp90 two hybrid system (in comparison toup to a 100 fold activation with other protein pairs such a p53 and the SV40 T antigen; Li and Fields, 1993), and as such, the Hsp90 interactors tested yielded no detectable β-galactosidase activity when compared to the negative plasmid controls. However, testing individual identified interactors for a functional effect upon loss of Hsp90

provided fruitful. One such interactor, Sam3, is a high affinity S-adenosyl-L-methionine (SAM) permease, required for the transport of SAM from the media into the cells (Rouillon *et. al.* 1999). The antifungal agent Sinefungin is also transported via Sam3 (Zheng *et. al.* 2007) and thus, yeast cells are unable to grow on plates treated with Sinefungin. I used a spot test assay to test for a functional effect of Hsp90 loss on Sam3 using the Hsp90 mutant strain G170D. While WT cells are able to grow on 1 μM Sinefungin, the Hsp90 G170D mutant strain showed a significant growth defect at this concentration (Fig. 10B), indicating that in the presence of a mutant Hsp90, Sam3 is hyperactivated. Indeed, measuring the incorporation of tritiated SAM showed a 2-fold increase in Sam3 activity in the G170D strain (Fig. 1C). This result agrees with previous studies highlighting a role for Hsp90 in suppressing certain cellular pathways (McClellan *et. al.* 2007).

Thus, my approach in capturing Hsp90 interactors using an *in vivo* kinetic trap by incorporating Bpa in a site specific manner within the Hsp90 sequence has generated a functional Hsp90 physical interactome.

2.2.4 Physical interactors associate with all three domains of Hsp90

The selection of Bpa sites across all three domains of Hsp90 enabled the analysis of the domain specificity of Hsp90 in client and co-chaperone selection. My results indicate that Hsp90 uses all 3 domains in a combinatorial manner to associate with other proteins, as each Bpa site mediated a comparable number of interactions with significant overlap between different sites (Fig. 11A; Table 2). The interaction interface generated using the known Hsp90-cochaperone/client crystal structures were biased towards the middle domain, likely due to more stable interactions being associated with the middle domain of Hsp90. As a result, I expected the middle domain to show a higher overlap with previously identified physical hits. While a high

overlap of previously identified physical hits is indeed seen with the middle domain Bpa sites, I see a surprising preference for known physical interactors with the N domain Bpa variant Hsp90-F120Bpa and a preferential association of the C domain Bpa variant Hsp90-F579Bpa with the previously established genetic interactors (Fig. 11B). The GO assessment of the 5 Hsp90-Bpa variants also revealed a differential use of the hsp90 sites with different pathways (Fig. 12). Specific enrichment of the protein folding pathway with the C domain Bpa variants is in agreement with the use of the 'MEEVD' tail of Hsp90 for interaction with the TPR domain containing proteins captured within this pathway (Fig. 11C).

My domain-centric interactome supports the idea that Hsp90 uses hydrophobic patches distributed over the entirety of its structure in conjunction with a combinatorial binding to the 3 different domains, to interact with a broad array of clients and cochaperones.

2.2.5 Client binding sites are enriched for intrinsically disordered regions

A benefit of using site specific Bpa incorporation in a protein sequence is the potential to exploit the Bpa as a tag in the mass spectrometry spectra to identify the target peptide sequence captured by crosslinking. While a software to identify crosslinked peptide pairs, MeroX (Götze *et. al.* 2015), is available, the algorithm for scoring the peptide pairs has been designed to function for highly enriched crosslinked species such as in the case of *in vitro* crosslinking or the crosslinking of two specific proteins *in vivo*. After using MeroX to identify crosslinked peptide pairs in the generated Hsp90-Bpa interactome, I created a set of criteria for further scoring and filtering the peptide pairs. Crosslinked peptide pairs were only retained if at least two b or y ions were present for both α and β peptides. Furthermore, more than 5% relative intensity for at least one ion that included the crosslink from both peptides was required.

Sti1 peptides identified aligned with a recently published crystal structure of the Hsp90-Sti1 complex, validating my approach (Fig. 13). In total, 181 crosslinked peptide pairs (Table 3) were identified with 29 corresponding to Hsp90-(co)chaperone (chaperone or cochaperone) interactions, and 152 corresponding to Hsp90-client interactions. Analysis of the client peptides yielded no consensus motif that could explain Hsp90 specific interaction. Rather, I found the client peptides to be preferentially located within intrinsically disordered regions (IDRs) in contrast to the (co)chaperone peptides that were within structured regions (Fig. 14A-E). The presence and locations of the IDRs was based upon the D^2P^2 prediction database (Oates *et. al.* 2013) that created disorder maps for each protein comprising of the predictions of 9 different disorder prediction algorithms and by visualizing the location of the peptide within AlphaFold predictions (Jumper *et. al.* 2021) of the protein structures (Fig. 14 A-D).

Having identified a client feature that could potentially determine Hsp90-client interaction, I tested the domain dependence of Hsp90-IDR interaction. While the M domain interactions recapitulated the overall association of Hsp90 with IDRs for clients, and structured regions for (co)chaperones, the C domain did not preferentially associate with (co)chaperones through structured regions (Fig. 14E). Instead, I see an increase in IDR dependent interactions of Hsp90 C domain with (co)chaperones. Since, IDRs are often thought to provide a docking surface for multiple protein interactions (van der Lee *et. al.* 2014), it is likely that through interactions with (co)chaperone IDRs, the Hsp90 C domain docks with multiple different (co)chaperones at the same time in a complex manner.

The propensity of Hsp90-client peptides to be within IDRs suggests that the selective pressures driving Hsp90-client interaction in nature have been biased towards a functional rather

than a structural effect which further breaks away from the canonical notion that structure informs function (van der Lee *et. al.* 2014).

2.2.6 Hsp90 functionally affects clients through IDR interactions

To test whether the interaction with an IDR was relevant to Hsp90 chaperone action, I investigated the established Hsp90 client Rsc3, which is a DNA binding subunit of the RSC chromatin remodeler. According to D^2P^2 and AlphaFold predictions, the Hsp90-Bpa crosslink to Rsc3 falls within an IDR (Fig. 15A). Hsp90 has been previously shown to disrupt the Rsc3 DNA binding activity *in vitro* as well as *in vivo* (Echtenkamp *et. al.* 2016). The functional effect of Hsp90 on Rsc3 DNA binding can be visualized by a Rsc3 yeast two hybrid assay that differs from a conventional two hybrid assay. Due to the presence of a Rsc3 consensus motif within the Gal4 DNA binding site, Rsc3-AD (activation domain) fusion can drive the expression of the *HIS3* reporter gene without a Gal4-DBD (DNA Binding Domain) bait. Hsp90 fused to the Gal4 DBD (Hsp90-DBD) localizes to the Gal4 promoter and is able to disrupt the Rsc3 DNA binding resulting in loss of *HIS3* reporter gene expression (Fig. 15B). Thus, in a Rsc3 two hybrid assay, the absence of a bait results in growth on synthetic media lacking Histidine, whereas the presence of the Hsp90-DBD bait results in an inability to grow on media lacking Histidine.

Deleting the IDR (Rsc3ΔIDR) associated with the Hsp90 crosslink prevented Hsp90 from disrupting the Rsc3ΔIDR DNA-binding (Fig. 15B) establishing a functional role for Hsp90-IDR interaction.

2.2.7 A Novel Hsp90 dependent process is further elucidated by the Hsp90-Bpa interactome

A parallel study being conducted by our group delineated the role for Hsp90 in long range chromosome motion. The directed motion of the *INO1* locus from the nucleoplasm to the nuclear periphery (Fig. 16A) under inositol starvation conditions requires several players including actin, myosin, transcription factors and chromatin remodellers. The molecular chaperones Hsp90 and p23 facilitate the dynamic interactions between these players and the *INO1* locus to enable the motion of the DNA.

Interestingly, the Hsp90-Bpa interactome captures two direct crosslinks (Fig. 16B), one to Bni1 – a formin involved in actin polymerisation regulation, and She4 – the budding yeast Unc45-Cro1-She4 (UCS) homolog. The UCS cochaperone enables Hsp90 regulation of type II myosins in fission yeast. With the directed motion of a DNA locus potentially requiring the movement of DNA as a myosin cargo upon actin tracks, I tested the role for actin polymerisation and myosin regulation in the chromosome process.

Both Bni1 and She4 were required for the motion of the *INO1* locus from the nucleoplasm to the nuclear periphery upon inositol starvation (Fig. 16C). The role for She4 is expected to be in activating the type II myosin as in the case of fission yeast while it is likely that the need for Bni1 stems from its role in regulating actin polymerisation. To directly test the role of actin polymerisation on the *INO1* locus motion, I generated nuclear localisation signal (NLS) tagged versions of wild type actin (Actin-NLS) as well as a polymerisation deficient mutant of actin (R62D-NLS). While Actin-NLS should not affect the polymerisation dynamics, expression of R62D-NLS should selectively disrupt the actin polymerisation within the nucleus. Indeed, *INO1* motion is abrogated only upon the expression of R62D-NLS (Fig. 16D). Aside from Bni1, another potential modulator of actin polymerisation is the Arp2/3 complex. A recent study

demonstrated that the Arp2/3 inhibitor CK-666 blocked the nuclear periphery clustering of double stranded heterochromatin DNA breaks. I tested whether Arp2/3 also modulates *INO1* movement. While CK-666 was able to disrupt the cytosolic actin patches, leaving the Bni1 dependent actin cables intact, Ck-666 only partially affected the movement of the *INO1* locus, even at the highest concentration tested (Fig. 16E, F).

Thus, the Hsp90 regulated pathway of long range chromosome motion is in part modulated by Hsp90 interactions with Bni1 which ultimately controls actin polymerisation, and by Hsp90 interactions with She4 which is required for active type II myosins. The capture of Bni1 and She4 in the Hsp90-Bpa interactome further validates the functionality of the physical interactome.

2.2.8 Hsp90 plays a multifaceted role in translation

Given a preferential interaction of Hsp90 with IDRs of clients, I decided to further investigate the Hsp90-IDR interaction by focusing on an Hsp90-linked process that is enriched with IDR containing proteins – translation (Fig. 1A, 17). Since Hsp90 could be involved in stabilizing the translation factors identified, I began by testing the stability of the translation hits upon Hsp90 inhibition. The steady state levels of all 32 hits remained unaffected by loss of Hsp90 activity (Fig. 18A). Ribosome fractionation showed that Hsp90 is primarily associated with the 40S small ribosomal subunit peak in contrast to the nascent chain binding Hsp70, which is present across all fractions (Fig. 18B). The 40S subunit is involved in scanning the 5'-UTR of the mRNA for the AUG start codon (Hershey *et. al.* 2012) and thus, I tested whether Hsp90 affects the fidelity of start codon selection using a dual luciferase assay system where the Firefly luciferase ORF begins with the non-canonical start codon UUG with the same plasmid harboring

a Renilla luciferase beginning with the canonical AUG start codon (Takacs *et. al.* 2011). Shifting the Hsp90 temperature sensitive mutant G170D to 37.5°C, which completely inactivates the mutant (Nathan and Lindquist, 1995), reduced the fidelity of translation as evidenced by the increase in UUG driven firefly luciferase activity (Fig. 18C). An increase in translation from non-canonical start codons, or a reduction in the fidelity of start codon selection would result in a global increase in out of frame translation. Surprisingly, RiboSeq analysis, an assay by which the ribosome protected fragments of mRNA can be captured and mapped to the genome (McGlincy and Ingolia, 2017), of both the WT and G170D mutant strains, showed out of frame translation in the G170D mutant even at 30°C (Fig. 18D). In fact, while the shift to 37.5°C slightly affects the translation frame for WT, as the G170D mutant strain already displays a significant translation frame defect (>50% translation is out of frame), no change is seen in G170D after the temperature shift.

Considering the dual luciferase assay displaying a decreased fidelity in start codon selection only after temperature shift, it is likely that the translation frame in G170D is also abrogated in additional ways such as during translation pausing and elongation. Inactivation of translation factors, such as during cellular stress, typically leads to the formation of stress granules (SG) (Protter and Parker, 2016). To assess whether Hsp90 affects SG formation, I followed heat-induced stress granules formed by the Hsp90 interactor Ded1. Ded1 us a DEAD-box RNA helicase that promotes the assembly of the 48S preinitiation complex (Guenther *et. al.* 2018) by fostering scanning of 5'-UTRs and forms SGs in an IDR dependent manner (Iserman *et. al.* 2020). While SG formation is typically visualized using super-physiological temperature shifts above 42°C that result in a substantial heat shock response (HSR) and cause cell death, the inhibition of Hsp90 at both 42°C and 46°C had no apparent effect on GFP-Ded1 SGs (Fig. 18E).

However, at 39°C and 40°C, the formation of GFP-Ded1 SGs increased in the presence of the Hsp90 inhibitor Radicicol (Fig. 18E).

A loss in fidelity of translation would result in the production of aberrant polypeptides which would in turn increase the degradation burden on the proteosome. Indeed, the temperature sensitive G170D mutant was more sensitive to the proteosome inhibitor MG-132 at progressively higher temperatures (Fig. 18F). In fact, even at lower doses of MG-132 where virtually no effect is seen on WT cell at 37.5°C, G170D show a heightened sensitivity to the proteosome inhibitor (Fig. 18G).

2.2.9 Physiological relevance of translation regulation by Hsp90

Hsp90 inhibitors have long been tested in cancer clinical trials, all of which have failed due the triggering of an HSR, and thereby HSF1 activation, upon Hsp90 inhibition through unknown mechanisms. The production of aberrant polypeptides as a result of loss of translation fidelity essentially mimics an HSR and could provide a mechanism for Hsp90 inhibition dependent HSF1 activation. To test whether active translation is required to induce the HSR upon Hsp90 inhibition, I measured the HSR of cells treated with elevated temperature (42°C), the proline analog azetidine-2-carboxylic acid (azetidine), or an Hsp90 inhibitor (Radicicol or Ganetespib). Addition of the translation inhibitor cycloheximide exacerbated the HSR triggered by 42°C, alleviated the azetidine effect, and prevent the HSR upon Hsp90 inhibitor treatment in both yeast (Fig. 19A) and human cell (Fig. 20B).

Thus, the Hsp90 inhibitor dependent HSR requires active translation and might provide an opportunity to further previously failed trials through the creation of a combination cocktail of Hsp90 inhibitors along with translation inhibitors.

2.3 DISCUSSION

In this study I have presented an Hsp90 physical interactome generated through the site-specific incorporation of a photoactivable non-natural amino-acid p-Benzoyl-L-Phenylalanine. I was able to identify 1114 Hsp90 interactors as well as 181 direct contact sites (Fig 8A; Table 1; Table 3). This physical interactome has provided insight into how Hsp90 might interact with a diverse clientele using all three of its domains and the various hydrophobic patches distributed across its structure in a combinatorial manner as well as recognizing clients through specific disordered regions within the client structure. The clients identified through this interactome have enabled the elucidation Hsp90 dependent regulation of two completely different pathways – Chromosome motion and Translation, with several more pathways waiting to be explored. Finally, the functional role of Hsp90 in translation regulation has the potential to reinvent previous failed Hsp90 inhibitor clinical trials, providing significant physiological relevance to the study.

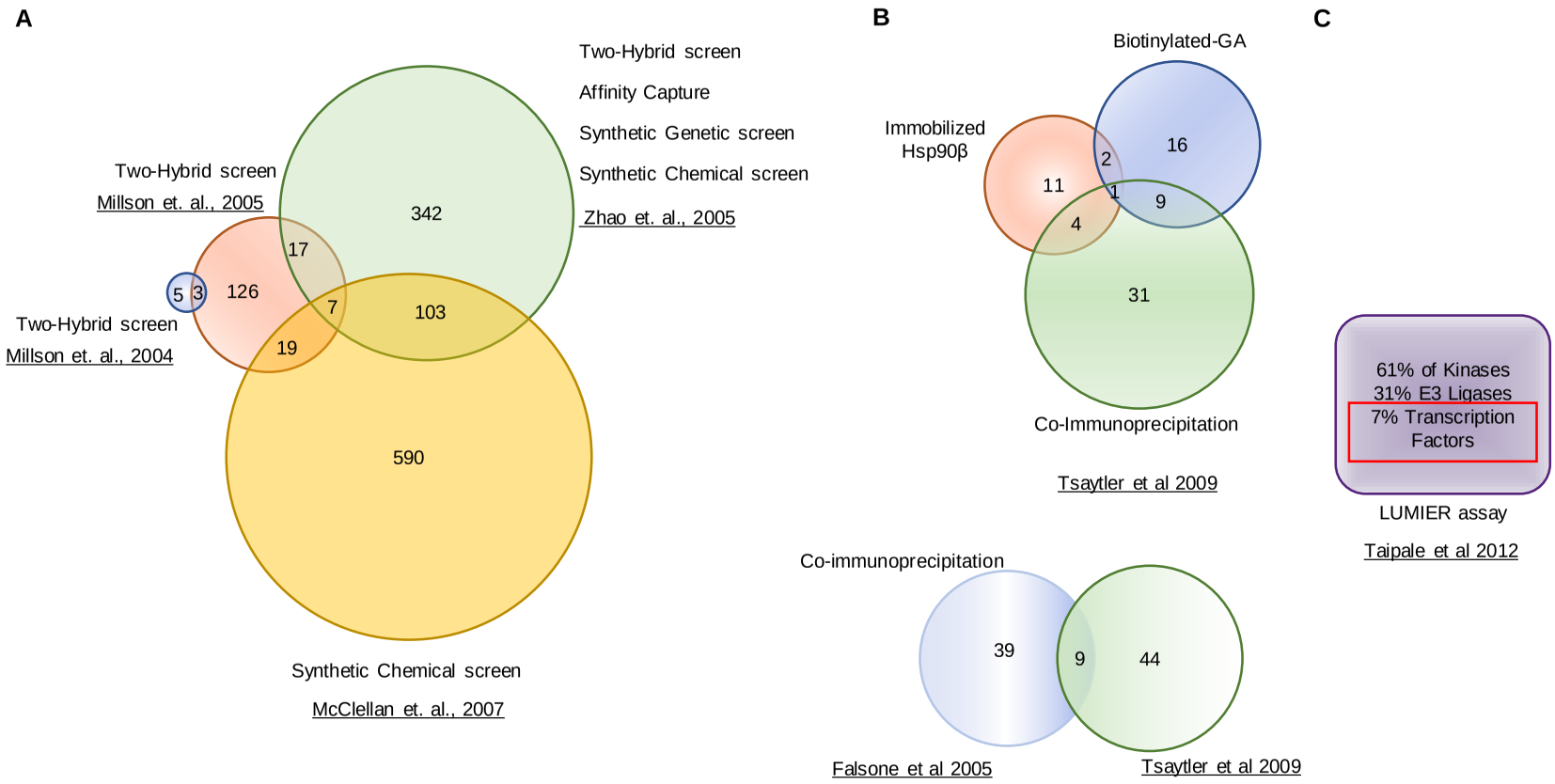

Figure 2. Overview of established Hsp90 interactomes at the start of the study. (A) Hsp90 interactomes established in yeast using a wide variety of techniques such as yeast two hybrid, affinity capture, synthetic genetic and synthetic chemical screens. **(B)** Hsp90 interactomes established using mammalian systems and affinity capture as the main techniques **(C)** Hsp90 interactors identified through a novel ELISA and luciferase based assay – LUMIER.

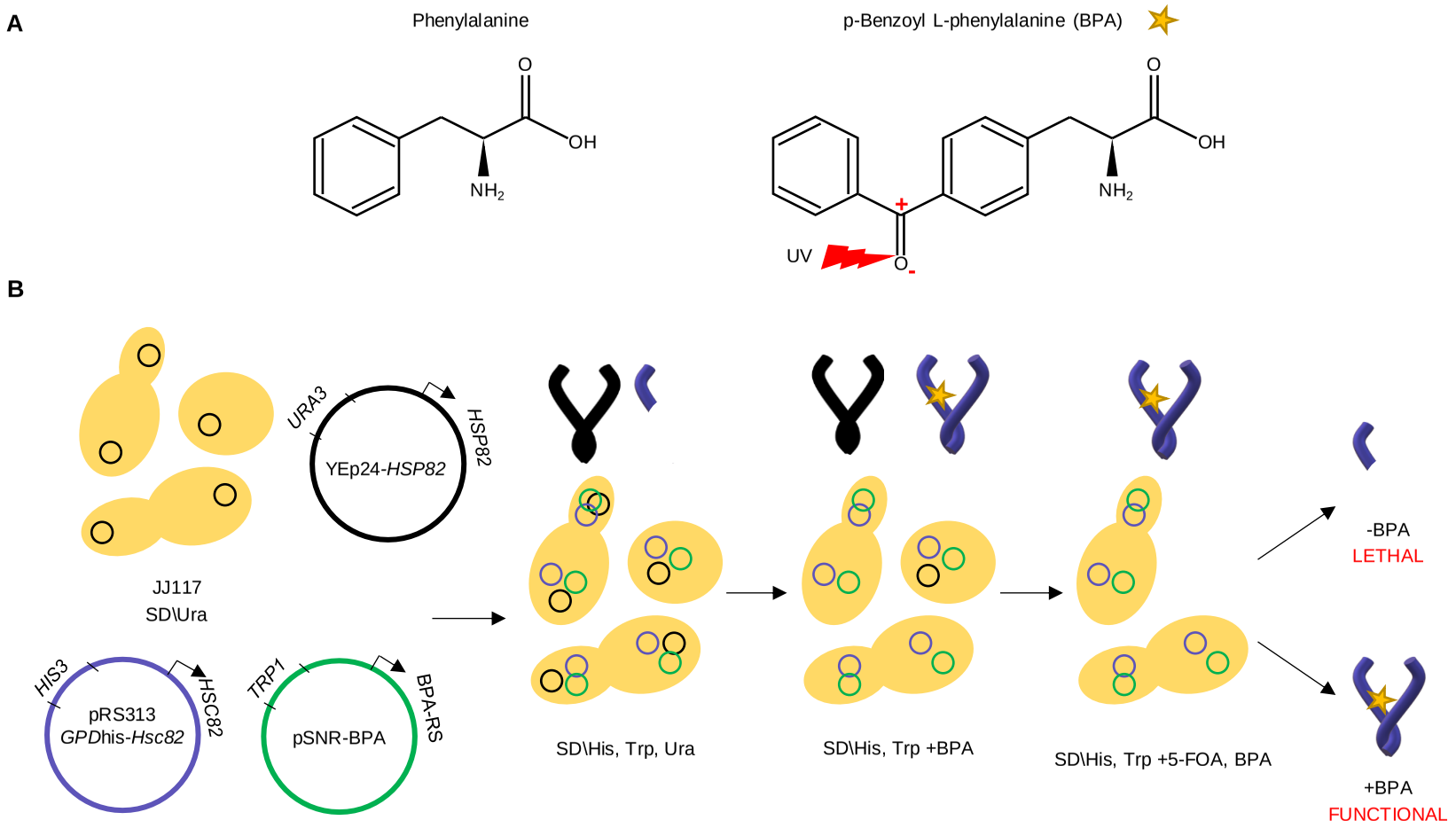

Figure 3. Overview of generating an *in vivo* kinetic trap for Hsp90-protein interactions. (A) The non-natural amino acid p-Benzoyl-L-phenylalanine (right) is an analogue of Phenylalanine (left). UV 365 nm exposure (red lighting bold) results in a negatively charged oxygen (charges indicated in red for after UV exposure) that is capable of crosslinking to any protein with 5 Å. **(B)** Schematic for generation of Hsp90-Bpa variant yeast strains. JJ117, a yeast strain deleted for both hsp90 isoforms and supported by Hsp82 on a plasmid was transformed with His-Hsc82 variants harboring an Amber (UAG) STOP codon at the sites of BPA incorporation as well as a Bpa tRNA synthetase plasmid. 5-FOA dependent plasmid shuffling allows for generation of strains only harboring the Hsc82-Bpa variants. Without Bpa in the media, these cells are expected to produce truncated Hsc82 which cannot sustain life.

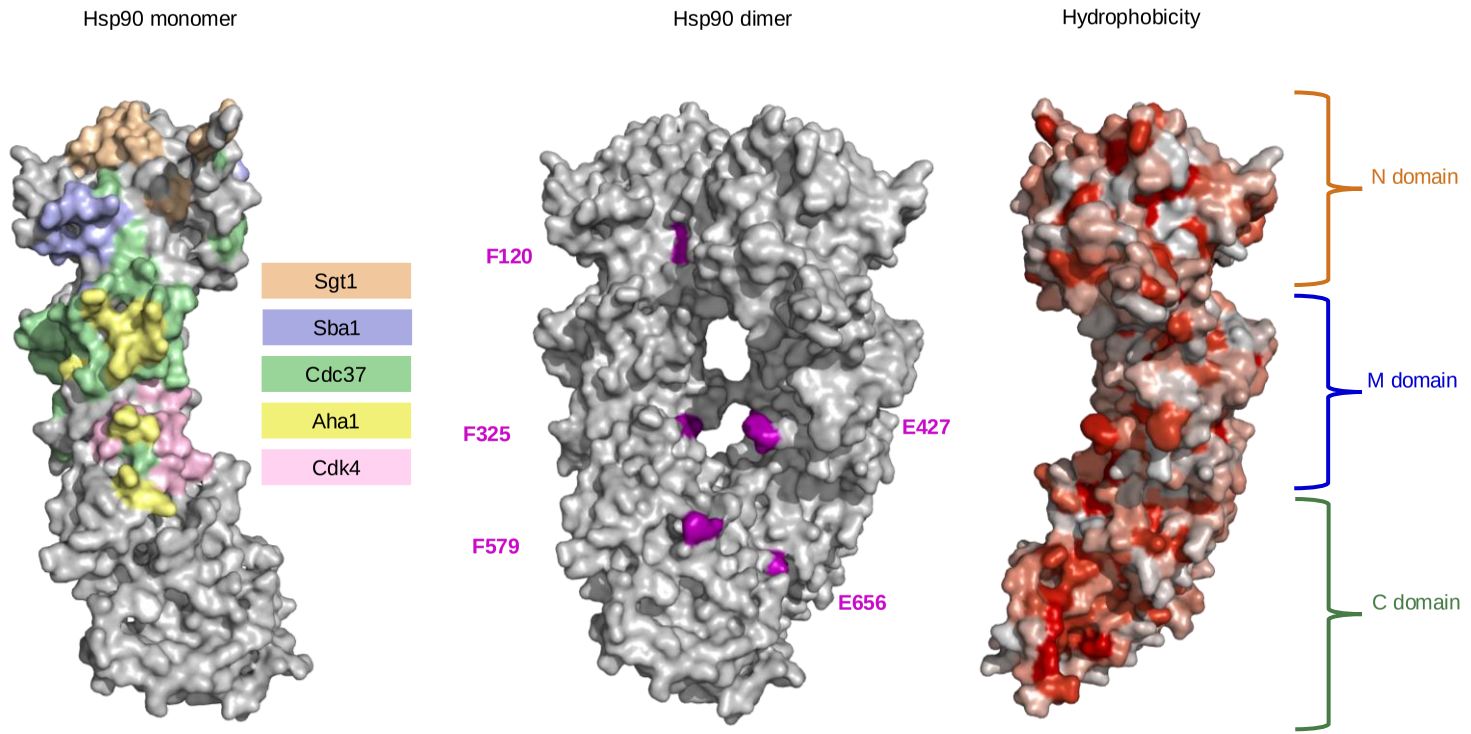

Figure 4. Selection of Bpa incorporation sites. Interaction interfaces (left structure) generated using Hs90-protein crystal structures for 4 Hsp90 co-chaperones and 1 client as well as the hydrophobicity plot of Hsp90 (right structure) were used to guide the selection of Bpa incorporation sites (middle structure). Sites of incorporation are labelled and highlighted in purple (Y24 is buried within the N-domain dimer and thus not highlighted). Domains of Hsp90 are indicated two the right in orange, blue and green.

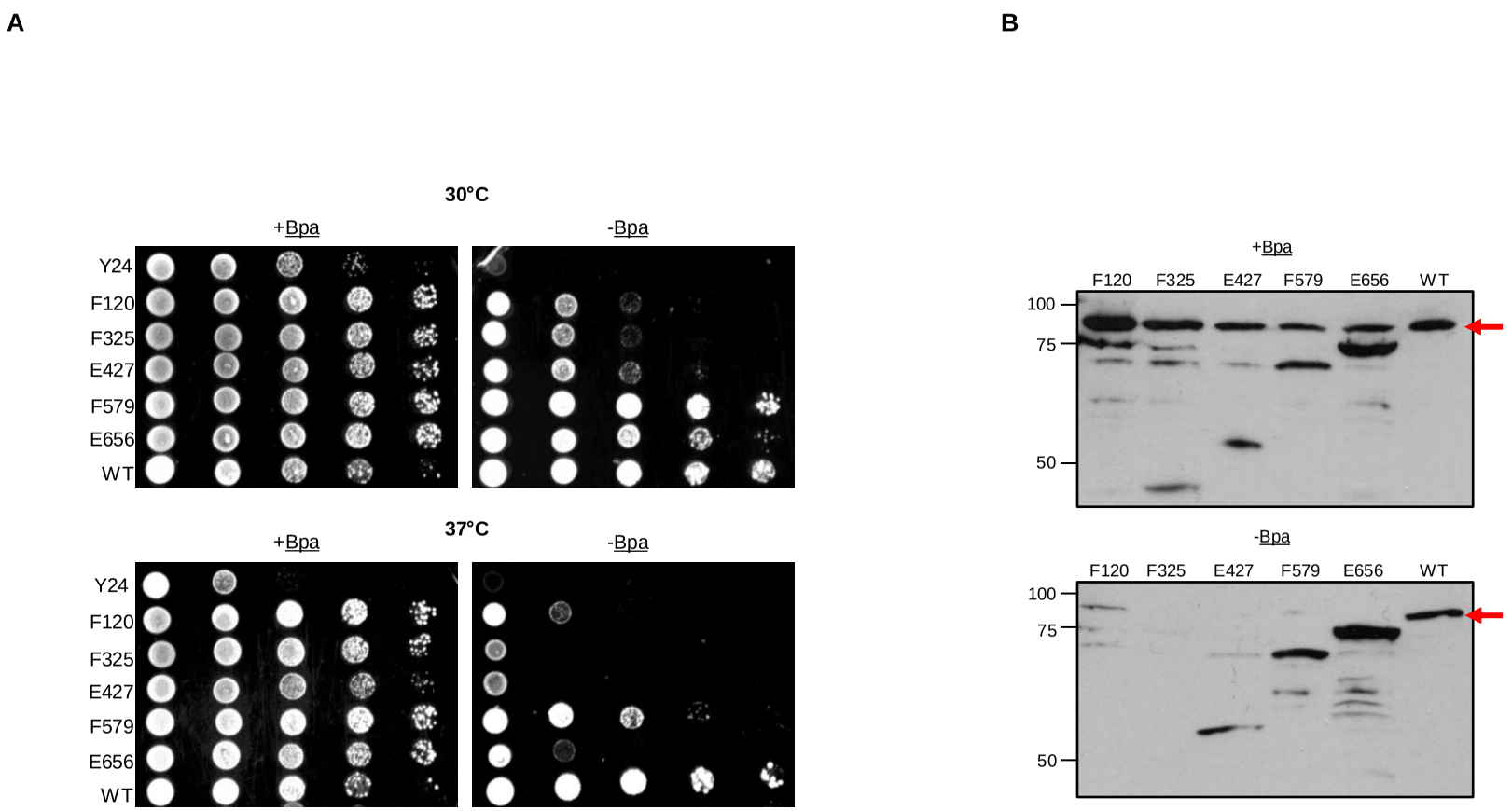

Figure 5. Validation of Hsp90-Bpa variant function. (A) Spot test assay performed with all Hsp90-Bpa variants (Y24,F120, F325, E427, F579, E656) in the presence and absence of Bpa at 30°C and 37°C. Absence of Bpa leads to reduced cell growth compared to cells harboring wild type Hsc82 (WT) which is exacerbated at 37°C. **(B)** Western blot analysis of Hsc82 production in the Hsp90-Bpa variant strains and WT. Blots were probed with anti-His antibody to capture full length as well as truncated forms of Hsp90.

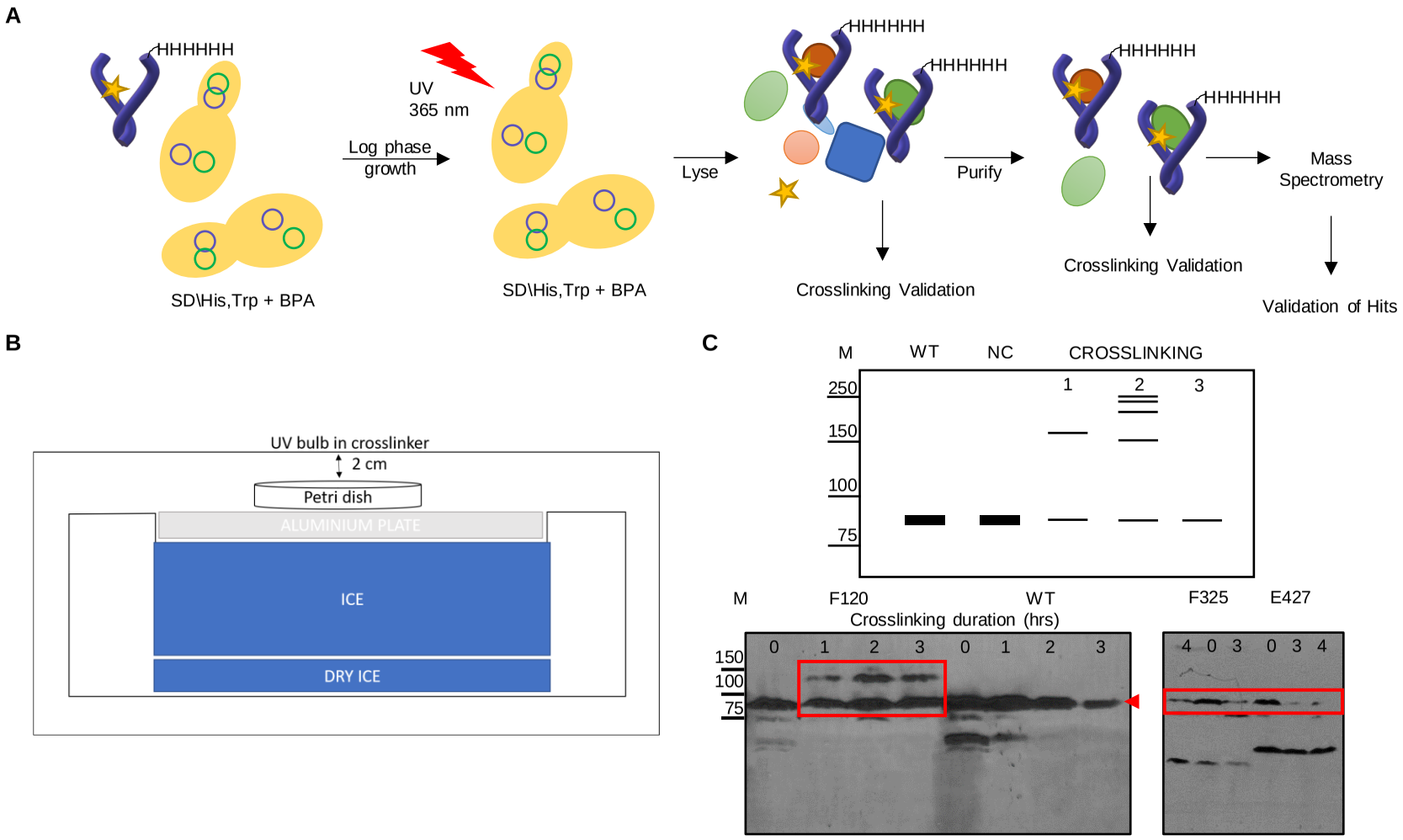

Figure 6. Overview of crosslinking protocol and validation strategy. (A) Schematic of approach – cells were grown to log phase and exposed to UV at 365 nm for various amounts of time. Crosslinking validation was attempted using whole cell extracts as well as after His-tag purification of the His-Hsc82.. **(B)** Schematic of crosslinking plate set up. **(C)** Schematic of expected results upon successful crosslinking (top) Crosslinking results obtained for 3 Hsp90-Bpa variants as analyzed by western blotting using an anti-His antibody. Appearance of higher molecular weight band with F120 and reduced levels of Hsp90 in F325 and E427 upon crosslinking (bottom).

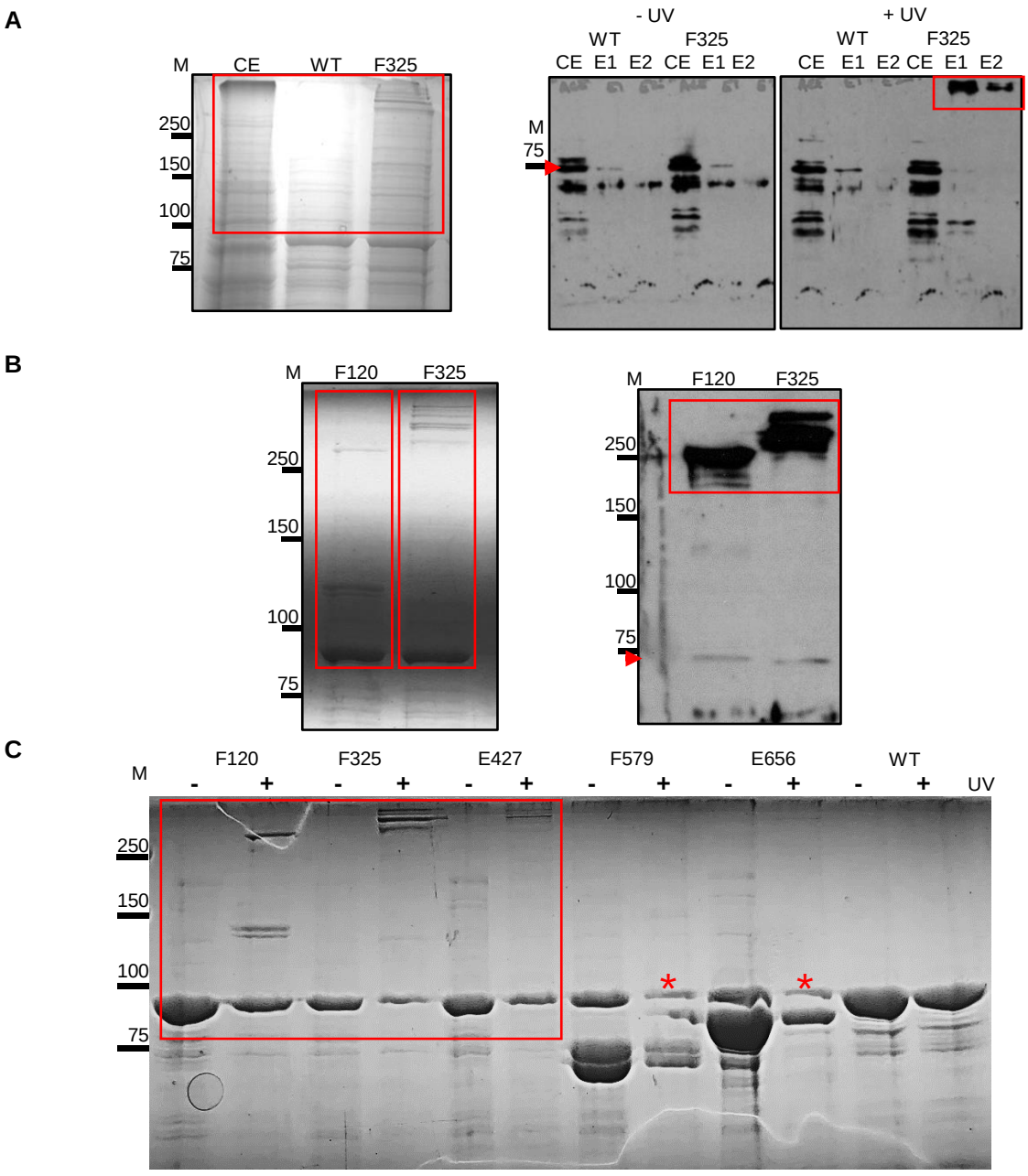

Figure 7. Preliminary crosslinking results. (A and B) Hsp90-Bpa variants F120 and F325 were crosslinked with WT as control. Hsp90-Bpa or WT was purified using His-tag affinity purification and eluants were resolved by SDS PAGE. Gel was stained with Coomassie (left panel) or taken further for western blot analysis (right panel) with an anti-Sti1 antibody. For Coomassie stained gels red rectangles highlight presences of higher molecular weight species in the Hsp90-Bpa variants that are absent in the WT control. In the western blot analysis, red arrowheads indicate Sti1 at it's expected molecular weight of ~75 kDa in the crude extract (CE) with red rectangles highlighting the shift of Sti1 in the eluants (E1 and E2) to ~250 kDa upon crosslinking to F120 and F325. **(C)** His tag purifications of all Hsp90-Bpa variants and WT with (-) and without (+) UV exposure were resolved on SDS PAGE and stained with Coomassie. Red rectangle highlights presence of higher molecular weight crosslinked species only upon UV exposure in F120, F325 and E427. For variants F579 and E656, while higher molecular weight species are hard to see, a reduction in Hsp90 levels (red asterisk) compared to non-crosslinked samples indicates successful crosslinking.

A

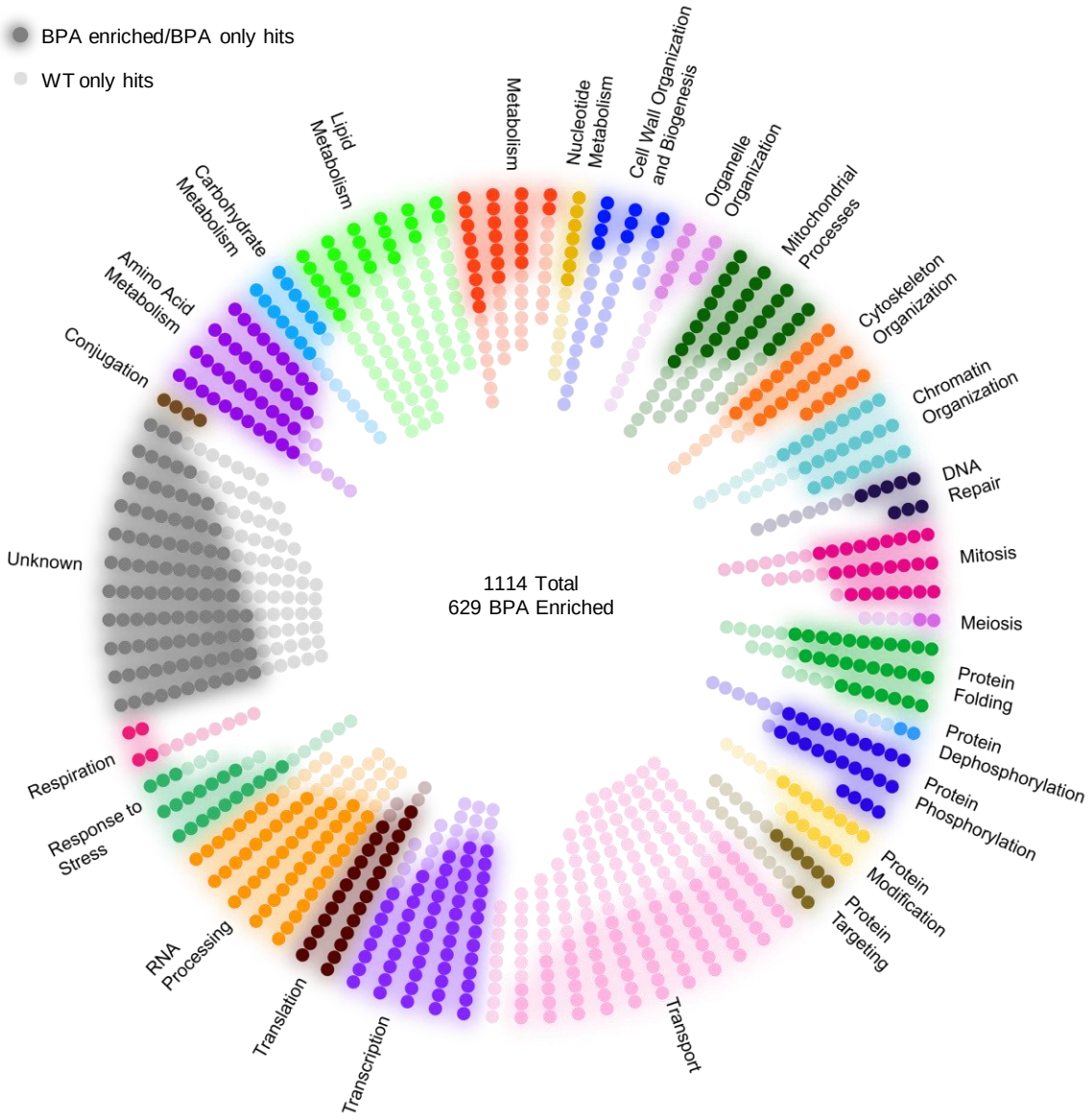

Figure 8. Establishing an Hsp90-Bpa Physical Interactome. (A) Bpa enriched and WT hits were categorized by GO Slim Analysis. Each hit was assigned to a n initial cellular process as displayed.

B

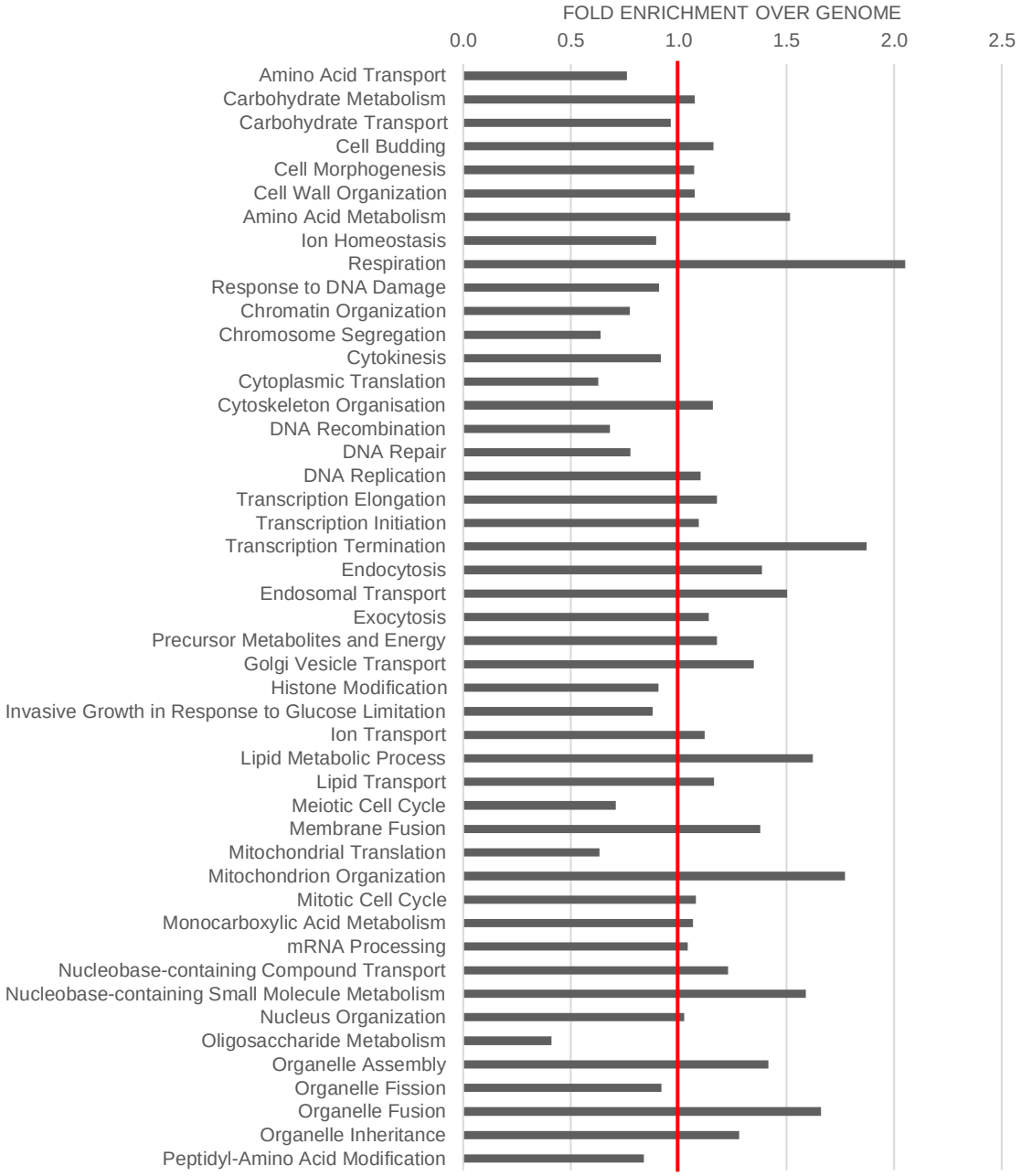

Figure 8. (cont.) (B) Bpa enriched and WT hits were categorized by GO Slim Analysis. All processes for each gene were considered and enrichments over all yeast ORFs (red line) were determined. First half of the generated list is presented here.

C

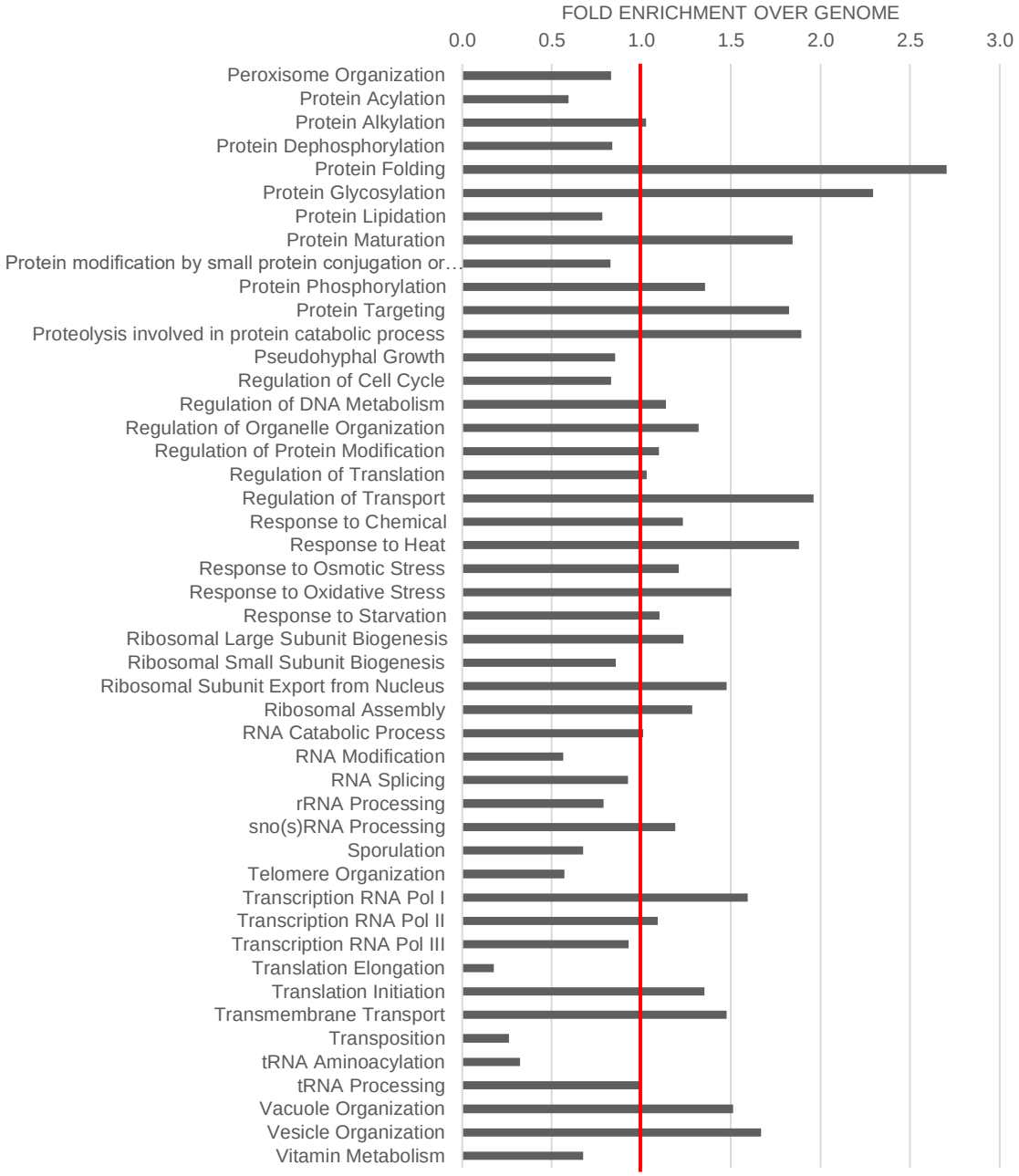

Figure 8. (cont.) (C) Bpa enriched and WT hits were categorized by GO Slim Analysis. All processes for each gene were considered and enrichments over all yeast ORFs (red line) were determined. Second half of the generated list is presented here.

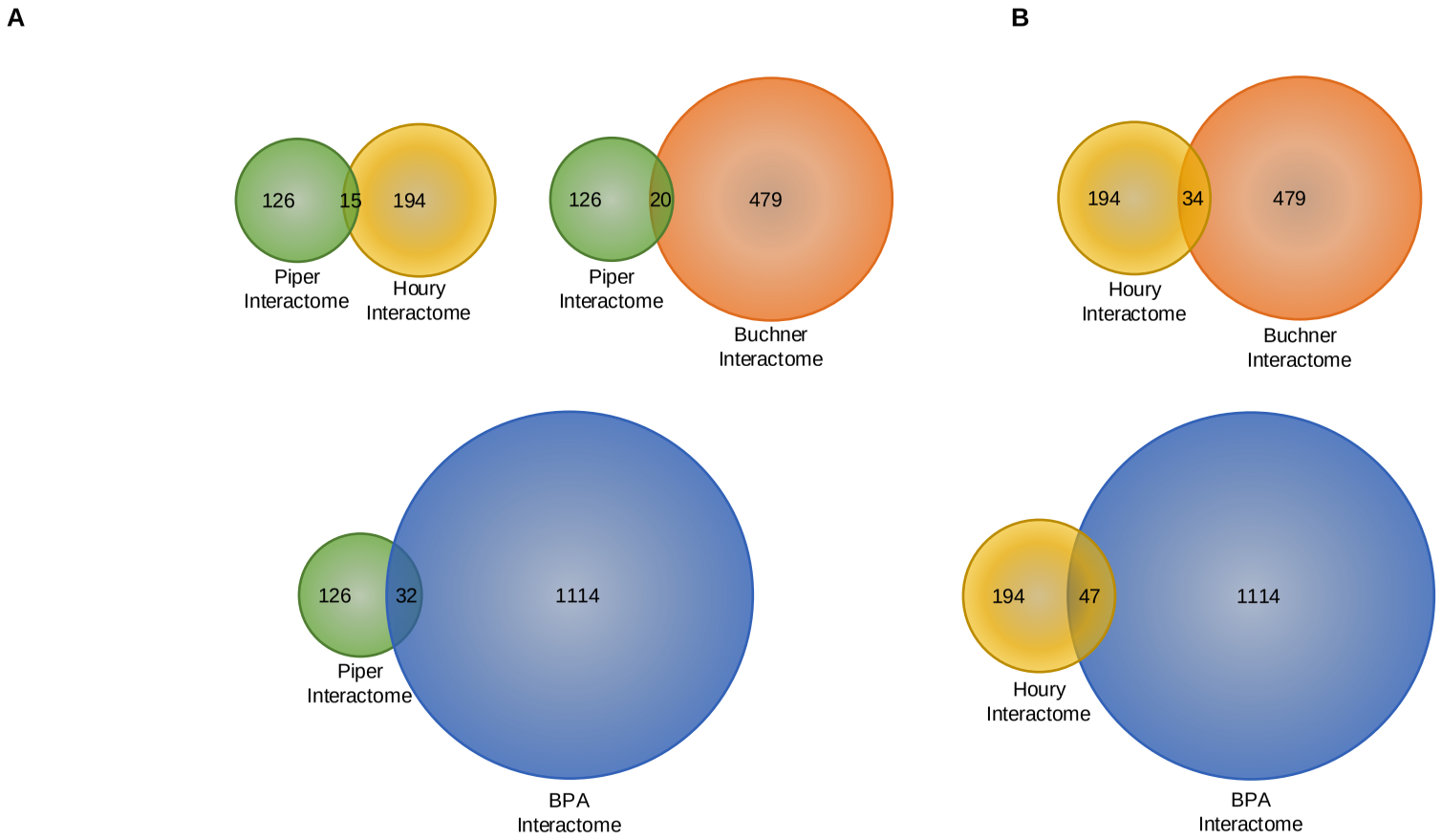

Figure 9. Overlap analysis of Hsp90-Bpa interactome with established Hsp90 interactomes. Overlap analysis of previously published Hsp90 interactomes with respect to **(A)** the original yeast Hsp90 interactome generated using yeast two hybrid from the Piper group and **(B)** the Hsp90 interactome generated using 4 different techniques by the Houry group. Comparisons were made in both cases with the Hsp90-Bpa interactome as well as another crosslinking based Hsp90 interactome established by the Buchner group.

C

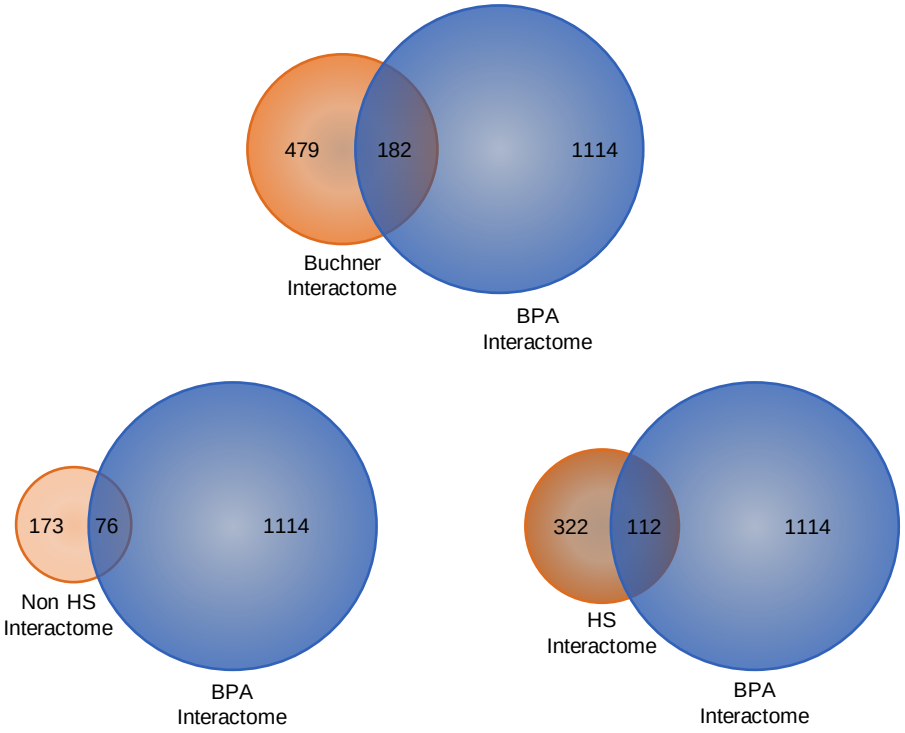

D

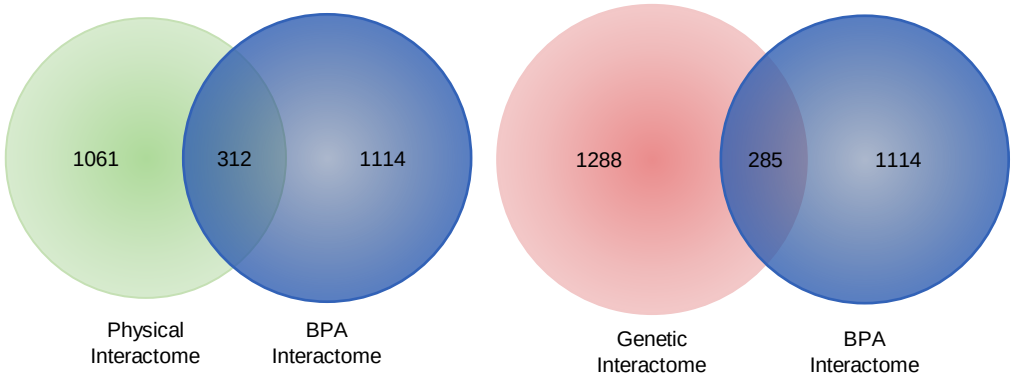

Figure 9. (cont.) (C) Overlap analysis between the Hsp90-Bpa crosslinking interactome and an Hsp90 interactome generated by the Buchner group using a non-specific crosslinker. Further comparisons with heat shock dependent and independent interactomes generated by the same group. **(D)** Comparison of the Hsp90-Bpa interactome with the complete physical (left) and genetic (right) Hsp90 interactomes as established by the Saccharomyces Genome Database.

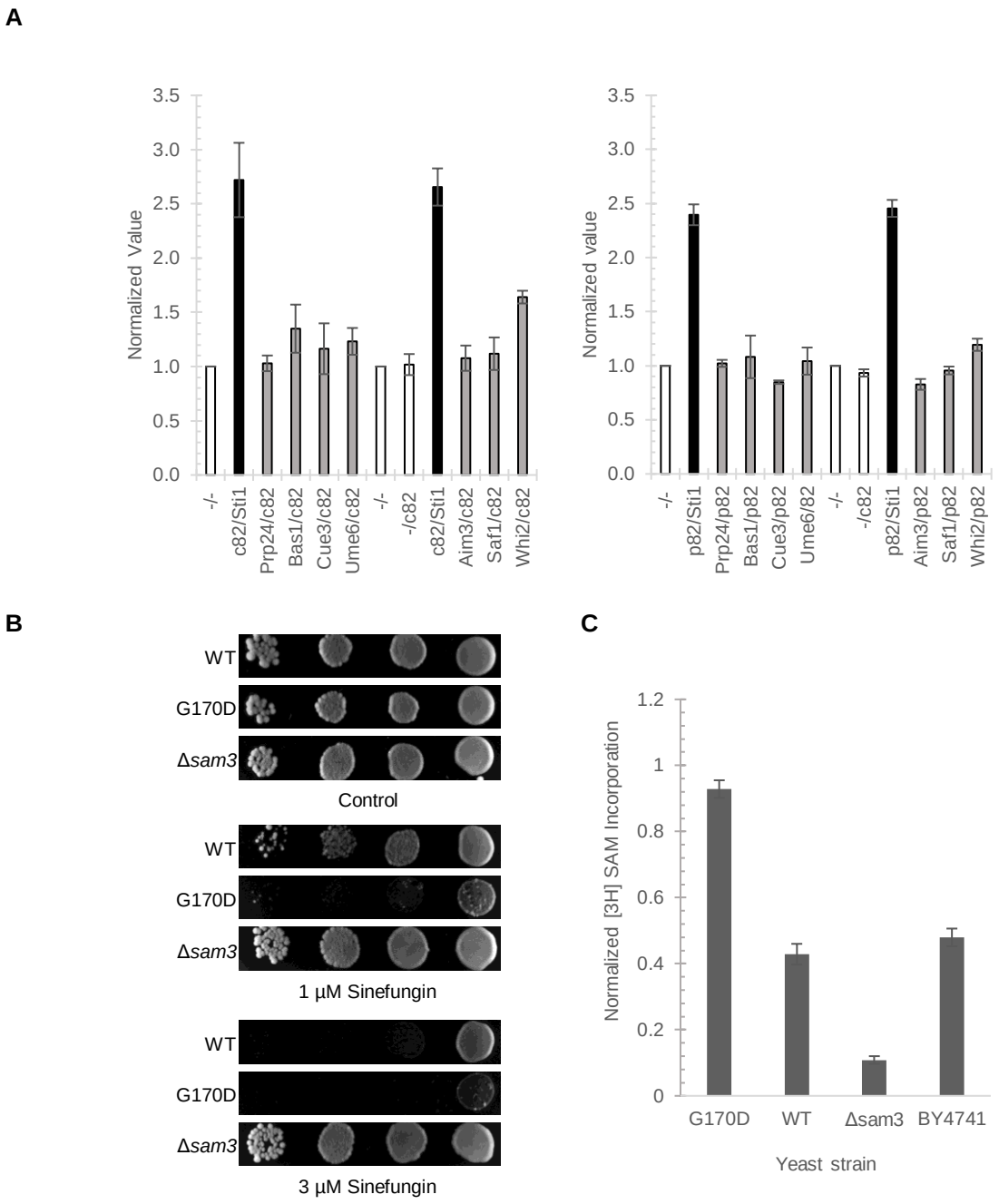

Figure 10. Validation of the Hsp90-Bpa interactome. (A) Yeast two hybrid analysis of 4 Bpa enriched hits (Prp24, Bas1, Cue3, Ume6) and 3 WT hits (Aim3, Saf1, Whi2) with Hsc82 or Hsp82 as bait and Sti1 as a positive control. Negative controls -/-, -/c82 and -/p82 indicated no bait or prey, and no prey with Hsc82 or Hsp82 as bait, respectively. **(B)** Sinefungin sensitivity spot test with WT, G170D and Δsam3 strains. **(C)** Sam3 permease activity as measured by [3H] SAM incorporation in WT, G170D, Δsam3 and BY4741 strains.

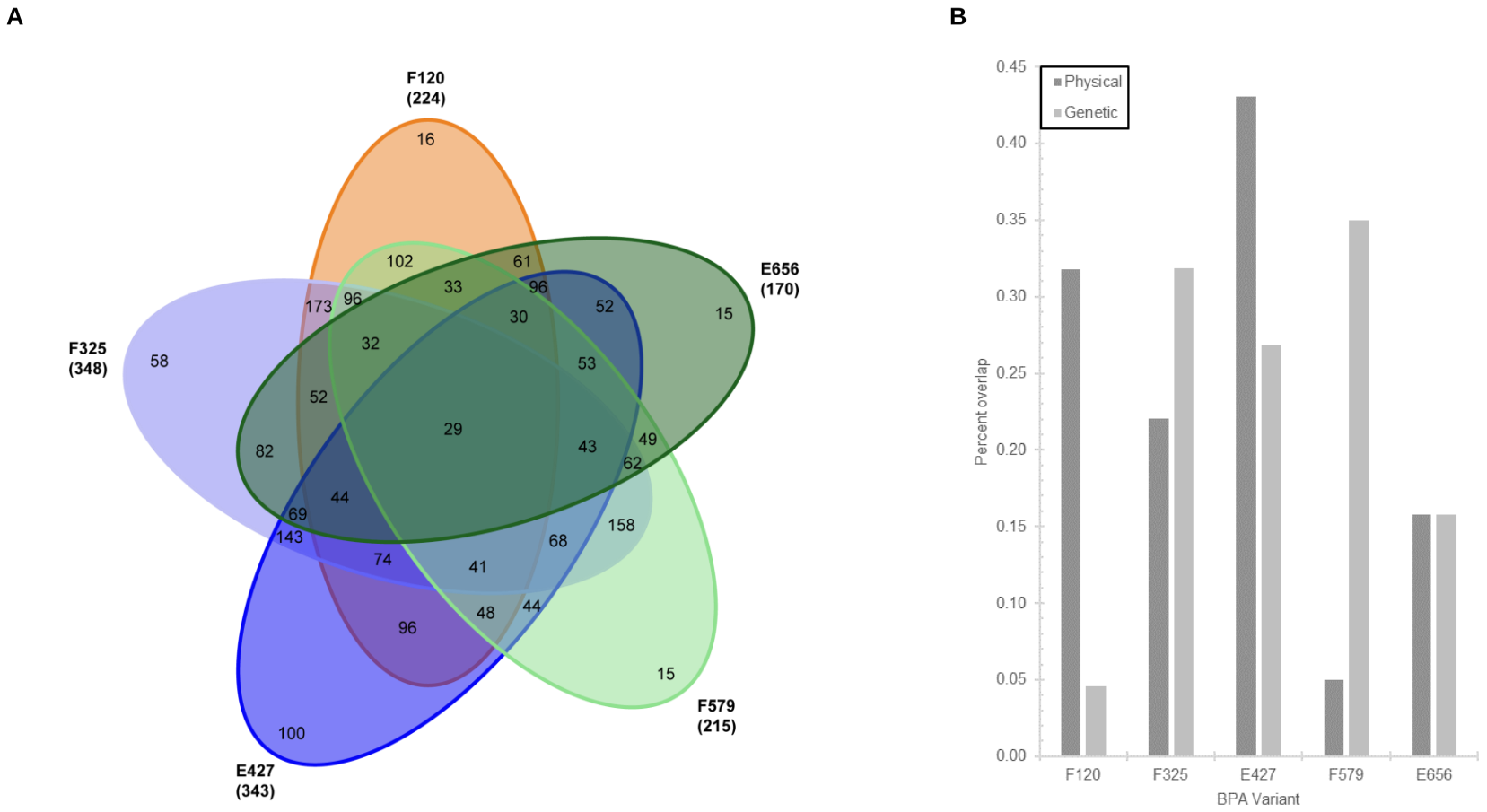

Figure 11. Physical interactors associate along the length of Hsp90. (A) Hsp90 hits enriched with each individual variant were compared to determine domain specificity. **(B)** Variant specific hits were compared to combined existing physical and genetic interactors of Hsc82 and Hsp82 from the Saccharomyces Genome Database.

A

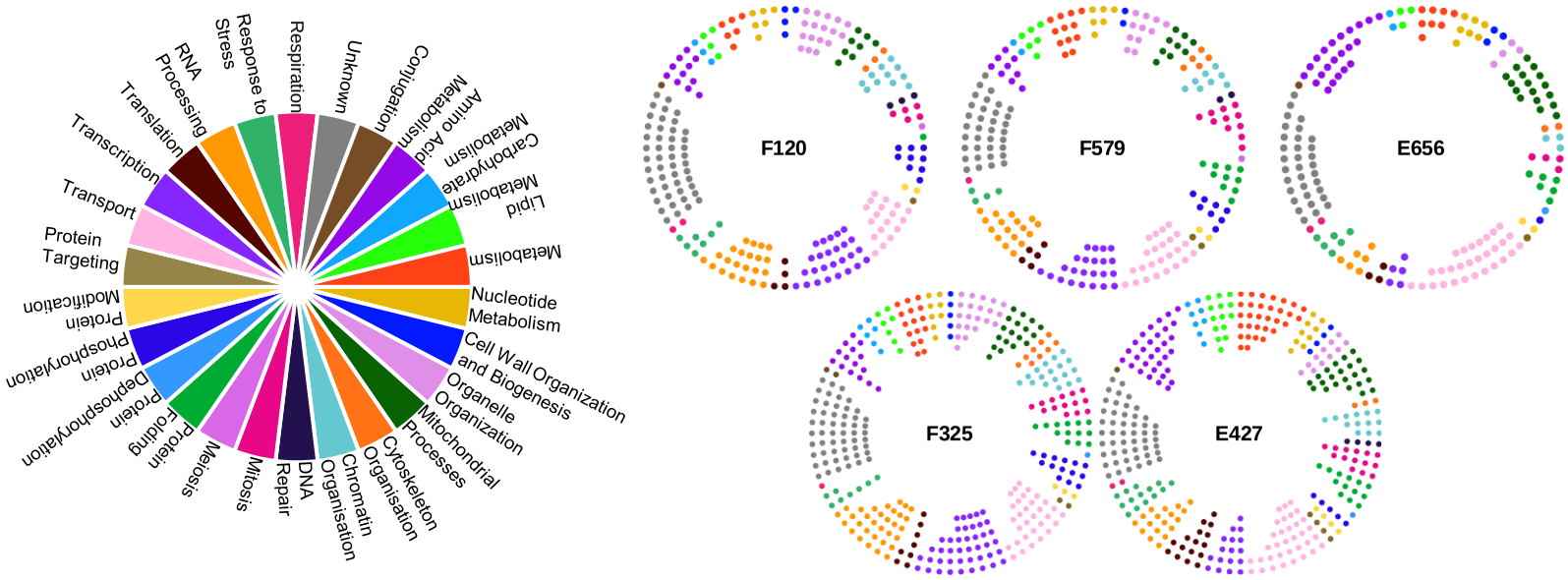

Figure 12. Differential use of Hsp90 domains in different pathways. (A) Hsp90-Bpa variant specific hits were cateforized by GO Slim Analysis and each hit was assigned to an initial cellular process as displayed (pin wheel to the left serves as a legend for the variant specific pin wheels).

B

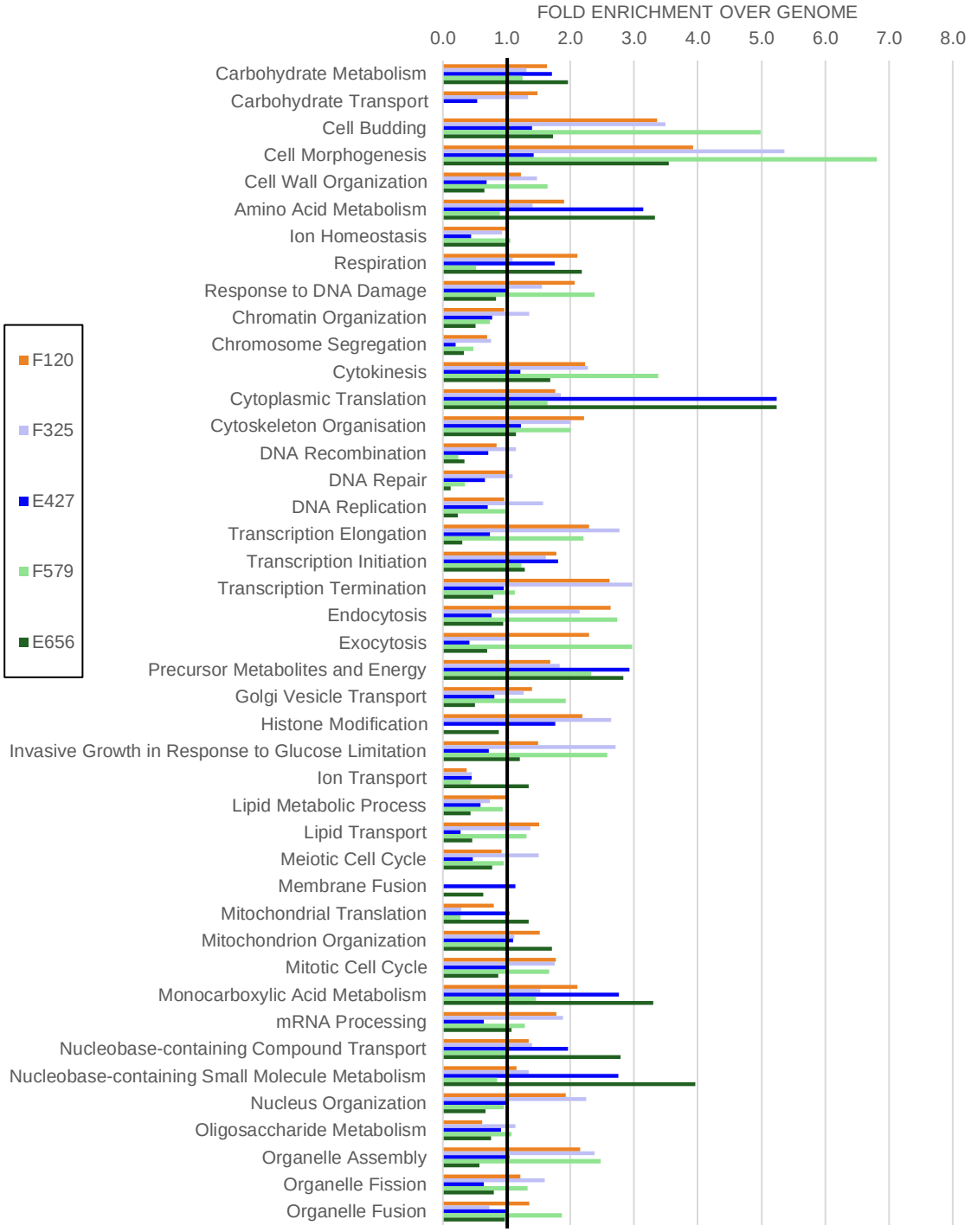

Figure 12. (cont.) (B) Hsp90-Bpa variant specific hits were categorized by GO Slim Analysis, all processes for each gene were considered and renrichments over all yeast ORFs were determined. First half of the generated list is presented here.

C

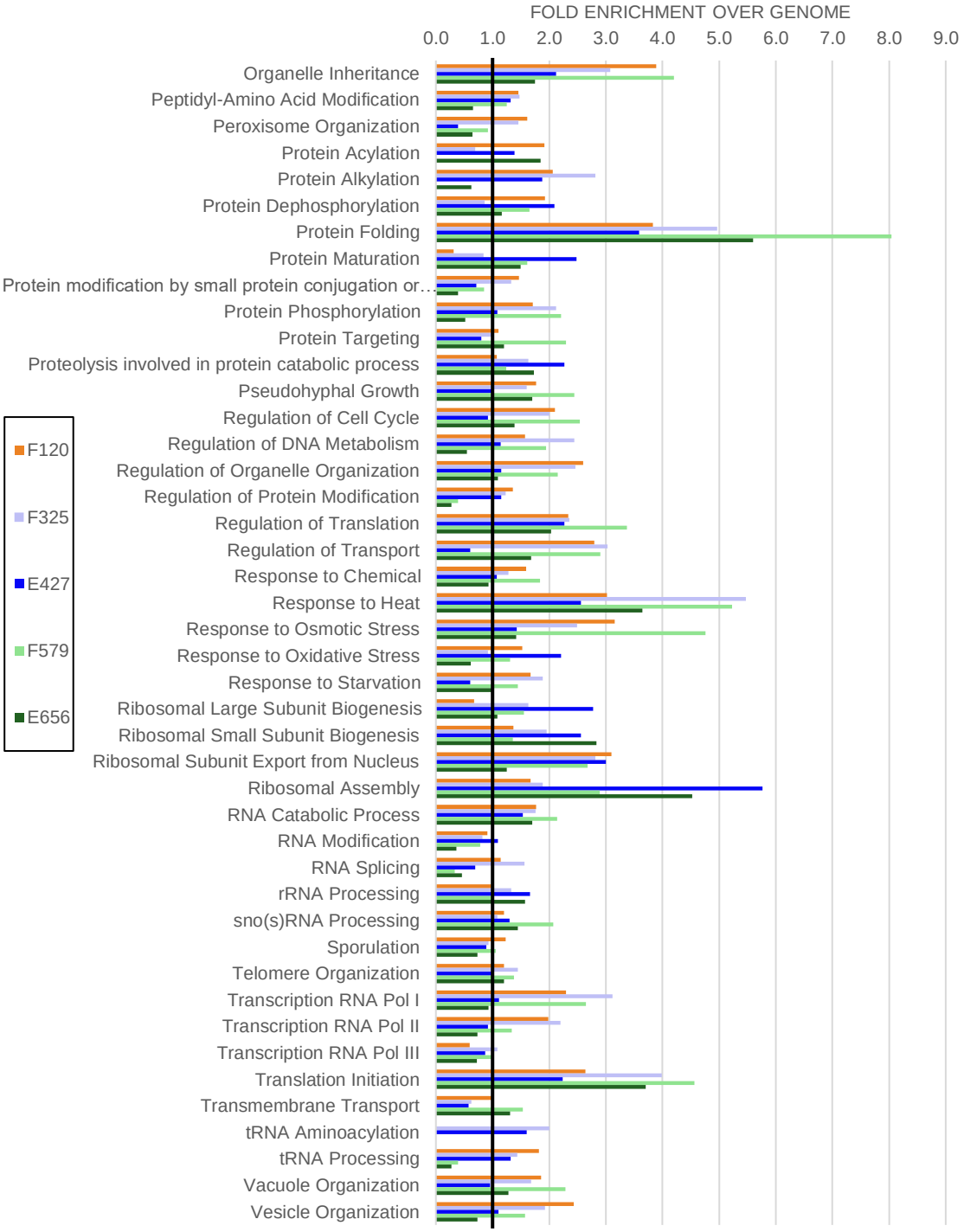

Figure 12. (cont.) (C) Hsp90-Bpa variant specific hits were categorized by GO Slim Analysis, all processes for each gene were considered and renrichments over all yeast ORFs were determined. Second half of the generated list is presented here.

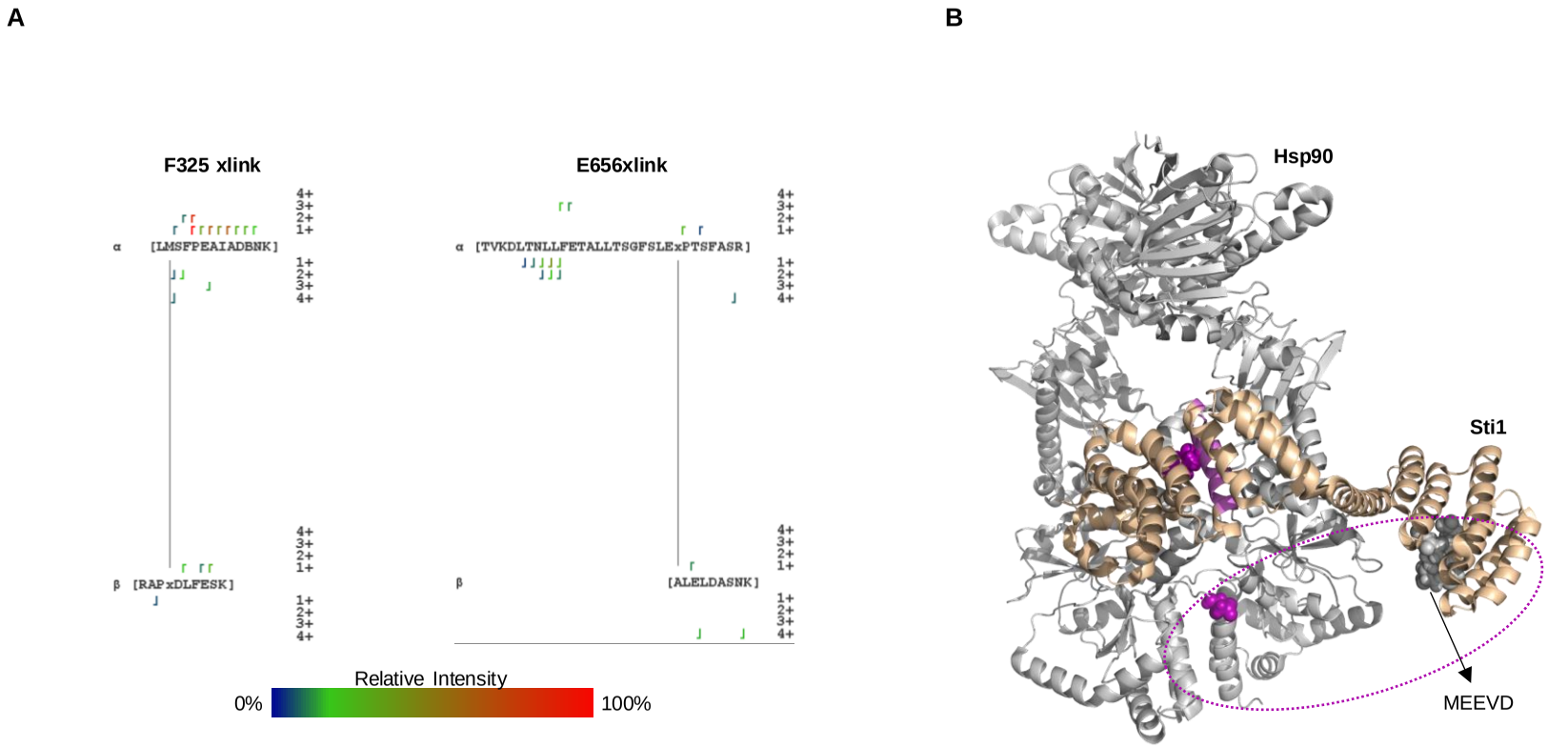

Figure 13. Hsp90-Sti1 crosslinks are in agreement with published crystal structures. (A) MeroX analysis of Hsp90-Bpa enriched hits identified two Sti1 corsslinks – one with F325 (F325 xlink) and the other with E656 (E656 xlink). **(B)** The rescently published crystal structure 7KW7 of Hsp90-Hop (mammalian Sti1) was used to highlight the crosslinked peptide within Sti1 (violet) and the corresponding Hsp90-Bpa incorporation sites (F325 and E656, violet and presented as spheres in the crystal structure).

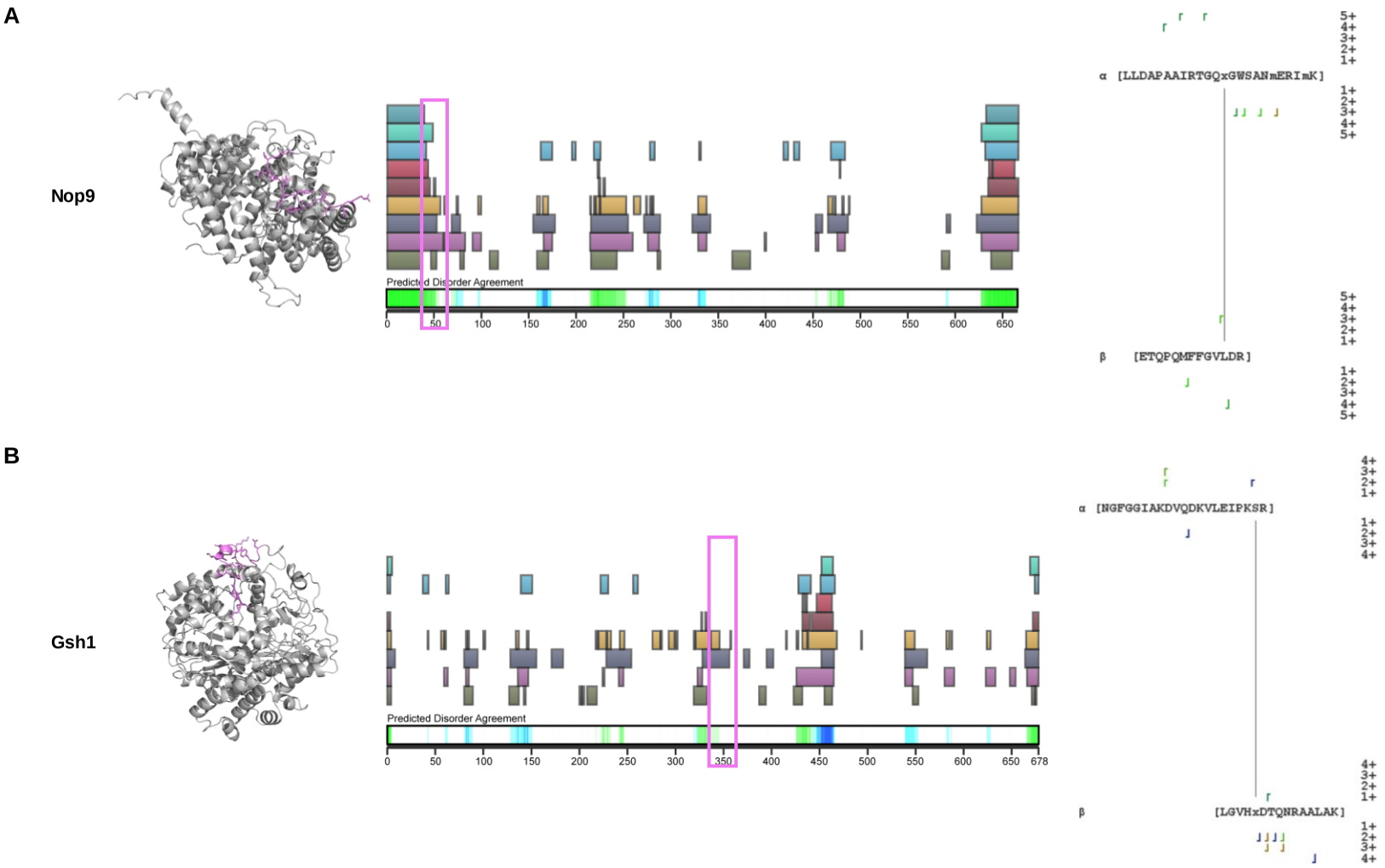

Figure 14. Hsp90 client interactions are enriched for IDRS. (A - D) Crosslinks identified for four different clients using MeroX are presented. For each client, the crosslinked peptide has been highlighted in the Alpha fold structure of the client in violet (left), in the D^2P^2 disorder plot the client using a violet rectangle (middle), and the crosslink itself from the MeroX interface has been presented (right).

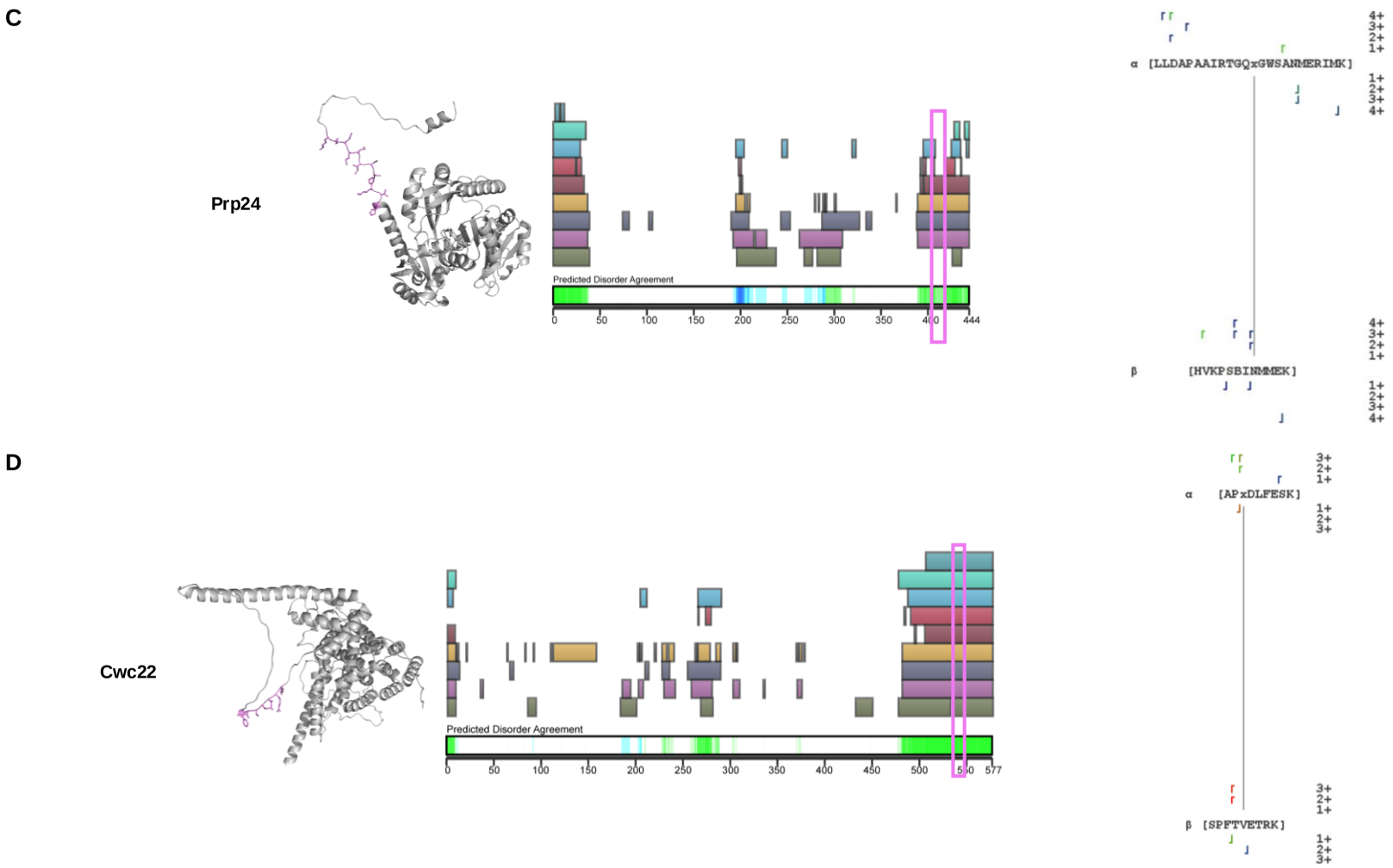

Figure 14. (cont.) (A - D) Crosslinks identified for four different clients using MeroX are presented. For each client, the crosslinked peptide has been highlighted in the Alpha fold structure of the client in violet (left), in the D^2P^2 disorder plot the client using a violet rectangle (middle), and the crosslink itself from the MeroX interface has been presented (right).

E

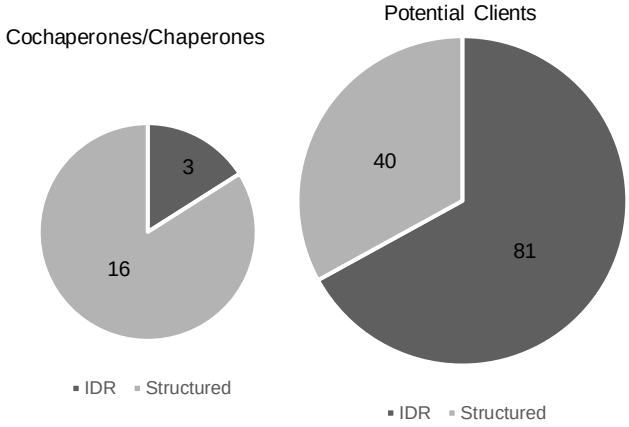

F

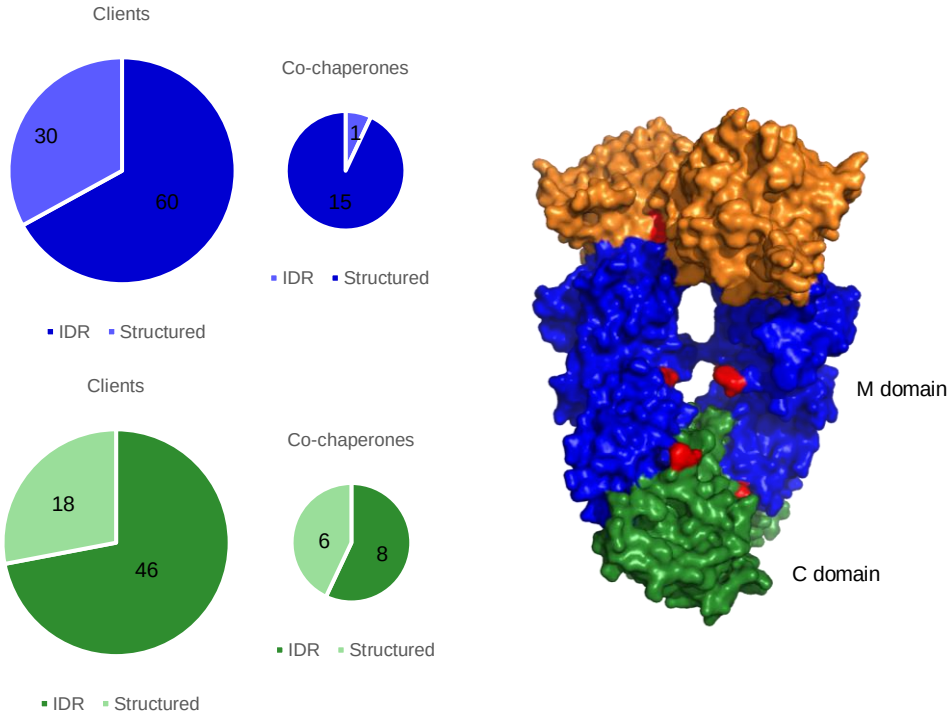

Figure 14. (cont.) (E) Crosslinked peptides identified using MeroX analysis were sorted into co-chaperone/client hits and determined to be either IDR or structured hits by comparison to the respective D^2P^2 plots. **(F)** Domain specific (blue – M domain, green – C domain) crosslinked peptides were analysed similar to (D) to determine domain specificity in IDR interaction.

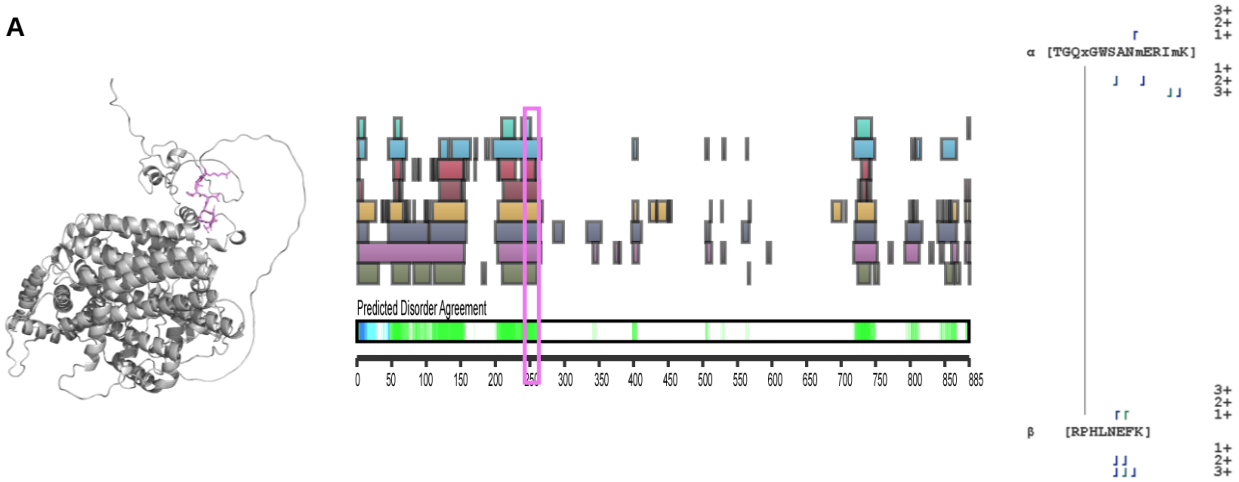

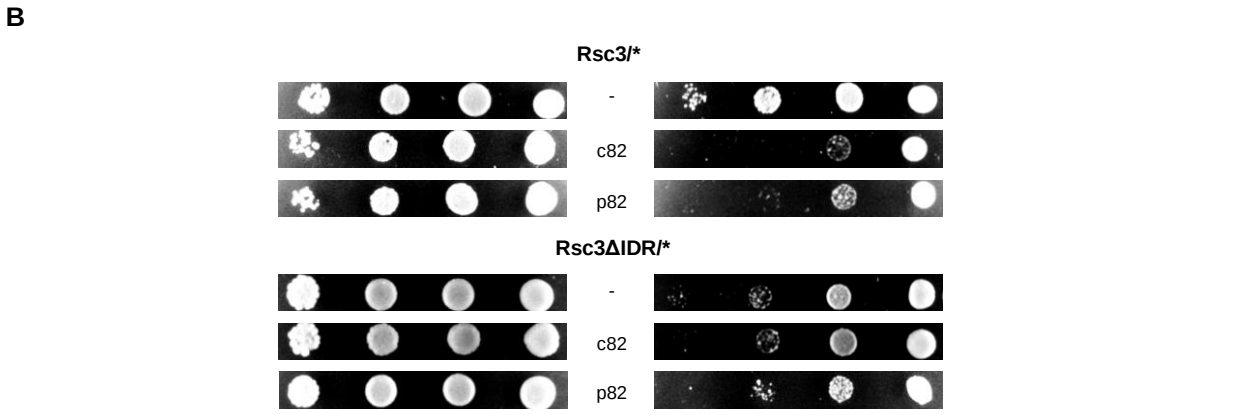

Figure 15. Hsp90 functionally affects clients through IDRs. (A) Crosslink identified for Hsp90 client Rsc3 is highlighted in the Alpha fold structure for Rsc3 in violet (left), in the D^2P^2 disorder plot of Rsc3 with a violet rectangle, and the crosslink itself from the MeroX interface is presented (right). **(B)** Rsc3 and Rsc3ΔIDR two hybrid assay was performed with Hsc82 or Hsp82 as bait.

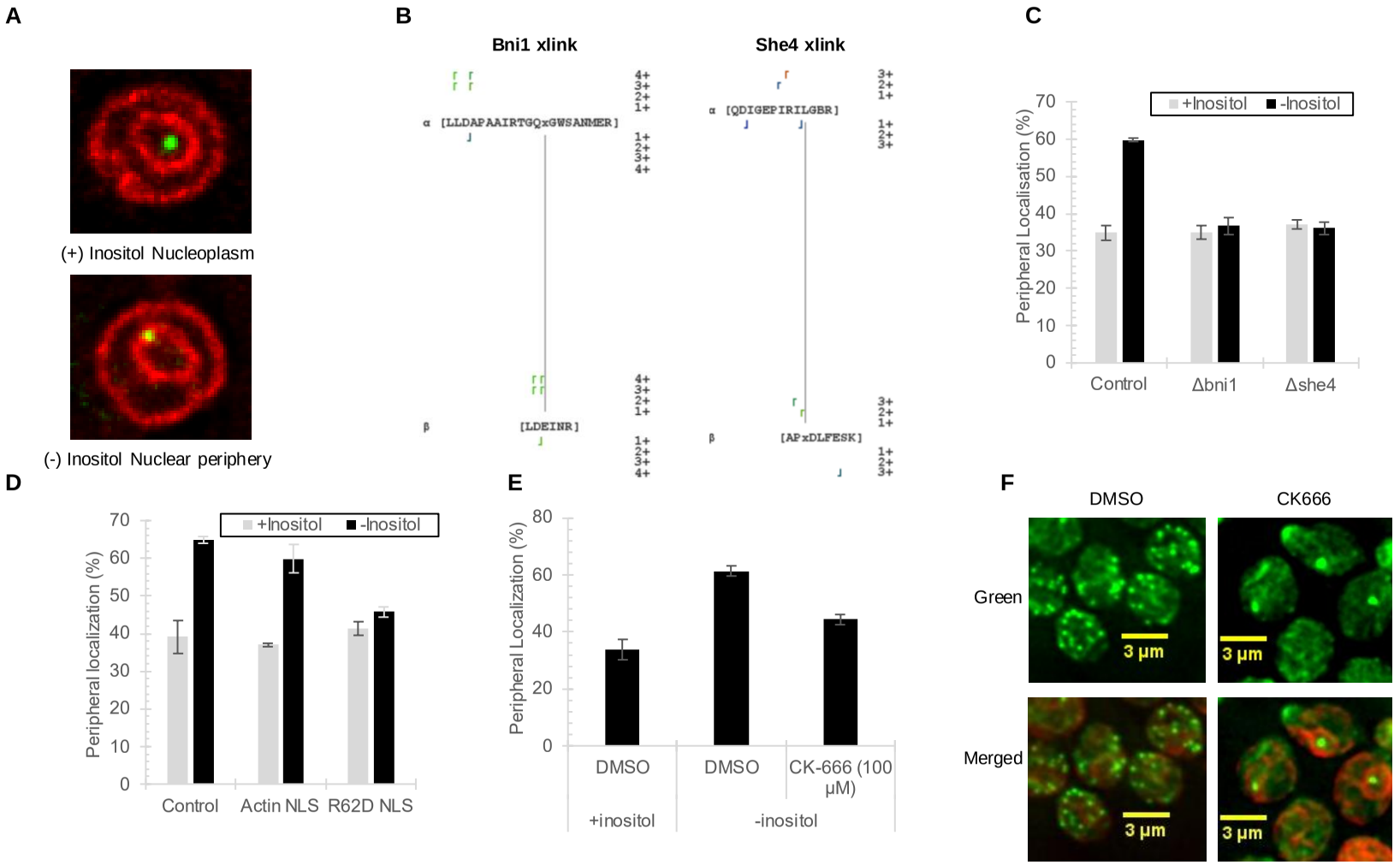

Figure 16. Functional validation of Hsp90-Bpa interactors in a novel Hsp90 associated pathway. (A) Yeast *INO1* locus chromosome motion system – membranes are tagged with an RFP membrane protein while the *INO1* locus is tagged with a GFP-LacI/LacO repeat system. **(B)** Crosslinked peptides identified for Bni1, an Hsp90 client and She4, an Hsp90 co-chaperone. **(C)** Quantification of *INO1* peripheral localisation in Δbni1 and Δshe4 strains. **(D)** *INO1* peripheral localisation upon over expression of WT or polymerisation deficient (R62D) actin in the nucleus. **(E)** *INO1* peripheral localisation upon inhibition of Arp2/3 complex using CK-666. **(F)** Phalloidin staining of yeast actin patches (green puncta) treated with and without CK66.

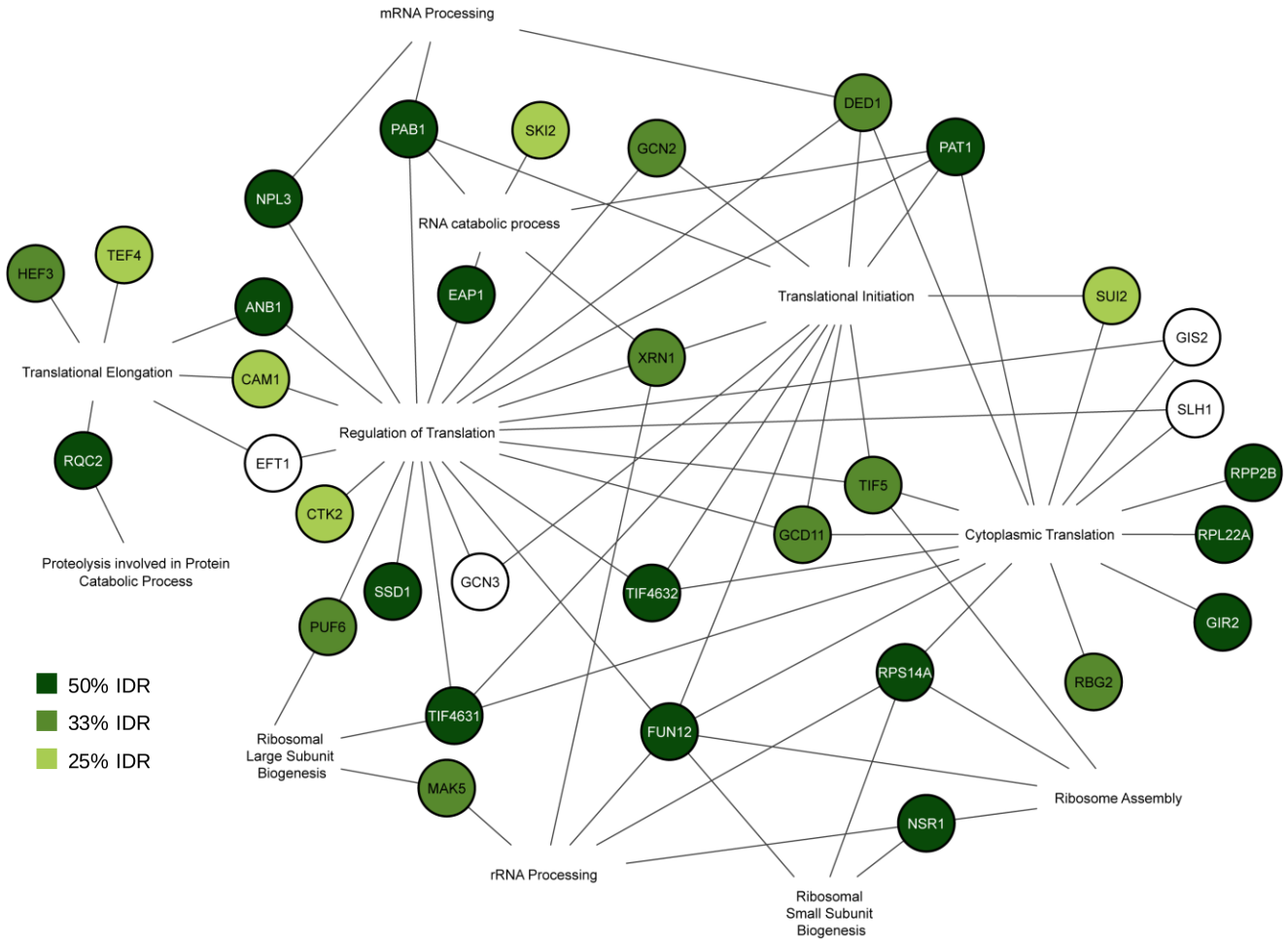

Figure 17. An IDR enriched Hsp90-dependent pathway. Hsp90-Bpa interactors in the translation pathway were analyzed for percentage of sequence within an IDR (50%, 33%, 25%) and cytoscape map generated was highlighted as marked.

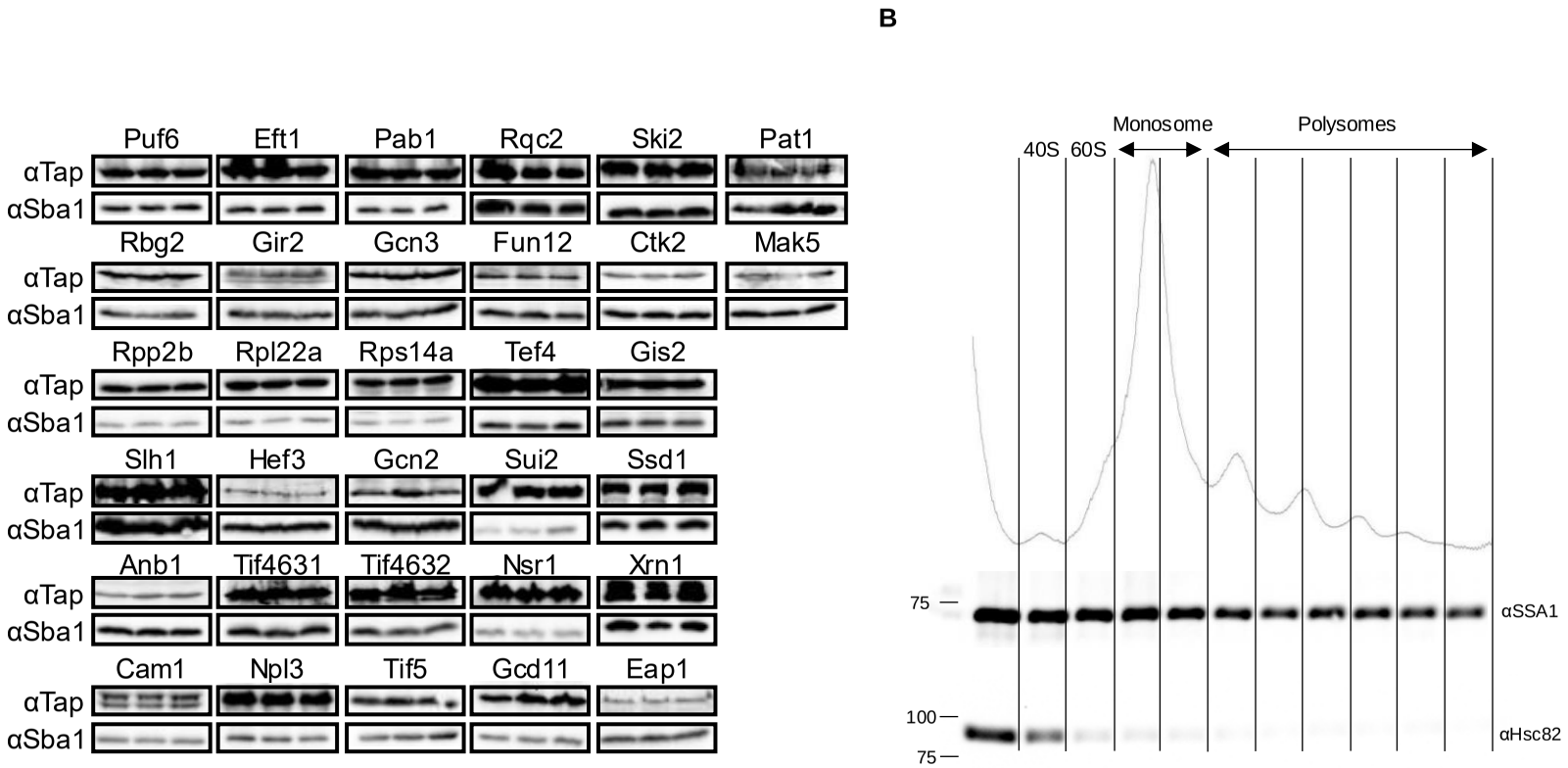

Figure 18. Hsp90 plays a multifaceted role in translation. (A) Stability analysis of Hsp90-Bpa associated translation factors upon exposure to Hsp90 inhibitor Radicicol (10 µM). For each protein blot, Sba1 was used as a loading control and protein levels were analyzed at 0/15/60 minutes, respectively. **(B)** Polysome fraction of WT yeast was assessed for presence of Hsp70 and Hsp90 across each fraction.

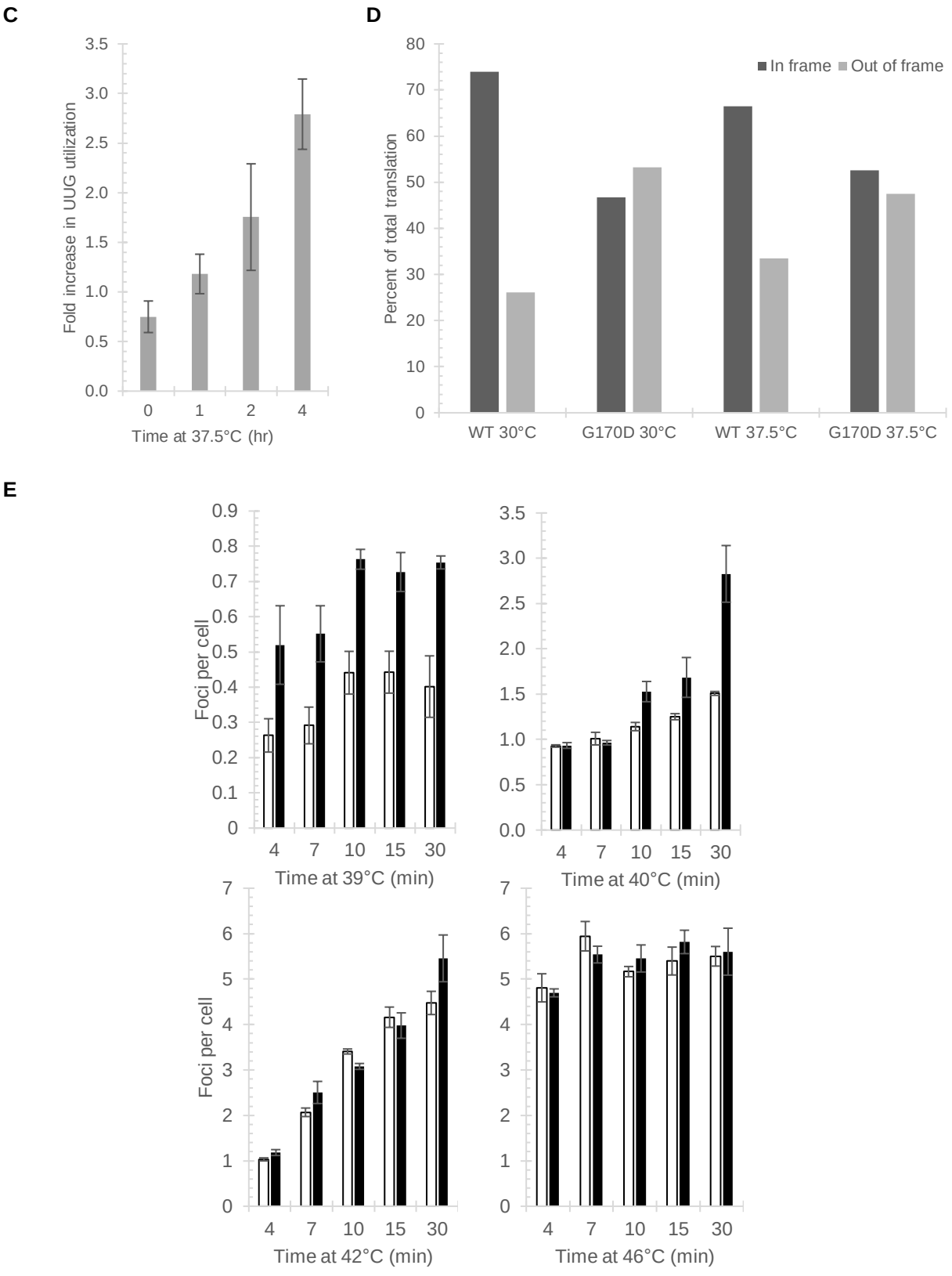

Figure 18. (cont.)

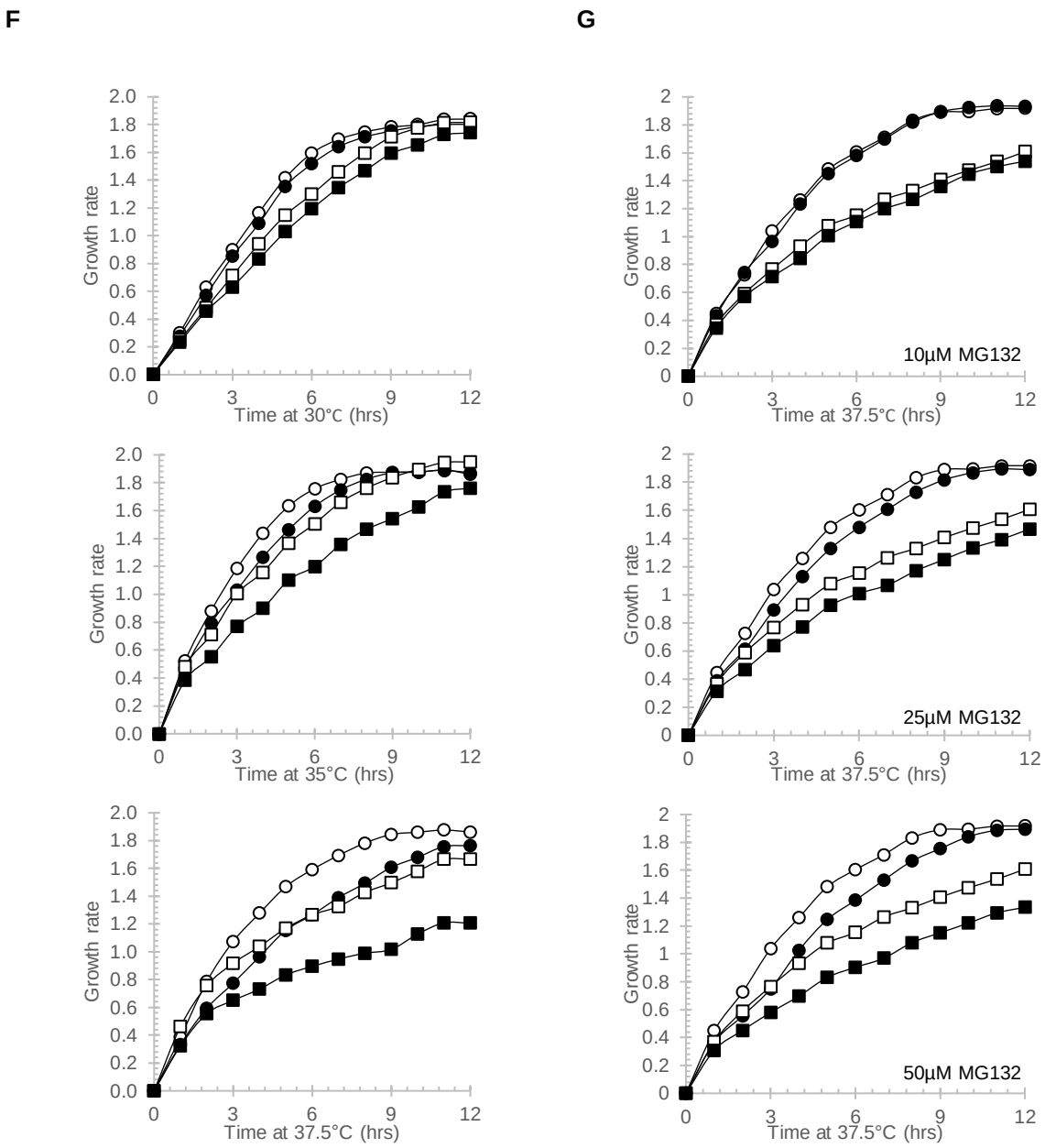

Figure 18. (cont.) (C) Dual luciferase assay to test fidelity of translation initiation in WT and G170D yeast strains. Data is presented as a fold change of G170D compared to WT. **(D)** RiboSeq analysis of translation frame in WT and G170D yeast strains at 30°C and 37.5°C for 15 min. **(E)** Stress granule formation in Ded1-GFP yeast upon exposure to 39°C/40°C/42°C/46°C in the presence (black bars) and absence (white bars) of 200 µM Radicicol. **(F)** MG132 (100 µM) sensitivity assay of WT and G170D cells at 30°C/35°C/37.5°C. **(G)** MG132 sensitivity assay of WT and G170D cells at 37.5°C for varying amounts of MG132 as indicated.

A

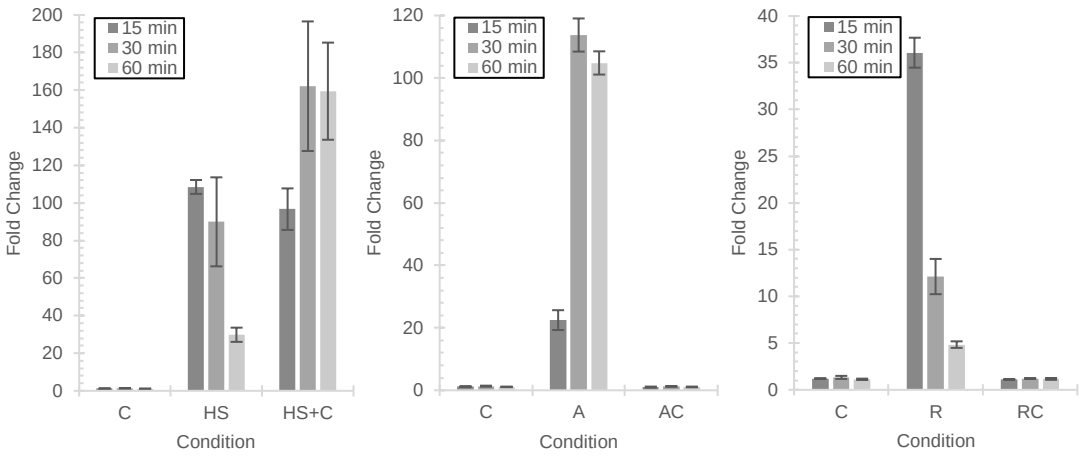

B

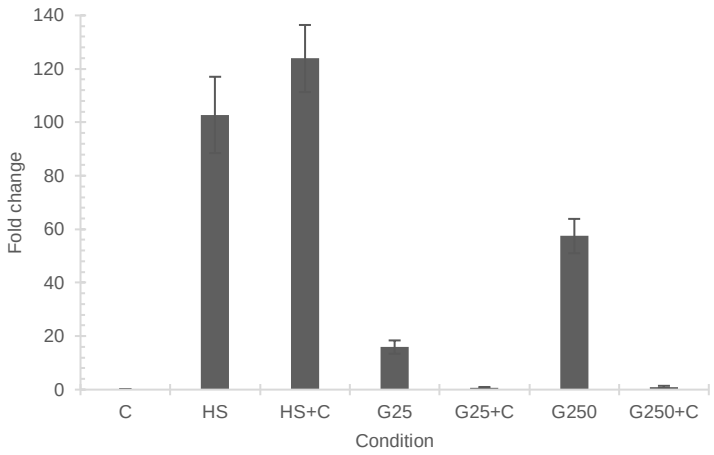

Figure 19. Physiological relevance of translation regulation by Hsp90 (A) qRT-PCR for stress inducible *SSA4* in yeast upon heat shock – HS (left panel), treatment with 20 µM azetidine-2-carboxylic acid – A (middle panel) or treatment 10 µM Radicicol – R (right panel), in the presence and absence of Cycloheximide – C. *TAF10* qRT PCR was used as an internal control and all values were normalized to respective DMSO controls. **(B)** qRT PCR for *HSP70* HeLa cells upon heat shock – HS, treatment with Hsp90 inhibitor Ganetespib at 25 nM – G25, or treatment with Ganetespib at 250 nM – G250, in the presence and absence of Cycloheximide – C.

Table 1: Bpa-dependent and -independent Hsp90 interactors

Bpa Only Hits	Bpa Enriched Hits	WT Hits
ACE2	AIM3	AAC1
ACF4	AIM36	ACS1
ACH1	ALD3	ADE12
ACK1	ANB1	ADR1
ADE3	APD1	AFG3
ADE6	ARC1	AGP1
ADH5	ARC18	AIM39
ADH6	AST1	AIM45
AEP1	ATP4	AIM46
AFG2	ATP7	ALG9
AHA1	BCY1	ALO1
AHP1	BDH2	ALT2
AIM14	BIK1	APM3
AIM19	BNA1	ARE1
AIM24	BNA2	ARE2
AIM25	BNI1	ART5
AIM32	BUR2	ASP1
AKL1	CAM1	AST2
ALD2	CAR1	ATG27
ALG5	CBR1	ATG9
ALR1	CDC37	ATP14
ALT1	CDC55	ATP20
ALY2	CDC73	ATP5
APA1	CHS3	AYR1
APE3	COX15	BAG7
APJ1	CPD1	BAP3
APL1	CPR6	BET3
ARC19	DBP3	BFR1
ARD1	DDP1	BIT61
ARG2	DYS1	BLM10
ARL1	EAP1	CAT5
ARO2	ENA2	CBP3
ARO3	ENO1	CBP4
ARO4	FRE1	CBP6
ARP8	FZF1	CCC1
ASE1	GIS2	CCS1
ATG13	GNP1	CCT6
ATG19	GUS1	CDC1
ATP1	HIS3	CDC53
ATP15	HSC82	CEX1
ATP16	HSP78	CFD1
ATP17	HYR1	CHO1
ATP2	IDH1	CKB1

Table 1 (cont.)

Bpa Only Hits	Bpa Enriched Hits	WT Hits
ATP3	IDH2	CLP1
AVT4	ITR1	CNB1
BAS1	KIN1	COQ1
BBC1	LIA1	COQ4
BCK2	LTE1	COQ9
BCP1	MAG2	COR1
BCS1	MCM4	COX11
BDH1	MCM6	COX12
BEM1	MCR1	COX20
BEM3	MDJ1	COX4
BIT2	MLC1	COX5A
BMH1	MNR2	COX6
BNA4	MPM1	COY1
BNA6	MRP1	CPA2
BOP3	NOP9	CPR4
BPL1	NPA3	CRM1
BPT1	NSG2	CSC1
BRE1	NTH2	CST26
BUD6	OCA6	CTF4
CBK1	OPI3	CTK2
CCA1	PAA1	CTR9
CCE1	PAD1	CUE4
CCT2	PDI1	CUE5
CCT3	PEX15	CWC21
CCT4	PIC2	CYB5
CCT8	PNC1	CYC2
CDC20	PPT1	CYC3
CDC48	PRR1	DAS2
CHO2	PRS4	DGA1
CHS2	PUF2	DGK1
CIA1	RHO5	DIA1
CIT2	RPA12	DLD1
CKB2	RPC10	DPL1
CMK2	RPN13	DPM1
CNS1	RPN2	DUG2
COG5	RRD2	ECM14
COX13	RTF1	ECM30
COX2	RTS1	EGD2
COX9	RTS3	EHT1
CPR3	SEC18	ELO2
CPR8	SEC8	EMC1
CST6	SHY1	EMC2
CTF18	SIS1	EMP24

Table 1 (cont.)

Bpa Only Hits	Bpa Enriched Hits	WT Hits
CTT1	SLM4	EMP47
CUE3	SSA1	EMP70
CWC22	SSA2	ENT5
CYS4	SSA3	EOS1
CYT1	SSA4	EPS1
DAS1	SSE1	ERG1
DAT1	SSM4	ERG11
DBP10	SSN8	ERG2
DBP5	STE50	ERG28
DCC1	STI1	ERG4
DCP1	STP4	ERG9
DED1	SYP1	ERJ5
DEP1	TFB1	ERP1
DIG1	TFB4	ERV2
DLD2	THG1	ERV29
DLD3	TIM9	ERV41
DRE2	TOM70	ERV46
DUG1	TRM82	FAA3
DSK2	TPS1	ETT1
DUR1,2	TRS33	FAA4
EAR1	TSA1	FBP26
ECM2	TY1A-MR1	FDC1
ECM29	TY1A-PR1	FKS3
ECM4	TY1B-MR1	FMP25
EDC3	TY1B-NL2	FRQ1
EFB1	TY2A-C	FRT1
EFT1	UBX4	FTR1
EGD1	UTR1	FUN12
ELP4	VAC7	FUN30
ELP6	WHI2	FYV8
ENO2	YBR053C	GAB1
ENP1	YDJ1	GAP1
ERG12	YGR250C	GAS1
ERG20	YHB1	GAS5
ERG26	YKR018C	GDA1
ESF1	YML131W	GDE1
ESS1	YMR155W	GET1
ETR1	YPL225W	GET2
FES1	YSC83	GGA2
FIS1	YTA12	GID7
FMP33	ZPR1	GIR2
FOL1		GMH1
FOL3		GPI11

Table 1 (cont.)

Bpa Only Hits	Bpa Enriched Hits	WT Hits
FPR3		GPT2
FPR4		GSC2
FSF1		GSF2
FSH3		GSY1
GAL11		GSY2
GCD11		GTR2
GCN3		GTT1
GDB1		GUT2
GEM1		GYP5
GFD1		HEM15
GIC2		HFD1
GLY1		HMG1
GNT1		HOC1
GPH1		HRD3
GRE1		HSV2
GRX5		HTA2
GRX7		HUL5
GSH1		HXT2
GTS1		HXT3
GUA1		HXT6
HAA1		HXT7
HAL5		IDP3
HAM1		IDS2
HAP2		ILM1
HAS1		IMP3
HBT1		IMP4
HEF3		IPI1
HEM14		IPI3
HCH1		INA17
HEM2		IRC22
HER1		IRR1
HGH1		ISC1
HIR1		KAP104
HIT1		KAP95
HLJ1		KEI1
HPA3		KIP3
HRT1		KRE2
HSF1		KRE6
HSP104		KTR1
HSP12		KTR3
HSP26		KTR4
HSP60		LAC1
HUA1		LAG1

Table 1 (cont.)

Bpa Only Hits	Bpa Enriched Hits	WT Hits
HXK1		LCB1
HXT5		LCB2
ICS2		LCB4
IDP1		LCB5
IKI1		LIP1
IKI3		LNP1
ILV3		LOS1
ILV5		LSM2
IRC21		MAK11
IRC7		MAP1
ISD11		MBP1
ISF1		MCD4
ISU1		MCM7
JAC1		MDL1
JJJ2		MDL2
JLP1		MDM1
KAP114		MDM10
KAR4		MDM38
KCS1		MED2
KEL1		MET3
KIC1		MET5
KIP2		MGR1
KOG1		MGR2
KSP1		MGR3
LCL3		MIC60
LHP1		MNN1
LHS1		MNN2
LIP5		MNN5
LOT6		MNT3
LRE1		MPC2
LSB3		MPD2
LSG1		MPP10
LSM1		MRD1
LSM3		MRH4
LSM4		MRS4
LSM7		MSC6
LSM8		MSC7
LYS12		MSN4
LSM6		MRX3
LYS20		MTG2
LYS9		MXR1
MAE1		NAB3
MAK5		NDE1

Table 1 (cont.)

Bpa Only Hits	Bpa Enriched Hits	WT Hits
MAM33		NDI1
MAS1		NOC2
MDJ2		NOP2
MDV1		NPR1
MEC1		NRD1
MED1		NUC1
MED4		NUP170
MET18		NUS1
MET22		NUT1
MET28		NYV1
MET31		OCA1
MEU1		OCA5
MEX67		OM45
MIC10		OMS1
MIC12		OSH6
MIR1		OSH7
MIT1		OSM1
MLF3		OST3
MMF1		PAC11
MOB2		PBN1
MRI1		PDC5
MRP17		PDR5
MRP49		PEP1
MRPL38		PEP4
MRPL50		PEX30
MRPL51		PGA2
MRPS16		PGA3
MRPS17		PGD1
MRPS8		PHO8
MRX12		PHO84
MRX6		PHO85
MRX9		PHO86
MSC3		PHO88
MSN1		PHO90
MSS116		PHO91
MSS51		PIM1
MTG1		PKP1
MTR2		PKR1
MUB1		PMR1
NAB2		PMT2
NAM9		PMT4
NAP1		PMT5
NAS6		PMU1

Table 1 (cont.)

Bpa Only Hits	Bpa Enriched Hits	WT Hits
NAT1		POM152
NBP35		POR1
NGL2		PPS1
NGR1		PRB1
NIP7		PRI2
NAT4		POM33
NMD5		PRM8
NNK1		PRP43
NOC3		PRS2
NOP1		PRS3
NOP15		PRS5
NOP53		PSD1
NPL3		PTC4
NRP1		PTH2
NSR1		PTK2
NTF2		PTM1
NUR1		PUB1
OAC1		PUF6
OCH1		PUN1
ODC1		QCR10
PAB1		QCR2
PAC10		QCR6
PAF1		QCR7
PAL1		QCR8
PAT1		RAD26
PCT1		RAS2
PDR17		RAX1
PDX3		RBG2
PEF1		RBL2
PEP3		RCF1
PET9		RCK2
PEX19		RER1
PFK26		RFC1
PHO2		RFC2
PIN4		RFC3
PIS1		RFC4
PLB3		RFC5
PMC1		RGD1
POM34		RGI1
PRE1		RHO1
PRE3		RIB4
PRE5		RIP1
PRE6		RIX1

Table 1 (cont.)

Bpa Only Hits	Bpa Enriched Hits	WT Hits
PRE7		RMD5
PRE8		RMD8
PRE9		RNH1
PRI1		RNR1
PRK1		RNR3
PRO1		RPA34
PRO2		RPA43
PRP18		RPN12
PRP24		RPN6
PRP4		RPN8
PST2		RSF1
PTC2		RSM25
PUP2		RSN1
PUP3		RVS161
PUT3		SAC1
PRX1		RRB1
PWP1		SAC6
RAD3		SAF1
RAD51		SAL1
RAI1		SAM3
RAT1		SAM37
RCF2		SAR1
RCM1		SBH1
RCO1		SCJ1
RDH54		SCS2
RDL1		SDH2
RDS3		SDH4
REB1		SEC1
REE1		SEC12
REP1		SEC17
REV1		SEC4
RGA2		SEC61
RHB1		SEC62
RIC1		SEC63
RIM2		SEC66
RIM4		SEC72
RIO1		SEY1
RMD1		SFA1
RNA1		SFT2
ROK1		SGD1
RPA49		SIP3
RPL22A		SKG3
RPN1		SLM1

Table 1 (cont.)

Bpa Only Hits	Bpa Enriched Hits	WT Hits
RPN10		SLM2
RPN7		SMF3
RPP2B		SNA2
RPS12		SNA3
RPS14A		SNL1
RPT1		SNX4
RPT5		SNX41
RQC2		SPB4
RRG7		SPC3
RSC3		SPF1
RSC30		SRB5
RSM26		SRB8
RSP5		SRF1
RTN2		SRL3
RTT101		SRP101
RTT103		SRP102
RXT2		SSB1
SAC3		SSB2
SAM50		SSN2
SAY1		SSP120
SBA1		SSP2
SCD5		SSS1
SCW10		STE13
SDS24		STE14
SEC11		STE18
SAP185		SSO1
SEC16		STE24
SEC23		STT3
SEC24		STT4
SEC26		SUR2
SEG2		SUR7
SER3		SVP26
SFB2		SWH1
SFL1		SXM1
SGN1		TAF1
SGT1		TAM41
SGT2		TCB2
SHE1		TED1
SHE3		TGL1
SHE4		TGL5
SHS1		TIM11
SIL1		TIM21
SIM1;SUN4		TIM22

Table 1 (cont.)

Bpa Only Hits	Bpa Enriched Hits	WT Hits
SKI2		TIM50
SKN7		TMN3
SLC1		TOM20
SLH1		TOM40
SLU7		TOM5
SMD1		TOM6
SMY1		TOM7
SNF5		TOS1
SNO1		TPD3
SNX3		TPK1
SNZ2		TPN1
SNZ2;SNZ3		TPO3
SOL2		TRS31
SPC29		TSC13
SPT15		TSC3
SPT5		TUM1
SRM1		TUS1
SRP14		TY1B-DR3
SRY1		TY1B-NL1
SSD1		TY2A-DR2
SSE2		TY2B-DR3
SSP1		TY2B-LR1
SST2		UBC7
STB3		UBP1
STE11		UBP11
STF2		UBP15
SUI2		UBP5
SWI6		UBP9
TAF5		URA2
TBF1		UTP15
TCB1		VAC8
TCO89		VAN1
TDA11		VIP1
TDH1		VMA13
TEF4		VPS21
SWP1		UBX2
TFB2		VPS27
TGL4		VPS34
THI80		VPS35
THP1		VPS45
TIF4631		VTC1
TIF4632		VTC2
TIF5		VTC3

Table 1 (cont.)

Bpa Only Hits	Bpa Enriched Hits	WT Hits
TMA10		VTC4
TOA2		WBP1
TOM71		XDJ1
TOR1		YBL029C-A
TRP1		YBR287W
TRR1		YBT1
TRS23		YCF1
TUB4		YCK3
TVP18		YCL042W
TY1B-ML1		YCP4
TY4B-J		YCR043C
UBC4		YDL121C
UBP7		YDR089W
UFD1		YDR132C
UGO1		YDR179W-A
UME6		YDR476C
UNG1		YER134C
URA5		YET1
URB2		YET3
URE2		YGR054W
UTH1		YHR177W
UTP30		YIL156W-B
VHS2		YJL016W
VID28		YJL171C
VPS29		YJU3
VPS52		YKL063C
VRP1		YKL075C
WWM1		YLR149C
XRN1		YLR225C
YAK1		YME1
YBL028C		YML020W
YCK1		YMR099C
YCR102C		YMR102C
YCS4		YMR209C
YDL144C		YMR265C
YDL218W		YNL011C
YDR119W-A		YNL181W
YDR248C		YNL320W
YDR391C		YNR021W
YDR461C-A		YOR385W
YFR045W		YOS1
YGL010W		YPL199C
YGL039W		YPP1

Table 1 (cont.)

Bpa Only Hits	Bpa Enriched Hits	WT Hits
YHR033W		YPR010C-A
YHR122W		YPR063C
YDR186C		YNL234W
YIL055C		YPR091C
YJL070C		YPR147C
YJR008W		YPT11
YJR085C		YPT52
YKL033W-A		YPT7
YKL151C		YRB1
YKR023W		YRO2
YLR108C		YVH1
YLR118C		ZEO1
YLR345W		
YMC2		
YML018C		
YMR111C		
YMR124W		
YNL131W		
YNL134C		
YNR068C		
YOL098C		
YOR131C		
YPK1		
YPL168W		
YPL247C		
YPR174C		
YRA2		
YRF1-6		
ZIM17		
ZWF1		

Table 2: Bpa site specific capture of Hsp90 interactors

F120	F325	E427	F579	E656
ACE2	ACE2	ACH1	ACF4	ACH1
ACF4	ACF4	ADE3	ADE6	ADH5
ADH5	ACK1	ADE6	ADH5	AHA1
AIM14	ADE6	ADH5	AEP1	AHP1
AIM3	ADH5	ADH6	AHA1	AIM14
AIM32	AHA1	AFG2	AIM3	AIM19
ALD3	AIM24	AHA1	AIM32	AIM25
ALR1	AIM3	AHP1	ALR1	AIM32
ALY2	AIM32	AIM14	APL1	AIM36
ANB1	AIM36	AIM19	ARO3	ALD2
APD1	AKL1	AIM24	ASE1	ALD3
APE3	ALR1	AIM25	ATP15	APA1
APL1	ALT1	AIM32	ATP16	ARC18
ARO3	ANB1	AIM36	AVT4	ARG2
ASE1	APA1	ALD3	BCY1	ATG19
AST1	APJ1	ALG5	BEM3	ATP15
ATP17	APL1	ANB1	BIT2	ATP16
BAS1	ARO2	APA1	BNI1	ATP17
BBC1	ARO3	APJ1	BOP3	ATP2
BCS1	ARP8	ARC1	BPT1	ATP3
BCY1	ASE1	ARC18	BRE1	ATP4
BDH1	AST1	ARC19	BUD6	ATP7
BDH2	ATG13	ARD1	BUR2	BDH1
BEM3	ATP15	ARL1	CAR1	BDH2
BIT2	ATP16	ARO3	CCE1	BNA2
BNA2	ATP3	ARO4	CCT3	BNA4
BNI1	AVT4	ARP8	CDC37	BPT1
BOP3	BAS1	ASE1	CDC55	CAR1
BUD6	BBC1	ATG19	CHS3	CCE1
BUR2	BCK2	ATP1	CIA1	CCT2
CAR1	BCS1	ATP15	CMK2	CDC37
CBK1	BCY1	ATP16	CNS1	CIA1
CCA1	BDH1	ATP17	COG5	COG5
CDC37	BDH2	ATP2	CPR3	COX13
CDC55	BEM1	ATP3	CPR6	COX9
CMK2	BEM3	BCP1	CPR8	CPR3
COX15	BIK1	BDH1	CTF18	CPR6
CPD1	BIT2	BDH2	CTT1	CTT1
CPR6	BNI1	BMH1	CUE3	CYT1
CTT1	BOP3	BNA1	DAS1	DBP5
CWC22	BPL1	BNA2	DBP3	DCP1

Table 2 (contd.)

F120	F325	E427	F579	E656
DBP10	BRE1	BNA6	DBP5	DDP1
DCC1	BUD6	BPL1	DCC1	ENP1
DDP1	BUR2	CAM1	DCP1	FMP33
EAP1	CAR1	CAR1	DSK2	FOL1
EAR1	CBK1	CBR1	DYS1	FPR3
ECM2	CCA1	CCE1	EGD1	FRE1
ECM4	CCT2	CCT2	ERG20	FSF1
ELP4	CCT3	CCT3	ESF1	GIC2
ELP6	CCT4	CCT4	FIS1	GLY1
ENO1	CCT8	CCT8	FMP33	GRE1
ESF1	CDC20	CDC37	FOL1	HAM1
ESS1	CDC37	CDC48	GAL11	HBT1
ETR1	CDC55	CHO2	GCD11	HEM14
FOL3	CDC73	CHS2	GEM1	HEM2
FZF1	CIA1	CIA1	GIC2	HIS3
GFD1	CMK2	CIT2	GNP1	HSC82
GIC2	CNS1	CKB2	HAA1	HSP104
GRE1	COX9	CMK2	HAL5	HSP78
GRX5	CPD1	COX2	HAP2	ICS2
GRX7	CPR6	CPR6	HEM14	IDH1
GTS1	CST6	CTT1	HEM2	IDH2
HAA1	CTF18	CYS4	HGH1	IDP1
HBT1	CTT1	CYT1	HIS3	IKI3
HER1	CUE3	DBP5	HIT1	ILV3
HIR1	CWC22	DCC1	HSP104	ISF1
HIS3	DAT1	DCP1	HUA1	JAC1
HIT1	DBP10	DDP1	HXK1	JLP1
HPA3	DBP5	DED1	HXT5	LCL3
HSP12	DCC1	DLD2	IKI1	LIP5
HSP78	DDP1	DLD3	IKI3	LSM8
HUA1	DEP1	DRE2	JAC1	LYS12
HXK1	DIG1	DSK2	JJJ2	MAE1
ICS2	DSK2	DUG1	KAP114	MEC1
IDH1	DYS1	DUR1,2	KIN1	MIC12
IKI1	EAR1	DYS1	KSP1	MIR1
IKI3	ECM2	ECM2	LCL3	MLF3
IRC21	EDC3	ECM29	LHS1	MPM1
ISD11	ELP4	ECM4	LOT6	MRI1
ISF1	ELP6	EFB1	LSM1	MRP1
ISU1	ENP1	EFT1	LSM4	MRP17
JAC1	ESF1	EGD1	LSM8	MRP49

Table 2 (contd.)

F120	F325	E427	F579	E656
JLP1	ESS1	ELP6	MCM6	MRPL38
KAR4	FIS1	ENA2	MCR1	MRPL51
KCS1	FOL1	ENO2	MDJ1	MRPS17
KIN1	FSH3	ENP1	MDJ2	MRPS8
KSP1	GCD11	ERG12	MED1	MRX6
LRE1	GEM1	ERG26	MET28	MTR2
LHP1	GDB1	ERG20	MET18	MRX9
LSM1	GFD1	ESS1	MEU1	NAT1
LSM3	GIC2	ETR1	MEX67	NBP35
LSM4	GNP1	FES1	MIC12	NTF2
LSM7	GRX7	FIS1	MLC1	OAC1
LSM8	GTS1	FOL3	MNR2	ODC1
MAG2	GUA1	FPR3	MOB2	PDX3
MCR1	HAA1	FPR4	MRI1	PIC2
MDJ2	HAP2	FRE1	MRPL38	PLB3
MEC1	HAS1	FSH3	MRX6	POM34
MED1	HER1	FZF1	MTR2	PPT1
MET18	HGH1	GCD11	MUB1	PRE3
MIC12	HIS3	GCN3	NAT4	PRO2
MIT1	HIT1	GDB1	NBP35	PRS4
MLF3	HRT1	GIC2	NNK1	RCF2
MNR2	HSF1	GIS2	NOC3	RDL1
MRPL38	HSP104	GLY1	NOP9	REE1
MRPL50	HSP78	GNT1	NRP1	REP1
MRPL51	HUA1	GPH1	NSG2	RIM2
MRX6	HXK1	GRE1	NTF2	RNA1
MSC3	HXT5	GRX5	NUR1	RPL22A
NNK1	ICS2	GSH1	PAC10	RPS14A
NOC3	IDH1	GTS1	PAD1	RRG7
NPL3	IDH2	GUS1	PEX15	RSM26
NUR1	IKI1	HAM1	PHO2	RTN2
PAC10	IKI3	HBT1	PIN4	SBA1
PAL1	IRC21	HCH1	POM34	SCW10
PAT1	JAC1	HEF3	PRE3	SEC18
PEF1	JJJ2	HEM2	PRK1	SER3
PEP3	JLP1	HER1	PRP24	SGT2
PFK26	KAR4	HGH1	PUF2	SHE3
PHO2	KCS1	HIS3	PUT3	SHS1
PIN4	KEL1	HLJ1	PWP1	SHY1
PRE3	KIC1	HPA3	RAD3	SIL1
PRK1	KIN1	HRT1	RAI1	SIS1

Table 2 (contd.)

F120	F325	E427	F579	E656
PRP18	KIP2	HSF1	RAT1	SLC1
PRP24	KOG1	HSP104	RDH54	SNZ2
PTC2	KSP1	HSP26	RDL1	SOL2
PUF2	LHP1	HSP60	REV1	SPT15
RAI1	LIP5	HSP78	RHO5	SRP14
RAT1	LOT6	HXK1	RMD1	SRY1
RCF2	LRE1	HYR1	ROK1	SSA1
RCO1	LSB3	ICS2	RPA12	SSA2
REV1	LSM1	IDH2	RPC10	SSA4
RHO5	LSM3	IDP1	RPS14A	SSE1
RDL1	LSG1	IDH1	RPA49	SSA3
RIM4	LSM4	IKI3	RRD2	SSM4
ROK1	LSM6	ILV5	RRG7	SSP1
RPA49	LSM7	IRC21	RSC3	STB3
RPC10	LSM8	IRC7	RTN2	STI1
RPS14A	LTE1	ISD11	RTS1	SUI2
RRD2	MAG2	ISF1	RTT101	SWP1
RRG7	MAK5	ITR1	SAP185	TDH1
RSP5	MCM4	JAC1	SBA1	TFB2
RTN2	MCM6	JLP1	SCD5	TIF5
RTS1	MDJ1	KIP2	SEC24	TIM9
RTS3	MDJ2	LIA1	SFL1	TOM70
SCW10	MDV1	LOT6	SGT1	TOM71
SDS24	MED1	LSB3	SGT2	TRP1
SEC16	MED4	LSM7	SHE3	TRR1
SEC23	MET22	LYS12	SHE4	TUB4
SER3	MET28	LYS20	SHS1	UTH1
SFB2	MET31	LYS9	SIL1	UTP30
SGN1	MEX67	MAM33	SIS1	VHS2
SGT2	MIC12	MAS1	SLH1	YDJ1
SHE1	MIR1	MCM4	SMY1	YDL218W
SHE3	MLC1	MCM6	SNZ2	YDR248C
SIM1;SUN4	MLF3	MDJ2	SOL2	YDR391C
SLH1	MNR2	MED1	SRP14	YDR461C-A
SMY1	MOB2	MET18	SSA1	YHR033W
SNF5	MPM1	MET22	SSA2	YJR008W
SNO1	MRPL38	MEU1	SSA3	YJR085C
SNZ2;SNZ3	MRPL51	MEX67	SSA4	YLR345W
SOL2	MRPS8	MIC10	SSE1	YML131W
SPT5	MRX12	MIC12	SSE2	YMR111C
SRM1	MRX6	MIR1	SSP1	YMR124W

Table 2 (contd.)

F120	F325	E427	F579	E656
SRP14	MRX9	MMF1	STB3	YNL134C
SSA4	MSC3	MPM1	STF2	YNR068C
SSD1	MSN1	MRI1	STI1	YOR131C
SSE1	MTG1	MRP17	STP4	YPL225W
SSN8	MTR2	MRP49	SWP1	YTA12
SSP1	NAM9	MRPL38	SYP1	ZPR1
SST2	NBP35	MRPS16	TBF1	
STI1	NGL2	MRPS8	TFB1	
STP4	NGR1	MRX9	TFB2	
SWP1	NMD5	MSS116	TGL4	
SYP1	NNK1	MSS51	THI80	
TFB1	NPA3	MUB1	TIF4631	
TFB4	NPL3	NAB2	TIF4632	
THG1	NRP1	NAM9	TMA10	
TBF1	NOP53	MTR2	THP1	
THP1	NUR1	NAP1	TOM70	
TIF4632	OCA6	NAS6	TOR1	
TMA10	OCH1	NAT1	TRS23	
TOM71	PAC10	NAT4	TUB4	
TRP1	PAD1	NBP35	TVP18	
TRR1	PAF1	NIP7	TY1A-MR1	
TVP18	PAL1	NMD5	TY1B-MR1	
TY1A-MR1	PAT1	NOP1	TY1B-NL2	
TY1A-PR1	PCT1	NOP15	UBX4	
TY1B-MR1	PDR17	NPA3	UME6	
TY1B-NL2	PDX3	NSR1	URA5	
TY2A-C	PEP3	NTF2	URE2	
TY4B-J	PEX15	NTH2	UTP30	
UBP7	PFK26	ODC1	VAC7	
UBX4	PHO2	OPI3	VHS2	
UME6	PIN4	PAA1	VID28	
UTH1	PMC1	PAB1	VPS29	
UTP30	POM34	PAC10	WHI2	
VHS2	PRE3	PCT1	YAK1	
VRP1	PRE9	PDI1	YBL028C	
YAK1	PRK1	PDX3	YCK1	
YBL028C	PRO1	PET9	YCS4	
YBR053C	PRP24	PEX19	YDJ1	
YCK1	PRP4	PIC2	YDR248C	
YCS4	PUF2	PIS1	YHR033W	
YDR119W-A	PUT3	PMC1	YJR008W	

Table 2 (contd.)

F120	F325	E427	F579	E656
YDR461C-A	RAD3	PNC1	YJR085C	
YFR045W	RAD51	PPT1	YKR023W	
YGL010W	RAI1	PRE1	YLR345W	
YGR250C	RAT1	PRE3	YML018C	
YHR033W	RCF2	PRE5	YML131W	
YIL055C	RCM1	PRE6	YMR124W	
YJL070C	RCO1	PRE7	YPK1	
YJR008W	RDL1	PRE8	YPL247C	
YKL033W-A	RDS3	PRE9	YPR174C	
YKL151C	REB1	PRI1	ZPR1	
YLR108C	RGA2	PRO2		
YLR345W	RHO5	PRR1		
YMR111C	RIM4	PRS4		
YMR155W	ROK1	PRX1		
YNL134C	RPA49	PTC2		
YNR068C	RPC10	PUP2		
YPL247C	RPN10	PUP3		
YRA2	RPS14A	PWP1		
YNL131W	RPA12	PST2		
	RRD2	RAD3		
	RRG7	RAD51		
	RSC3	RAT1		
	RSC30	RDL1		
	RSP5	RDS3		
	RTF1	REP1		
	RTN2	RHB1		
	RTS1	RIC1		
	RTS3	RIM2		
	RTT101	RIM4		
	RTT103	RIO1		
	RXT2	RNA1		
	SAC3	RPL22A		
	SAP185	RPN1		
	SBA1	RPN10		
	SCD5	RPN13		
	SCW10	RPN2		
	SDS24	RPN7		
	SEC16	RPP2B		
	SEC23	RPS12		
	SEC24	RPS14A		
	SEC26	RPT1		

Table 2 (contd.)

F120	F325	E427	F579	E656
	SEC8	RPT5		
	SEG2	RQC2		
	SER3	RRD2		
	SFB2	RRG7		
	SFL1	RSM26		
	SGN1	RSP5		
	SGT2	RTN2		
	SHE1	RTT103		
	SHE3	SAC3		
	SHE4	SAM50		
	SIL1	SAY1		
	SIS1	SBA1		
	SKN7	SCW10		
	SLH1	SEC11		
	SLU7	SEC18		
	SMD1	SER3		
	SMY1	SGT2		
	SNO1	SHE3		
	SOL2	SHY1		
	SPC29	SIS1		
	SPT5	SKI2		
	SRM1	SLH1		
	SNF5	SHE1		
	SRP14	SLM4		
	SSD1	SNF5		
	SSE1	SNO1		
	SSP1	SNX3		
	SST2	SNZ2		
	STE11	SOL2		
	STE50	SPC29		
	STI1	SPT15		
	STP4	SRM1		
	SWI6	SSA1		
	SWP1	SSA4		
	SYP1	SSD1		
	TAF5	SSE1		
	TBF1	SSE2		
	TCB1	SSP1		
	TCO89	STI1		
	TDA11	SUI2		
	TFB2	SWP1		

Table 2 (contd.)

F120	F325	E427	F579	E656
	TFB4	TCB1		
	THP1	TEF4		
	TIF4631	TFB1		
	TIF4632	TFB2		
	TMA10	THI80		
	TOA2	TIF5		
	TOM71	TIM9		
	TPS1	TOM71		
	TRM82	TRP1		
	TRP1	TRR1		
	TRR1	TSA1		
	TRS23	TUB4		
	TRS33	TY4B-J		
	TVP18	UBC4		
	TY1A-MR1	UFD1		
	TY1B-ML1	UGO1		
	TY1B-MR1	UNG1		
	TY1B-NL2	URB2		
	TY4B-J	URE2		
	UBX4	UTH1		
	UGO1	VHS2		
	UME6	VID28		
	UTH1	VPS29		
	UTP30	YBR053C		
	UTR1	YCR102C		
	VAC7	YCS4		
	UFD1	UTP30		
	VHS2	YDJ1		
	VID28	YDL144C		
	VPS29	YDR119W-A		
	VPS52	YDR186C		
	VRP1	YDR248C		
	WWM1	YDR391C		
	XRN1	YDR461C-A		
	YAK1	YFR045W		
	YBL028C	YGL010W		
	YBR053C	YGL039W		
	YCK1	YHB1		
	YCS4	YHR033W		
	YDJ1	YJR008W		
	YDR119W-A	YKL033W-A		

Table 2 (contd.)

F120	F325	E427	F579	E656
	YDR461C-A	YKR018C		
	YGL039W	YLR118C		
	YHR033W	YLR345W		
	YHR122W	YML131W		
	YJR008W	YMR155W		
	YKR023W	YNL134C		
	YLR108C	YOL098C		
	YLR345W	YOR131C		
	YMC2	YPL225W		
	YML018C	YRF1-6		
	YML131W	YSC83		
	YMR111C	YTA12		
	YNL134C	ZIM17		
	YNR068C	ZPR1		
	YPK1	ZWF1		
	YPL168W			
	YPL247C			
	YRA2			
	ZPR1			
	ZWF1			

Table 3: Peptide Sequences of Bpa crosslinked targets

Chaperones			
Target	**Sequence**	**Residues**	**Bpa Site**
CCT3	IVDMVSYGIWEPEVIK	491-506	F325
CCT3	IPGGDVLDSR	209-218	F325
CCT4	LSKEAR	425-430	E427
CCT8	GLmKPSGGK	410-418	F325
HGH1	IVNMLMRGEPGAGAVEEMPSK	348-368	F579
HGH1	DPIPAIICCHLESILLLCTTHAGREYLR	294-321	F579
HGH1	EGVASTIK	229-236	E427
HSP104	YKGDFEERFK	257-266	F579
SSA1	ITITNDKGR	499-507	E427
SSA1	NFTPEQISSMVLGK	111-124	E427
SSA3	MKETAENYLGTTVNDAVVTVPAYFNDSQR	125-153	F579
SSE2	EVTKTIKK	523-530	F579
Hsp90 Co-chaperones			
Target	**Sequence**	**Residues**	**Bpa Site**
CNS1	AGGLIKAGK	327-335	F579
CPR6	LKRK	353-356	F579
SBA1	LTKEK	107-111	F325
SGT1	LLSAETASK	300-308	F579
SGT1	GTVKTSPPEGMEPK	380-393	F579
SGT2	EYDQAVKDAESAISIDPSYFR	151-171	E656
SHE4	QDIGEPIRILGCR	522-534	F325
STI1	ALELDASNK	100-108	E656
STI1	LMSFPEAIADCNK	443-455	F325
Potential chaperones			
Target	**Sequence**	**Residues**	**Bpa Site**
TOM70	AIELFPRVNSYIYMALIMADR	356-376	F579
TOM70	IQETLAKLREQGLm	604-618	F579
TOM71	IGLAQLK	568-574	E427
UTP30	NTSYIPNNDNCLSVR	186-200	F579
UTP30	LPYmIRmSKEVK	150-161	F325
UTP30	VGYIQK	201-206	F325
SEC18	LGISHVK	269-275	E427
SEC18	GATKLNTKDIAKLK	483-496	E427

Table 3 (cont.)

Clients			
Target	**Sequence**	**Residues**	**Bpa Site**
ACK1	SIYWYSK	519-525	F325
BAS1	LLNPSPNSVR	652-661	F325
BEM1	SEmVHSLFVVLNNGFDR	390-406	F325
BIK1	NDGSFMGK	47-54	F325
BIT2	VGIIWK	414-419	F325
BUD6	SNNAPNASDDDDALSQLK	226-243	F325
CCA1	LETKK	461-465	F325
CDC55	QNSLCDNK	265-272	F325
CWC22	SPFTVETRK	540-548	F325
DBP10	KVEKALQSGISVKGYNNAPGLR	942-963	F325
DDP1	LVAGCICLTPDK	33-44	F325
DIG1	KSLKRGR	94-100	F325
ECM2	NEKGANEVK	165-173	F325
ECM2	NDKKKTSK	338-345	F325
EDC3	LQNSNPEPLVVILASDSNRSGAK	332-354	F325
EDC3	KDSWNK	162-167	F325
GDB1	EANAGPNLDRVmTDK	1207-1221	F325
HER1	ISDSTDEPDK	822-831	F325
HSF1	LmNEANLGDK	332-341	F325
HSF1	AQPSSGTTNAQPR	148-160	F325
KCS1	DDFLSDLDQENNGK	392-405	F325
KEL1	TSSPPmFARKQVSESR	65-80	F325
KIN1	VSSSQGmPK	102-110	F325
LHP1	QFDLQREASK	216-225	F325
LSM7	FEGPKREAILDLAK	19-32	F325
MAG2	TIWGTSIAVTEDEKASKENKEFQDMLLQR	600-628	F325
MCM6	EARSYLVEKYK	768-778	F325
MDJ1	SSSmFR	190-195	F325
MDJ1	KIKGDK	504-509	F325
MED1	SNRHGSVVEASR	399-410	F325
MNR2	ADVIKGFAK	835-843	F325
PIN4	NIPFAIKK	91-98	F325
PUF2	QHPQGFHSPGR	887-897	F325
ROK1	VLTRGASVKK	6-15	F325
SAC3	TPYKGNVNSSFMLSSSDK	844-861	F325
SAC3	KASRTK	230-235	F325
SEC8	RYTEALEKLSNLEKEQSK	1025-1042	F325
SEC8	EQSKEGARTK	1039-1048	F325
SEG2	RTSSLPNQGHK	77-87	F325
SGN1	LSKEEKHAHQLEADSR	49-84	F325

Table 3 (cont.)

Clients			
Target	**Sequence**	**Residues**	**Bpa Site**
SPC29	VKSPLDDK	75-82	F325
SPT5	AmGKK	314-318	F325
XRN1	KALEKKK	1248-12543	F325
YAK1	EILAVK	393-398	F325
YBL028C	GVFQK	20-24	F325
YBR053C	LRSNDGNVSPDGK	147-159	F325
YCS4	IEAETRNGK	873-881	F325
ZWF1	YVMPEK	484-489	F325
AFG2	LGISAPK	545-551	E427
ANB1	RSEYQLLDIDDGYLSLMTMDGETK	87-110	E427
ARP8	SEMEK	328-332	E427
ASE1	LIKKLISDSWDKIQELWR	459-476	E427
BDH2	mRALAYFGK	0-9	E427
ECM2	NILLR	141-145	E427
ECM29	QLVEKAELR	12-20	E427
ECM29	FDPFQAVSR	1151-1159	E427
ECM29	KSmKYVK	1646-1652	E427
ECM29	AELRLAIADSPQK	17-29	E427
GDB1	LGVNRR	1342-1347	E427
GSH1	IAHHR	519-523	E427
GSH1	NGFGGIAKDVQDKVLEIPKSR	341-361	E427
GUS1	TIEYR	401-405	E427
HBT1	NLETK	63-67	E427
HEF3	TPSEYIQWR	751-759	E427
HEF3	INSGKKK	1005-1011	E427
HER1	LLCKFLLQNK	579-588	E427
KIP2	LSADK	405-409	E427
MCM4	GLVLR	330-334	E427
MRX9	EISSRMGIPNEFAK	409-421	E427
NOP1	NMAPGESVYGEK	110-121	E427
PDI1	SLDSLFDFIK	472-481	E427
PDX3	QSDVIKNR	153-160	E427
PDX3	ILLFK	74-78	E427
PMC1	EDDEDQLFKNVNKGR	551-565	E427
PRE8	VAHTSYK	92-98	E427
PRI1	DTLLKSELK	94-102	E427
PRO2	ETGLADSLLK	57-66	E427
RPT1	VATEKDFLK	437-445	E427
RTT103	IIQFQDSFGK	76-85	E427
SLH1	GDELLMIK	1911-1918	E427

Table 3 (cont.)

Clients			
Target	**Sequence**	**Residues**	**Bpa Site**
SND1	LLNDTSKK	661-668	E427
SND1	SLSINRKSNR	332-341	E427
SPT15	LASRKYAR	134-141	E427
SSD1	ISGGEAGVTVK	182-192	E427
SUI2	RVSSEDIIK	89-97	E427
UGO1	LLIQVGEFK	138-146	E427
YCS4	AIQGCSK	378-384	E427
YOL098C	SIATVDSYK	526-534	E427
YRF1-6	EFYGLESK	1235-1242	E427
ZPR1	LKEAIAGK	428-435	E427
ACF4	LSIVDK	17-22	F579
ADE6	EDIVLAYHDR	921-931	F579
ADH5	SPIHLAGLSDVPEIFAK	319-335	F579
ALR1	AFGIHPLTAEDIR	473-485	F579
AVT4	LRRPRSMENVTPK	160-172	F579
BCY1	LDSDSK	188-193	F579
BIT2	LLPYKPHNSIGK	213-224	F579
BNI1	LDEINR	1021-1026	F579
BPT1	AILGQLPCMSGSR	684-696	F579
BPT1	LIIRSSSVAYCSQESWImNASVR	703-725	F579
CHS3	TMDKHTNDIEDWSNNIQTK	493-511	F579
CPR8	VSmIKDDKGLK	152-162	F579
CUE3	LFERSKRGTK	494-503	F579
DBP5	GIYAmKFQKPSK	106-117	F579
GAL11	LEISSR	863-868	F579
GAL11	NGTPNPNNmK	818-827	F579
GAL11	AAQRARDQDSIDISIKDNK	924-942	F579
HAL5	LINALSEK	445-452	F579
HAL5	KNSLSTPRSPPmK	231-243	F579
HEM14	NFKPLFDKLSTNPNALNKYTK	407-427	F579
IKI1	FLSEIASPHCTMVATYHKDIKDENR	120-144	F579
IKI3	GKHPSIVCEFPK	509-520	F579
LSM1	GIFmIRGENVVmLGEVDIDK	100-119	F579
MCM6	LHFPSSSQPHVSNSQTGPFVNDSTQFSSQR	43-72	F579
MLC1	ELDATTK	74-80	F579
MOB2	EmAPLLPLIESFEKQGK	267-283	F579
NOP9	ETQPQMFFGVLDR	46-58	F579
NRP1	RTACFRCSFPAPSNSQIHTANSNNNVNSSR	372-402	F579
NUR1	REFEALPK	354-361	F579
PEX15	CCIKVIQFNLTDHTEQEEK	141-159	F579

Table 3 (cont.)

Clients			
Target	**Sequence**	**Residues**	**Bpa Site**
PIN4	EKYYYELAYPMGISASHK	319-336	F579
PRP24	HVKPSCINMMEK	404-415	F579
PUT3	RQQRSSVACLSCR	26-38	F579
RAD3	VLRGKDDYGVmVLADR	669-684	F579
RAI1	MIPRDEDPHSQIR	330-342	F579
RAT1	FHVTPQDIEQLRKDmVK	613-629	F579
RDH54	NDGGKYQMPLSQLFSLNTVKR	214-234	F579
ROK1	QSGCEVSEWMDKMAKMTR	493-510	F579
RPS14A	ETIARVTGGmK	37-47	F579
RSC3	RPHLNEFK	254-261	F579
SCD5	IKNLNFKSKK	264-273	F579
SEC24	NESGVVNTSKETAQLLSCQDSFYK	461-484	F579
SHS1	RGITYTMLLCGPAGTGK	20-36	F579
SIL1	NNKDKQLQIK	276-285	F579
SNZ2	EIMEAVSIPVmAK	66-78	F579
STB3	LTATSEPTSR	333-342	F579
TBF1	ILDLYGPGGK	434-443	F579
TIF4631	IEITTKSGEHLDLK	134-147	F579
UBX4	MPMVTVKYNFQLFK	0-14	F579
UME6	ESSNNNEIGGYLR	296-308	F579
YAK1	FMKKLAPEESSSSTQK	603-618	F579
YCS4	mLHLVWMKGTNDEGTSISVHLIECYK	584-609	F579
YCS4	TLVYLEKCEAEFK	857-869	F579
YKR023W	REKYVVSmNIGSNGK	395-409	F579
YMR124W	LESESAVANRASLSTFSSTFSDSPSK	564-589	F579
YMR124W	mVSANYSRSNSLmSGPPGQFR	287-307	F579
ZPR1	NCEIQPASQIQEK	90-102	F579
TIF5	mPPIQAKVEGR	18-28	E656
YLR345W	QLNPGSIADLTDQQIMDK	393-410	E656
SNZ2	INEGAAMIR	136-144	E656
YTA12	NNTIPANWKEQKR	86-98	E656
MRPL38	ImANDGCVDRTLKDK	111-125	E656

CHAPTER 3: DISCUSSION

Hsp90s have evolved from a single non-essential factor (HtpG) in bacteria to an essential family in eukaryotes (Bardwell and Craig, 1988, Borkovich *et. al.* 1989). In addition to the cytosolic forms of Hsp90, which include a constitutively expressed isoform and a heat-induced isoform, organelle-specific Hs90s have evolved through gene duplication in multicellular eukaryotes – TRAP1 in mitochondria, Grp94 in the endoplasmic reticulum (ER) and chloroplast Hsp90 (cHsp90). Hsp90 was first identified with metastable factors, including unactivated hormone receptors and kinases (Pratt and Toft, 1997; Joab *et. al.* 1984; Catelli *et. al.* 1985; Sanchez *et. al.* 1985), leading to the concept that Hsp90 recognizes polypeptides late in the folding process with recent efforts extending Hsp90's reach to native proteins. Large-scale genetic interaction screens showed that this abundant chaperone is linked to a wide variety of cellular processes (Millson *et. al.* 2005, Zhou *et. al.* 2005, McClellan *et. al.* 2007), nevertheless most physical interaction screens only identified a limited number of hits. Likely, Hsp90 transiently interacts with its clients thereby abating detection by standard methods. A study incorporating a chemical crosslinker followed by mass spectrometry found Hsp90 associated with ~8% of the yeast proteome (Girstmair *et. al.* 2019). How Hsp90 recognizes these diverse clients was unresolved.

Hsp90 consists of an amino (N), middle (M), and carboxyl (C) terminal domain with the N-domain housing ATPase activity and the C-domain mediating Hsp90 dimerization (Prodromou *et. al.* 1997; Harris *et. al.* 2004; Wayne and Bolon, 2007). A high-resolution structural study showed that Hsp90 contacted the Cdk4 kinase client primarily using its M-

domains (Verba *et. al.* 2016). Whether Hsp90 uses one or all three domains to recognize other clients had not been determined.

To better understand the mechanistic features driving client recognition by the Hsp90 molecular chaperone, I exploited the non-natural amino acid p-Benzoyl-L-Phenylalanine (Bpa), which a photoactivable crosslinker, and large scale mass spectrometry to build a domain-centric Hsp90 interaction map. I have identified 1114 yeast proteins to be Hsp90 interactors and provided insight into a potential mechanism driving Hsp90-client interaction – the usage of all three domains of Hsp90 and the hydrophobic patches distributed across them as sites for interactions with specific intrinsic regions of disorder within the client. While my study provides mechanistic insights into Hsp90 function, it also opens the field of Hsp90 biology to several interesting questions that I discuss further.

3.1 THE ATPASE CYCLE OF HSP90

Hsp90 is a low affinity ATPase with an abysmal enzymatic activity of 0.1 ATP min^{-1} in humans and 1 ATP min^{-1} in yeast.(Scheibel *et. al.* 1997). Co-chaperones have been shown to bind to Hsp90 in a sequential manner, promoting or inhibiting certain conformational changes (Li *et. al.* 2011). However, the single crystal structure of Hsp90 with a client, Cdk4 (Verba *et. al.* 2016) pushed forth the idea that Hsp90-client interactions might occur exclusively through the M domain cleft – an interaction that is likely initiated during the open conformation of Hsp90 whereby the client is positioned within the open M domain following which the Hsp90 dimer closes on stabilizes the client (Bieble *et. al.* 2019). While the ATPase activity has been shown to be essential *in vivo* (Obermann *et. al.* 1998; Panaretou *et. al.* 1998; Mishra and Bolon, 2014).

Recent findings with the Hsp82 E33A mutant, which can bind ATP and undergo conformational changes, but is unable to hydrolyse ATP suggest that rather than ATP hydrolysis, the duration of time spent in different conformations due to Hsp90's inherently low ATPase activity might be sufficient to support the essential function of Hsp90 (Zierer *et. al.* 2016).

The Hsp90 physical interactome generated in this study establishes 629 Bpa enriched interactors that utilize all three Hsp90 domains in a combinatorial manner, likely through the hydrophobic surfaces spread across all three domains. Since the Bpa was incorporated at residues that remain on the surface throughout the Hsp90 conformation cycle, it is possible that subsets of the captures interactors were captured during different steps of the conformation cycle. This puts forth the interesting hypothesis as to whether the indispensability of the Hsp90 conformation cycle is due to a difference in the clients that interact with different steps of the cycle. It is possible that the Hsp90 conformation cycle exposes different hydrophobic patches across all three domains that enables a broad range of client binding. The necessity of a particular stage in the conformation cycle would then depend on the necessity of the clients that interact with that specific conformational stage of Hsp90 and the degree to which the client is affected by an inability to interact with Hsp90. This idea could be probed further by using ATPase cycle mutants in conjunction with Bpa crosslinking and mass spectrometry to further understand the conformation cycle specificity of Hsp90-client interaction.

3.2 HSP90 GOVERNS CLIENT FUNCTION THROUGH IDRS

The canonical Structure-Function paradigm dictates that protein sequences define structures which in turn determines function and thus, the function of domains or proteins can be

determined through its structure. This paradigm establishes a framework useful in understanding gene and protein evolution where the overall fold of the structure of two distantly evolved genes might remain the same despite the sequences being different. (Laskowski and Thornton, 2008). This framework has also given rise to many useful protein classification systems that correlate structure with function (SCOP; Murzin *et. al.* 1995, CATH; Sillitoe *et. al.* 2012).

While many proteins do have a well-defined structure that is required for their function, a large fraction of the proteome of any organism has now shown to consist of polypeptides that do not form a well-defined three-dimensional structure, but are functional (Dyson and Wright, 2005). These polypeptides are referred to as intrinsically disordered regions (IDRs). Traditionally considered to be non-functional "linker" segments of protein sequence, IDRs have slowly been established as active functional components of many proteins (Kriwacki *et. al.* 1996; Iakoucheva *et. al.* 2004; Collins *et. al.* 2008). The length, sequence and function of IDRs varies drastically making not only classification, but even prediction of IDRs of proteins extremely challenging.

Nine different algorithms predict IDRs based on different criteria, the results of which are collated on the D^2P^2 database (Oates *et. al.* 2013). Using this resource, I was able to ascertain that the majority of the Hsp90-client crosslinks found in the Hsp90-Bpa physical interactome are within or near IDRs. I was also able show that the deletion of a specific predicted IDR within the client RSC3 resulted in a lack of functional regulation of RSC3 by Hsp90. Finally, I demonstrated that Hsp90 can also regulate the physical state of a protein through its IDR, since the inhibition of Hsp90 lead to stress granule formation by the Hsp90 interactor Ded1. Intriguingly, several Hsp90 clients, including RSC3, possess more than one IDR which would indicate that at least in the case of RSC3, Hsp90 regulates protein function through a specific

IDR. This suggests that regions of intrinsic disorder must have evolved in the context of selective pressures that ensure chaperone-client binding and/or chaperone-client functional regulation. It would be of interest to consider the specific features of IDRs that determine Hsp90 dependent binding and/or regulation in future studies.

3.3 THERAPEUTIC TARGETING OF HSP90

Hsp90 inhibitors have been tested in clinical trials as potential anti-cancer drugs (Whitesell *et. al.* 2003; Whitesell and Lindquist 2005). However, induction of a heat shock response (HSR) results in activation of the Heat Shock Factor 1 (HSF1) transcription factor, which upregulated the transcription of other heat shock proteins (HSPs), thereby compensating for the inhibition of Hsp90. This HSR has led to the failure of the clinical trials (Neckers and Workman, 2012), however, the exact cause for the induction of the HSR remains unknown.

The Hsp90-Bpa physical interactome identified several translation factors as Hsp90 clients. I demonstrated a multifaceted role of Hsp90 in translation regulation using the Hsp90 inhibitor Radicicol or Ganetespib, and the Hsp90 mutant G170D. Since inhibition of Hsp90 led to gross translational defects including a change in translation frame, loss in fidelity of translation start codon selection, and increase in heat stress independent stress granule formation, I hypothesized that translation dysregulation due to Hsp90 inhibition might account for the Hsp90 inhibition dependent HSR. Indeed, in yeast and in mammalian cells, Hsp90 inhibitor induced HSR was dependent on active translation. My discovery that Hsp90 governs translation initiation affords an opportunity to hone Hsp90 therapeutic trials to avoid triggering an HSR,

potentially through the incorporation of existing translational inhibitors in the Hsp90 inhibitor cocktails.

In conclusion, the Hsp90-Bpa physical interactome generated in this study provides significant insight into the workings of an essential eukaryotic molecular chaperone. The interactome provides several other Hsp90-linked pathways waiting to be explored and raises additional interesting questions with respect to the mechanistic action of Hsp90-client regulation. Future studies expanding the Hsp90-Bpa interactome to different physiological conditions will further deepen our understanding of this complex, multifaceted modulator of cellular processes.

CHAPTER 4: MATERIALS AND METHODS

The focus of this chapter will be to describe several methodologies designed to create a high throughput screen involving p-Benzoyl-L-Phenylalanine crosslinking, validate the interactome thus generated and probe the function of Hsp90 in various cellular pathways identified through the interactome. The specific goals of these assay were to elucidate the mechanisms by which Hsp90 recognizes clients and functionally modulates them.

4.1 EXPERIMENTAL MODEL AND MEDIA

Saccharomyces cerevisiae cultures were grown in complete (YPD) or minimal media supplemented with the required amino acids at 30°C unless otherwise noted. The parent yeast strain (JJ117) used in this study has the endogenous Hsp90 genes disrupted (*hsc82*D*hsp82*D) and is supported by plasmid (Yep24-HSP82-URA) borne expression of Hsp82 protein. The Bpa Hsc82 derivatives were generated by introducing Amber stop codons (UAG) into an Hsc82 expression plasmid (pRS313GPD His-Hsc82) at the positions encoding for the indicated amino acid codons of Hsc82 (F120, F325, E427, F579, and E656) by one-step overlap extension PCR. Plasmids to express wild type Hsc82 (WT) or each Bpa variant were introduced in parental yeast transformed with pSNR-BPA (**16**) and YEp24-HSP82-URA. Plasmid shuffling with 5-FOA selection was used to eventually drop the YEp24-HSP82 plasmid. All yeast used in the described experiments express a variant of Hsc82, which is referred to as Hsp90. The strains used in this study are described in Table S6.

Bpa supplemented liquid media was prepared with sterile, Synthetic Dextrose (SD) media supplemented with the required amino acids or complete (YPD) media. 200 mM Bpa stock solution (prepared by dissolving 53.8 mg of BPA in 1 mL of 1 M NaOH) was added by slowly dripping the solution into the liquid media prior to inoculation to a final concentration of 2 mM. The pH was neutralized with equal volume of 1 M HCl. Bpa supplemented solid media was prepared with autoclaved SD media with 2% agar, cooled to 55°C, required amino acid drop out mix was added while stirring with a magnetic stir bar, Bpa stock solution was slowly dripped into the media to a final concentration of 2 mM, and pH was neutralized with equal volume of 1 M HCl.

4.2 BPA VARIANT PRODUCTION AND GROWTH TESTS

To check the ability of each Hsp90 derivative to support cell growth, yeast expressing either Hsp90 WT or a Bpa variant were grown to exponential log phase, collected by centrifugation, and resuspended to a OD_{595}=1.0. Each sample was serially diluted 10-fold and 5 µL of each dilution was spotted onto selective SD media plates supplement with or without Bpa. Plates were incubated at 30°C or 37°C and imaged after two days of growth.

To assess the production length of each Hsp90 variant, each variant was grown overnight to saturation in SD\His,Trp with and without Bpa. Cell pellets thus collected were used to generate whole cell extracts by glass bead beating for 37 min with a 1 min ON 2 min OFF cycle. Lysates were collected and clarified by centrifugation at 14000 rpm for 15 min. 100 µg of each extract was resolved by SDS PAGE. The Hsp90 proteins were detected by immunoblot analysis using anti-His antibody.

4.3 BPA CROSSLINKING

Yeast transformants expressing either wild type His-Hsp90 (WT) or a Bpa variant were maintained on 2 mM Bpa supplemented selective SD solid media as described under 'Experimental model and media'. Briefly, a 200 mM Bpa stock solution (freshly prepared by dissolving 53.8 mg of Bpa in 1 mL 1 M NaOH was slowly dripped in the solid or liquid media to a final concentration of 2 mM. The pH was neutralised with an equal volume of 1 M HCl). Overnight cultures in selective SD media supplemented with Bpa at 2 mM were used to seed ~325 mL YPD media supplemented with Bpa (since each variant produced full length Hsp90-Bpa only in the presence of Bpa, there is an inherent selective pressure to retain the Hsp90-Bpa variant plasmid, thus, YPD media was used for growth of crosslinking cultures as cells were empirically determined to grow better in the YPD media supplemented with Bpa when compared to selective SD media supplemented with Bpa) to a final OD_{595} of 0.3. Cells were harvested at OD_{595} 0.6-0.7, collected by centrifugation, and resuspended in 25 mL YPD without Bpa. 5 mL was spread onto five 10 cm^2 plates each. (~0.8 OD_{595} units of cells per cm^2 surface area to achieve a 0.1 cm thickness of cell suspension). To maintain temperature during the UV crosslinking step, a Styrofoam box was prepared by adding crushed dry ice to fill the bottom third of the bottom of the box, followed by wet ice packed over the top. A metal plate was placed over the ice for levelling and support. The petri plate containing cells was placed on top of the metal plate and the box was placed in the crosslinker with paper towels added under it to raise the box till the petri plate was ~2 cm from the UV bulbs. Crosslinking was carried out with default energy settings for 3 hours. After UV exposure, cells were collected by centrifugation, washed once with water, and pellet was flash frozen in liquid nitrogen.

WT culture was used to detect stable Hsp90 interactors, while Hsp90-Bpa variants were used to generate an Hsp90-Bpa dependent interactor list. The crosslinking procedure was also carried out with W303 yeast grown with an untagged Hsp90 without selective pressure but in YPD media to serve as a negative control for analysis of the mass spectrometry data.

4.4 PURIFICATION OF CROSSLINKED HSP90

Frozen pellets were resuspended in TALON Binding Buffer (TBB; 50 mM Sodium phosphate, 300 mM NaCl, pH 7.2) with 0.75% Triton-X and lysed using glass bead beating with a 1 min ON and 2 min OFF cycle for 37 min at 1400 rpm. Lysates were collected and clarified by centrifugation at 14000 rpm for 15 minutes. TALON Cobalt beads prewashed with TBB were added and the mixture was nutated for 2 hours at 4°C. Beads were collected by centrifugation at 3000 rpm for 3 min and the lysate was discarded. The beads were washed 4x with 10x bead volume of TBB supplemented with 20 mM Imidazole. Samples were eluted with a 1x bead volume of TBB containing 150 mM Imidazole for 15 min at 4°C and pooled with a second round of elution. 325 mL of crosslinked culture was purified using 200 µL of beads and yielded ~500 µL of combined eluant which was concentrated down to ~200 uL. A 10 µL aliquot of the samples was analysed by SDS-PAGE and visualized by Coomassie blue or SYPRO Ruby Protein gel staining for crosslinking using manufacturer's instructions. The remaining sample was flash frozen in Dry Ice/Methanol and stored at -20°C until mass spectrometry analysis.

4.5 MASS SPECTROMETRY

Multidimensional Protein Identification Technology mass spectrometry was performed on the purified samples by the Sanford Burnham Prebys Proteomics facility. The Bioconductor package artMS was used for analysis of the mass spectrometry data (31). Default settings were used for relative quantification of identified proteins using triplicates of samples generated for Hsp90-BPA variants (Hsp90-BPA), wild type His-Hsc82 (WTL) and untagged Hsc82 (W303). Relative quantification tables were generated by providing a contrast text file comparing WT and Hsp90-BPA with W303 and Hsp90-BPA with FL. Hsp90 interacting proteins (stable interactors) were identified as proteins with a 1.5 fold or higher enrichment and adjusted p value of 0.05 or lower in Hsp90-BPA and/or WT when compared to W303. Crosslinked proteins (transient interactors) were determined as proteins with a 1.5 fold or higher enrichment and adjusted p value of 0.05 or lower in Hsp90-BPA when compared to WT.

To identify the Bpa crosslinked peptide pairs, files for each Hsp90 variant were generated in accordance with the MeroX software's guidelines. Briefly, the site of Bpa incorporation in the Hsc82 fasta sequence was replaced with an 'x' and fasta sequences of the variant specific hits were combined into the same file (due to many variants specific hits, multiple files were generated for each variant with a subset of the hits to significantly reduce computational time of the software). After crosslinked peptide list was generated, peptides were filtered to select those with more than two b and/or y ions from both α and β ions as well as more than 5% relative intensity for at least one ion that included the crosslink from both peptides.

4.6 YEAST TWO HYBRID TO VALIDATE THE BPA INTERACTOME

Two-hybrid (Y2H) interaction analysis was carried out using Matchmaker Gal4 2-hybrid system (Clonetech). Cloning in pGAD-T7 and pGBK-T7 was carried out using Takara Bio InFusion cloning kit and all plasmids generated are described in Table S5. IDR deletion in Rsc3 were created by Q5 Site Directed Mutagenesis protocol. AH109 cells were transformed with the required pGBK-T7 and pGAD-T7 plasmid combinations.

To validate interactors identified in the Hsp90-Bpa interactome, the production of b-galactosidase was assessed in three single colonies from each Y2H combination were patched onto fresh plates and used for overnight cultures in selective SD media. Overnight cultures were used to inoculate 25 mL selective SD media at OD_{595} 0.05 and allowed to grow for ~12 hours to an OD_{595} of 0.4-0.6. Cells were collected by centrifugation and washed 3 times in wash buffer (10 mM Tris pH 7.5, 5 mM DTT). Cells were resuspended in ~5x pellet volume of wash buffer and lysed with glass bead beating using a vortexer with a 1 min ON/1 min OFF cycle on ice for a total of 5 cycles. Lysates were filtered and 3M KCl was added to 1/10 lysate volume. Lysates were then clarified for 10 min at 14000 rpm and moved to fresh tubes. 20 µL of lysates was incubated with 100 µL of substrate buffer (12 mM Na_2HPO_4, 8 mM NaH_2PO_4, 2 mM KCl, 0.2 mM $MgSO_4$, pH 7, 0.5 mM CPRG, 0.14% β-Mercaptoethanol) in a 96 well plate for 4 hours at 37°C and absorbance at 560 nm was read using TECAN Evolution plate reader. Lysate protein concentration was determined by BCA assay and used for normalisation of b-galactosidase values.

For the Rsc3 yeast two hybrid (Y2H) analysis to assess the effects of Hsp90 on Rsc3 or Rsc3ΔIDR DNA binding activity, spot test assay was carried out to test the activation of the *HIS3* reporter. Single colonies from each Y2H combination were patched onto fresh plates and

inoculated from the patches into selective SD media for 2 days to saturation. 10-fold serial dilution was carried out from saturated cultures and 5 µL of each dilution was spotted onto selective solid SD media with and without Histidine. Plates were imaged every two days for 6 days.

4.7 RSC3 ELECTROPHORETIC MOBILITY SHIFT ASSAY

IDR deletion (Rsc3ΔIDR) in Rsc3 was generated using the Q5 Site directed mutagenesis protocol with pET SUMO Rsc3 as a template (Table S5). Recombinant Rsc3 or Rsc3ΔIDR (region deleted G197-Q303) proteins were purified as His_6-SUMO fusion proteins following expression in Rosetta transformants. The DNA binding assay used a radiolabelled ACC1_TIM23 probe (Table S5) in Binding Buffer (10 mM Tris pH 7.4, 40 mM NaCl, 1 mM DTT, 4% glycerol, 50 mg/mL BSA). Where indicated, reactions were supplemented with Hsp90 (1, 4, 16 mM) or BSA to balance total protein levels (16 mM total). Reactions were resolved on 4% native polyacrylamide 1x GTG, gels were dried, and resolved products were visualized using a PhosphoImager (Molecular Dynamics).

4.8 POLYSOME FRACTIONATION

To determine the locations of the yeast Hsp90 and Hsp70 molecular chaperones relative to established ribosome complexes, we used a standard polysome fractionation procedure (32) with some modification. In brief, an overnight culture of wild type yeast (BY4741) was used to inoculate 100 mL of YPD to OD_{595} 0.25 and allowed to grow till OD_{595} 0.7. Cycloheximide

(CHX) was added to the culture to a final concentration of 100 µg/mL for 15 minutes followed by collection of cells by centrifugation at 4°C, 4000 rpm for 1 min. Cells were resuspended in chilled polysome gradient buffer (20 mM Tris pH 7.4, 150 mM NaCl, 5 mM $MgCl_2$, 1 mM DTT, 100 µg/mL CHX). Resuspended cells were dripped into liquid N_2 to create frozen cell pellets. Lysates were prepared by grinding the frozen cells in liquid N_2 using a mortar and pestle and thawing the frozen powder at 4°C. A_{260} of the lysates was measured and lysate corresponding to 200 µg of RNA was layered onto a premade 10%-50% sucrose gradient. Fractionation in sucrose density gradient was carried out using the SW41Ti rotor and ultra-centrifugation at 32000 rpm for 3 hours. AKTA fraction collector set up with a UV reader was flushed with 50% sucrose solution and then used for sample fractionation with a fraction volume of 1 mL. Fractions were collected corresponding to the crude extract, 40S, 60S, monosome and polysome fractions based on A_{260} readings. Fractions were TCA precipitated with 25% TCA and washed twice with acetone. Pellets were dried on a 95°C heat block and resuspended in 40 µL 2xSDS PAGE loading dye. Aliquots (20 µL) of each fraction were resolved by SDS-PAGE. The positions of yeast Hsp90 and Hsp70 were visualized by immunoblot analysis using anti-Ssa1/2 or anti-Hsc/p82 antibodies.

4.9 INHIBITOR INDUCED HEATSHOCK

Yeast: W303 was grown in YPD from OD_{595} 0.25 to OD_{595} 0.5-0.6. Cells were concentrated 4-fold. Radicicol (10 µM), L-azetidine 2-carboxylic acid (5 mM), and CHX (100 µg/mL) were added in the required combinations. Cultures were then kept at 30°C or 42°C for heatshock for the specified duration. Cells were collected by centrifugation and total RNA was

extracted by hot acidic phenol method. Briefly, cell pellet was resuspend in 400 µL TES buffer (10 mM Tris-Cl pH 7.5, 10 mM EDTA, 0.5% SDS) and 400 µL of acid phenol preheated to 65°C. Cells were incubated at 65°C for 60 minutes with brief vortexing for 10 sec every 15 min. Phases were separated by centrifugation at 14000 rpm at 4°C for 5 min. Aqueous phase was transferred to a clean microcentrifuge tube and 400 µL of chloroform was added followed by vigorous vortexing and centrifugation at 14000 rpm, 4°C for 5 min. 300 µL of aqueous phase was transferred to a new tube and 30 µL 3 M sodium acetate, pH 5.3 and 750 µL of 100% ethanol was added. Samples were incubated overnight at -80°C and precipitated by centrifugation at 14000 rpm at 4°C for 5 min. RNA pellet was washed in ice-cold 70% ethanol and dried for 5 min. RNA pellet was resuspended in 50 µL of H_2O and concentration was measured by nanodrop. 100 ng RNA was used for qRT PCR with SSA4 and TAF10 qRT primers (Table S5) using Power SYBR Green RNA-to-C_T 1-Step kit according to manufacturer's instructions with t_m at 58°C.

Mammalian cell culture: HeLa cells were cultured to 70%-80% confluency in 6 well plates. Ganetespib (25 nM or 250 nM) and CHX (1 ng/mL) were added in the required combinations to each well for the specified duration. For heatshock, an entire 6 well plate was parafilm wrapped twice and submerged in a 42°C water bath for the specified duration. Cells were lysed directly in the well using TRIzol and manufacturer instructions were followed for RNA isolation. 100 ng RNA was used for qRT PCR with HSP70 and GAPDH qRT primers (Table S5) using Power SYBR Green RNA-to-C_T 1-Step kit according to manufacturer's instructions with t_m at 58°C.

4.10 DUAL LUCIFERASE ASSAY

To determine if Hsp90 influences the fidelity of translation initiation, we used a standard dual luciferase expression system (23). In brief, plasmids expressing firefly luciferase under a noncanonical (UUG) or canonical (AUG) start codon and Renilla luciferase under the canonical AUG start codon were kind gifts of Dr. Jon Lorsch (NIH). WT (JJ117) and G170D yeast were transformed with each plasmid and four single colonies were assayed for dual luciferase activity. Overnight cultures for each transformant were inoculated to OD_{595} 0.2 in a 96 well plate and incubated at 30°C for 4-6 hours to OD_{595} 0.6-0.8. 50 µL of cultures were moved to a new 96 well plate and 50 µL of SD Ura- media prewarmed to 45°C was added to bring the temperature to 37.5°C. Cultures were allowed to grow for another 4-6 hours at 37.5°C. 2 µL of cultures (30°C and 37.5°C) were added to 50 µL 1x Passive lysis buffer and incubated at room temperature with shaking for 50 min. Firefly luciferase activity was measured in the TECAN Evolution plate reader at 560 nm by the addition of 50 µL luciferin in substrate buffer (15 mM Tris pH 8, 25 mM glycylclycine, 4 mM EGTA, 15 mM $MgSO_4$, 1 mM DTT, 2 mM ATP, 0.1 mM CoA, 75 µM Luciferin). Renilla luciferase activity was subsequently measured at 440 nm by the addition of 50 µL coelenterazine substrate (0.22 M citric acid-sodium citrate pH 5, 1.1 M NaCl, 2.2 mM EDTA, 1.3 mM NaN_3, 0.44 mg/mL BSA, 1.43 µM Coelenterazine) to the same wells.

To calculate UUG utilisation, UUG and AUG Firefly luciferase values were first normalized their respective AUG Renilla luciferase values (from the same plasmid as the Firefly luciferase) to determine the F_{UUG} and F_{AUG} values. F_{UUG} was then normalized to F_{AUG} for the final UUG utilisation value.

F_{UUG} = UUG Firefly/ AUG Renilla F_{AUG} = AUG Firefly/ AUG Renilla

$$\text{UUG utilisation} = F_{UUG}/F_{AUG}$$

To determine fold change, the G170D UUG utilization value was compared to the WT UUG utilization value.

4.11 TRANSLATION FACTOR STABILITY ASSAY

TAP tagged strains of the required translation factors were grown from OD_{595} 0.25 to OD_{595} 0.5-0.6. Cells were concentrated 5-fold and an aliquot was immediately collected by centrifugation and pellet was frozen as time 0. Radicicol was added to a final concentration of 25 µM to the remaining culture and incubated at 30°C, with aliquots being taken at 15 min and 60 min. Frozen pellets were lysed by bead beating in TENG (Tris pH 7.4, EDTA, NaCl, 10% Glycerol) buffer and lysates were clarified. BCA assay was used to determine concentration of proteins in the lysate. Proteins were TCA precipitated and resuspended in 1X SDS loading buffer to a final concentration of 25 µg/µL. Protein expression levels based on placement in the TAP tag library were used to determine amount of whole cell extract (WCE) resolved. For TAP tagged strains from the S1 labelled plates in the library 100µg WCE, for TAP tagged strains in the S2 and S3 categories 250 µg WCE and for TAP tagged strains in the S4 category, 500 µg of WCE was resolved on 10% SDS polyacrylamide gel and analysed by immunoblotting using αTAP and αSBA1 antibodies.

4.12 MG132 GROWTH CURVES

Overnight cultures of JJ117 WT and G170D were inoculated to an OD_{595} 0.25 and grown to OD_{595} 0.6-0.7. Cultures were diluted down to OD_{595} 0.5 and added 1:1 to tubes pre-aliquoted with media containing MG132 (100 µM) or equivalent amounts of DMSO. Culture tubes were shifted to 30°C/35°C/37.5°C water baths and absorbance was measured every hour for 12 hours. Growth rate was calculated as $\log(X_t/X_0)$ with X_t being the absorbance at time t and X_0 being the initial absorbance of the cultures.

4.13 STRESS GRANULE MICROSCOPY AND ANALYSIS

Ded1-GFP strain from the N-terminal GFP library kindly provided by Dr. Maya Schuldiner (Weizmann Institute of Science), was grown to OD_{595} 0.5. Required volume of culture was aliquoted into conical tubes and DMSO or Radicicol at 200 µM was added to each. DMSO/Radicicol containing cultures were then aliquoted into test tubes and moved to the required water bath (39°C/40°C/42°C/46°C). Samples were collected at 4/7/10/15/30 min and added to formaldehyde to a final formaldehyde concentration of 3.7%. Cells were fixed on ice for 10 min followed by 2 washed in KPO_4 buffer pH 6.5. Cells were resuspended in KPO_4 buffer and mounted onto polylysine coated slides using vectashield. Ded1-GFP was visualised using DeltaVision OMX with the FITC channel, 30 s exposure and 50% transmission. 2 µM stacks were generated and deconvoluted. A custom Fiji script provided by Dr. Titus Franzmann (TU Dresden) was modified and used for identification and counting of stress granules and cells.

4.14 PHALLOIDIN STAINING OF ACTIN CYTOSKELETON

Phalloidin staining was carried out as per Higuchi et al. (2013). Briefly, cells were fixed by addition of 3.7% paraformaldehyde directly to the growth medium at 30°C with shaking for 50 min. Cells were then collected by centrifugation and washed three times with wash solution (0.025M KPi pH 7.5, 0.8M KCl), followed by one wash with PBT (PBS, 1% w/v BSA, 0.1% v/v Triton X-100, 0.1% NaN3). Staining was carried out with 1.65 □M FITC-phalloidin for 35 min at RT in the dark. After three washed in PBS, cells were mounted onto slides and visualized immediately.

4.15 *INO1* LOCUS MICROSCOPY

INO1 nuclear positioning was determined by analyzing z-stack images acquired with a DeltaVision OMX microscope (GE Life Science) with 100x/1.40 NA oil immersion objective (Olympus). INO1 nuclear periphery localization was determined by stringent criteria as previously described (Brickner and Walter, 2004). All INO1 motion data represent averages of 3 independent trials with 50 counted cells in each and the error bars represent the SEM.

4.16 RIBOSEQ

Samples for Riboseq were prepared in accordance with McGlincy and Ingolia 2017. Briefly, 200 mL yeast strains carrying WT Hsp90 and G170D temperature sensitive Hsp90 were grown to OD_{595} 0.5-0.6 in YPD at 30°C. 100 mL of each culture was collected by filtration, resuspended in 100 mL YPD prewarmed to 37.5°C and incubated with shaking for 15 minutes.

Cultures at 30°C and 37.5°C were then collected by filtration, cells were scraped off the filter with a straight-edge metal spatula and plunged into liquid nitrogen in a 15 mL conical tube. 1.5 mL of lysis buffer (20 mM Tris pH 7.4, 150 mM NaCl, 5 mM $MgCl_2$, 1 mM DTT, 100 µg/mL CHX) was dripped into the liquid nitrogen containing 15 mL conical tube. Frozen cells and lysis buffer were ground using a pre-chilled mortar and pestle and lysate powder was allowed to thaw at 4°C in the 15 mL conical with a pierced cap to allow the liquid nitrogen to evaporate. RNA concentration of each cell lysate was determined using Quant-iT RiboGreen assay kit following manufacturer's instructions, 30 µg of RNA was diluted to 200 µl in lysis buffer and 1.5 µL of RNase I was added. Samples were incubated at room temperature with gentle agitation for 45 min. 10 µL SUPERase*In RNase inhibitor was added to stop the nuclease digestion and sample was transferred to a 13 mm x 51 mm polycarbonate ultracentrifuge tube on ice. Sucrose cushion of 0.9 mL was underlayed and ribosomes were pelleted by centrifugation in a TLA100.3 rotor at 100000 rpm, 4°C for 1 hour. Ribosomal pellet was resuspended in 300 µL TRIzol reagent and purified using Direct-zol kit according to manufacturer's instructions. RNA was precipitated overnight at -20°C. Footprint fragments in the size range of 17-34 nt were separated using a TBE-Urea polyacrylamide gel and excised. RNA was extracted from excised gel slice, dephosphorylated with T4 PNK and ligated to barcoded linkers. Samples were then pooled and purified. Ribosomal RNA was depleted using RiboMinus Eukaryote kit according to manufacturer's instructions. Reverse transcription was carried out and footprints were separated by gel electrophoresis and excised from the gel. Footprints were extracted from the gel, circularized, quantified by qPCR and library was generated by PCR using the number of cycles determined by qPCR. Library was sequenced on NovaSeq SP with a 50 bp single-end sequencing run.

4.17 RIBOSEQ BIONIFORMATIC ANALYSIS

Sequencing data was uploaded to the Galaxy web platform (Afgan *et. al.* 2018) and RiboGalaxy web platform (Michel *et. al.* 2016) and the public servers at usegalaxy.org and ribogalaxy.genomicsdatascience.ie were used to analyze the data. CutAdapt tool on Galaxy was used to removed the adapter from the reads and filter reads by size >11 after adapter removal. Barcode Splitter was then used to split the sequencing data into each individual sample followed by CutAdapt again to trim the barcode from the reads. UMI to header tool on RiboGalaxy was used to move the UMI from each read to the header. rRNA removal was carried out using Bowtie 2.0 on Galaxy with a custom index built using the ncRNA fasta file available on the Saccharomyces Cerevisiae Genome Database (SGD, rna_coding.fasta.gz). Unaligned reads were then aligned to orf_coding_all.fasta.gz from SGD.

Aligned bam files were processed through RiboWaltz (Lauria *et. al.* 2018) to generate Ribosome mRNA frame plots and read length distributions. Annotation file for RiboWaltz was generated using TxDB and annotation file was manually modified to set length of 5' and 3' UTR to 150 and transcript length to CDS+300. Automatic settings were used for analysis.

4.18 SINEFUNGIN SPOT TEST ASSAY

WT, G170D and Δsam3 strains were inoculated from overnight cultures to an OD595 of 0.25 and allowed to grow to OD_{595} 0.5-0.6. Cells were collected by centrifugation and resuspended in water to an OD_{595} of 1.0 following which 10-fold serial dilution was carried out and 5 µL of each dilution was spotted on YPD agar plates supplemented with 0/60/120 µL of 0.5 mM Sinefungin.

4.19 [3H] S-ADENOSYL-L-METHIONINE INCORPORATION

WT, G170D, Δsam3 and BY4741 cultures were grown from OD_{595} 0.25 to OD_{595} 0.5, Cell numbers for each strain were determined using a hemocytometer. [3H]-SAM at 1 mCi/mL was diluted a thousand fold and 25 µL was added to an aliquot (1 mL) of each culture. Cultures were collected by centrifugation 3 min after addition of [3H]-SAM and pellet was immediately chilled on ice and washed 2x with ice cold water. Pellet was resuspended in 50 µL ice cold water and added to 1 mL scintillation fluid in a scintillation vial. Scintillation counter set to read [3H] isotope averaging over 5 min for each vial was used to estimate incorporation of SAM as counts per minute (CPM)

4.20 QUANTIFICATION AND STATISTICAL ANALYSIS

All experiments were performed in 3 biological replicates. Additionally, in the microscopy experiments, at least 50 cells were counted in each condition. The error bars represent the SEM of the 3 biological replicates. Student's t-test (unpaired or paired when appropriate) was used to compare with WT or DMSO controls to determine significance.

4.21 TABLES

Table 4: Materials

REAGENT or RESOURCE		IDENTIFIER
Antibodies and Affinity Resin		
Anti TAP	ThermoFisher	CAB1001
Anti-His	ThermoFisher	MA1-21315
TALON Metal Affinity Resin	Takara Bio	635503
Bacterial and Virus Strains		
DH5α	N/A	N/A
Mammalian Cell Culture		
HeLa Cells	ATCC	CCL-2
Chemicals, Peptides, and Recombinant Proteins		
All chemicals unless otherwise noted	Sigma-Aldrich	N/A
Yeast Media Components	DIFCO	N/A
LB Media Components	DIFCO	N/A
p-Benzoyl-L-phenylalanine Bachem	Fisher Scientific	NC0169631
Radicicol	AG Scientific	R-1130
Ganetespib	Selleckchem	S1159
L-Azetidine-2-carboxylic Acid	TCI	A1043
Cycloheximide	GoldBio	C-930-10
D-Luciferin, Potassium salt	GoldBio	LUCK-100
Coelenterazine	GoldBio	CZ2.5
CPRG	Roche	99792-50-4
ATP [γ-^{32}P]	Perkin Elmer	BLU002Z250UC
SYPRO Ruby Protein Gel Stain	ThermoFisher	S12000
Restriction Enzymes	New England Biolabs	N/A
Critical Commercial Assays		
Pierce BCA Assay Kit	Fisher Scientific	PI23223
Power SYBR Green RNA-to-CT 1-Step kit	Applied Biosystems	4388869
In-Fusion Snap Assembly kit	Takara Bio	638946
Experimental Models: Organisms/Strains		
Saccharomyces cerevisiae	Strain Table S2	N/A
TAP tag strain library	Open Biosystems	YSC1177
Knockout library	Open Biosystems	
GFP Library	Maya Schuldiner	(Weizmann Institute)

Table 4 (cont.)

Oligonucleotides		
SSA4 qRT FP	GCTCAACGTGTTCAAGCTAA	N/A
SSA4 qRT RP	ACCCACCTTCTCCTTGAAGT	N/A
TAF10 qRT FP	TACGAATATTCCAGGATCAGG	N/A
TAF10 qRT RP	CAATAGCTGCCTAGCTCTC	N/A
Hsp70 qRT FP	CAGAGCGGAGCCGACAGAG	N/A
Hsp70 qRT RP	CCACCTTGCCGTGTTGGAAC	N/A
GAPDH qRT FP	ACACCCACTCCTCCACCTTTGAC	N/A
GAPDH qRT RP	ACCACCCTGTTGCTGTAGCCA	N/A
pGBK Hsc82 N FP	GAATTCCCGGGGATCATGGCTGGTG AAACTTTTGAATTTC	N/A
pGBK Hsc82 N RP	GCAGGTCGACGGATCCTTACTTAGT CTTGTTCAACTCTTCTAATTC	N/A
pGBK Hsc82 M FP	GAATTCCCGGGGATCGTTCCAATTC CAGAAGAAGAAAAGA	N/A
pGBK Hsc82 M RP	GCAGGTCGACGGATCCTTATTCTTC CAATTCGAAATCTTTAGT	N/A
pGBK Hsc82 C FP	GAATTCCCGGGGATCACTAAAGATT TCGAATTGGAAGAAA	N/A
pGBK Hsc82 C RP	GCAGGTCGACGGATCCTTAATCAAC TTCTTCCATCTCGGT	N/A
pGAD Hsc82 N FP	GGAGGCCAGTGAATTCATGGCTGGT GAAACTTTTGA	N/A
pGAD Hsc82 N RP	CACCCGGGTGGAATTTTACTTAGTC TTGTTCAACTCTTCT	N/A
pGAD Hsc82 M FP	GGAGGCCAGTGAATTCGTTCCAATT CCAGAAGAAGAAAAG	N/A
pGAD Hsc82 M RP	CACCCGGGTGGAATTTTATTCTTCCA ATTCGAAATCTTT	N/A
pGAD Hsc82 C FP	GGAGGCCAGTGAATTCACTAAAGAT TTCGAATTGGAAGAA	N/A
pGAD Hsc82 C RP	CACCCGGGTGGAATTTTAATCAACT TCTTCCATCTCGGTG	N/A
Hsc82 N FP	TTGTTGTCTAGAATGGCTGGTGAAA CTTTTGAATTTC	N/A
Hsc82 N RP	TTGTTGCTGCAGTTACTTAGTCTTGT TCAACTCTTCTAATTC	N/A
Hsc82 M FP	TTGTTGTCTAGAGTTCCAATTCCAGA AGAAGAAAAG	N/A
Hsc82 M RP	TTGTTGCTGCAGTTATTCTTCCAATT CGAAATCTTTAGT	N/A
Hsc82 C FP	TTGTTGTCTAGAACTAAAGATTTCG AATTGGAAGAA	N/A
Hsc82 C RP	TTGTTGCTGCAGTTAATCAACTTCTT CCATCTCGG	N/A

Table 4 (cont.)

Oligonucleotides		
pGBK Rsc3 FP	CATGGAGGCCGAATTCATGGATATTCGTGGTAGAAAAATG	N/A
pGBK Rsc3 RP	GGATCCCCGGGAATTTTAGCTACGAATAGCCTCAAAAAC	N/A
Rsc3 Del RP	TGTAATTTCTTGCAATTCC	N/A
Rsc3 Del FP 1	ATTCAGTATTTGATTGAACG	N/A
Rsc3 Del FP 2	ACTAATAAAGTTTTTAATGTGTTTAATTC	N/A
F120-BPA FP	GCCGATGTATCCATGATTGGTCAATAGGGTGTTGGTTTTTACTCTTTATTC	N/A
F120-BPA RP	GAATAAAGAGTAAAAACCAACACCCTATTGACCAATCATGGATACATCGGC	N/A
F325-BPA FP	TTGTTCATTCCAAAGAGAGCACCATAGGACTTATTTGAGAGTAAGAAGAAG	N/A
F325-BPA RP	CTTCTTCTTACTCTCAAATAAGTCCTATGGTGCTCTCTTTGGAATGAACAA	N/A
E427-BPA FP	AAGAACATTAAGCTGGGTGTACATTAGGACACTCAAAACAGAGCTGCTTTA	N/A
E427-BPA RP	TAAAGCAGCTCTGTTTTGAGTGTCCTAATGTACACCCAGCTTAATGTTCTT	N/A
F579-BPA FP	CATCAGAACTGGTCAATAGGGCTGGTCTGCTAACAT	N/A
F579-BPA RP	ATGTTAGCAGACCAGCCCTATTGACCAGTTCTGATG	N/A
E656-BPA FP	TTGACTTCTGGTTTCAGTTTGGAATAGCCAACTTCTTTTGCATCAAGAATA	N/A
E656-BPA RP	TATTCTTGATGCAAAAGAAGTTGGCTATTCCAAACTGAAACCAGAAGTCAA	N/A
ACC1_TIM23 F	ACGCGCGCGCGGCCGGGCCA	N/A
ACC1_TIM23 R	TGGCCCGGCCGCGCGCGCGT	N/A
Recombinant DNA		
pTGPD *HSP82*	S. Lindquist	N/A
pTGPD *hsp82* G170D	S. Lindquist	N/A
pSNR-tRNA-pBpaRS	A. Mapp	N/A
pRS313GPD His-Hsc82	E. Craig	N/A
pRS313GPD His-Hsc82 F120-BPA	This manuscript	N/A
pRS313GPD His-Hsc82 F325-BPA	This manuscript	N/A

Table 4 (cont.)

Recombinant DNA		
pRS313GPD His-Hsc82 E427-BPA	This manuscript	N/A
pRS313GPD His-Hsc82 F579-BPA	This manuscript	N/A
pRS313GPD His-Hsc82E656-BPA	This manuscript	N/A
pFJZ1052 (AUG)	J. Lorsch	N/A
pFJZ1054 (UUG)	J. Lorsch	N/A
pFJZ1055 (GUG)	J. Lorsch	N/A
pFJZ1056 (AUC)	J. Lorsch	N/A
pFJZ1057 (AUU)	J. Lorsch	N/A
pFJZ1058 (AUA)	J. Lorsch	N/A
pFJZ1059 (ACG)	J. Lorsch	N/A
pFJZ1060 (AAG)	J. Lorsch	N/A
pFJZ1061 (AGG)	J. Lorsch	N/A
pGADT7	Clonetech Matchmaker	630442
pGBKT7	Clonetech Matchmaker	630489
pGBKT7 Hsp82	Echtenkamp et al 2016	N/A
pGADT7 Hsp82	Echtenkamp et al 2016	N/A
pGADT7 Rsc3	Echtenkamp et al 2016	N/A
pGADT7 Rsc3 ΔIDR-1	This manuscript	N/A
pGADT7 Rsc3 ΔIDR-2	This manuscript	N/A
pGBKT7 Rsc3	This manuscript	N/A
pGBKT7 Rsc3 ΔIDR-1	This manuscript	N/A
pGBKT7 Rsc3 ΔIDR-2	This manuscript	N/A
pGADT7 Bas1	This manuscript	N/A
pGADT7 Aim3	This manuscript	N/A
pGADT7 Cue3	This manuscript	N/A
pGADT7 Saf1	This manuscript	N/A
pGADT7 Ume6	This manuscript	N/A
pGADT7 Whi2	This manuscript	N/A
pGADT7 Hsc82	This manuscript	N/A
pGADT7 Hsc82-N	This manuscript	N/A
pGADT7 Hsc82-M	This manuscript	N/A
pGADT7 Hsc82-C	This manuscript	N/A
pGADT7 Hsc82-NM	This manuscript	N/A
pGADT7 Hsc82-MC	This manuscript	N/A
pGBKT7 Hsc82	This manuscript	N/A
pGBKT7 Hsc82-N	This manuscript	N/A
pGBKT7 Hsc82-M	This manuscript	N/A
pGBKT7 Hsc82-C	This manuscript	N/A
pGBKT7 Hsc82-NM	This manuscript	N/A
pGBKT7 Hsc82-MC	This manuscript	N/A
p405 ADH1 3xHA Hsc82	This manuscript	N/A

Table 4 (cont.)

Recombinant DNA		
p405 ADH1 3xHA Hsc82-N	This manuscript	N/A
p405 ADH1 3xHA Hsc82-M	This manuscript	N/A
p405 ADH1 3xHA Hsc82-C	This manuscript	N/A
p405 ADH1 3xHA Hsc82-NM	This manuscript	N/A
p405 ADH1 3xHA Hsc82-MC	This manuscript	N/A
pET28a SUMO Rsc3	Echtenkamp et. al. 2016	N/A
pET28a SUMO Rsc3ΔIDR	This manuscript	N/A
pRS405 GAL1 3xNLS ACT1	Wang et. al. 2020	N/A
pRS405 GAL1 3xNLS Act1-R62D	Wang et. al. 2020	N/A
Software and Algorithms		
artMS	Jimenez-Morales et. al. 2022	N/A
MeroX	Götze et. al. 2014	

Table 5: Strains

Strain	Source
W3031-A	R. Rothstein
SL WT (W3031-A piH GpD/p82)	S. Lindquist
SL WT (W3031-A piH GpD/G170D)	S. Lindquist
JJ117	J. Johnson
JJ117 WT	This manuscript
JJ117 G170D	This manuscript
NDY05	Jason Brickner (Northwestern University)

REFERENCES

Afgan E, Baker D, Batut B, van den Beek M, Bouvier D, Cech M, Chilton J, Clements D, Coraor N, Grüning BA, Guerler A, Hillman-Jackson J, Hiltemann S, Jalili V, Rasche H, Soranzo N, Goecks J, Taylor J, Nekrutenko A, Blankenberg D. The Galaxy platform for accessible, reproducible and collaborative biomedical analyses: 2018 update. Nucleic Acids Res. 2018 Jul 2;46(W1):W537-W544. doi: 10.1093/nar/gky379. PMID: 29790989; PMCID: PMC6030816.

Ali MM, Roe SM, Vaughan CK, Meyer P, Panaretou B, Piper PW, Prodromou C, Pearl LH. Crystal structure of an Hsp90-nucleotide-p23/Sba1 closed chaperone complex. Nature. 2006 Apr 20;440(7087):1013-7. doi: 10.1038/nature04716. PMID: 16625188; PMCID: PMC5703407.

Balchin D, Miličić G, Strauss M, Hayer-Hartl M, Hartl FU. Pathway of Actin Folding Directed by the Eukaryotic Chaperonin TRiC. Cell. 2018 Sep 6;174(6):1507-1521.e16. doi: 10.1016/j.cell.2018.07.006. Epub 2018 Aug 9. PMID: 30100183.

Bardwell JC, Craig EA. Ancient heat shock gene is dispensable. J Bacteriol. 1988 Jul;170(7):2977-83. doi: 10.1128/jb.170.7.2977-2983.1988. Erratum in: J Bacteriol 1988 Oct;170(10):4999. PMID: 3290192; PMCID: PMC211237.

Biebl MM, Buchner J. Structure, Function, and Regulation of the Hsp90 Machinery. Cold Spring Harb Perspect Biol. 2019 Sep 3;11(9):a034017. doi: 10.1101/cshperspect.a034017. PMID: 30745292; PMCID: PMC6719599.

Borkovich KA, Farrelly FW, Finkelstein DB, Taulien J, Lindquist S. hsp82 is an essential protein that is required in higher concentrations for growth of cells at higher temperatures. Mol Cell Biol. 1989 Sep;9(9):3919-30. doi: 10.1128/mcb.9.9.3919-3930.1989. PMID: 2674684; PMCID: PMC362454.

Brehme M, Voisine C, Rolland T, Wachi S, Soper JH, Zhu Y, Orton K, Villella A, Garza D, Vidal M, Ge H, Morimoto RI. A chaperome subnetwork safeguards proteostasis in aging and neurodegenerative disease. Cell Rep. 2014 Nov 6;9(3):1135-50. doi: 10.1016/j.celrep.2014.09.042. Epub 2014 Oct 23. PMID: 25437566; PMCID: PMC4255334.

Brugge J, Yonemoto W, Darrow D. Interaction between the Rous sarcoma virus transforming protein and two cellular phosphoproteins: analysis of the turnover and distribution of this complex. Mol Cell Biol. 1983 Jan;3(1):9-19. doi: 10.1128/mcb.3.1.9-19.1983. PMID: 6298609; PMCID: PMC368498.

Brugge JS, Erikson E, Erikson RL. The specific interaction of the Rous sarcoma virus transforming protein, pp60src, with two cellular proteins. Cell. 1981 Aug;25(2):363-72. doi: 10.1016/0092-8674(81)90055-6. PMID: 6269742.

Buchner J. Hsp90 & Co. - a holding for folding. Trends Biochem Sci. 1999 Apr;24(4):136-41. doi: 10.1016/s0968-0004(99)01373-0. PMID: 10322418.

Catelli MG, Binart N, Jung-Testas I, Renoir JM, Baulieu EE, Feramisco JR, Welch WJ. The common 90-kd protein component of non-transformed '8S' steroid receptors is a heat-shock protein. EMBO J. 1985 Dec 1;4(12):3131-5. doi: 10.1002/j.1460-2075.1985.tb04055.x. PMID: 2419124; PMCID: PMC554632.

Catlett MG, Kaplan KB. Sgt1p is a unique co-chaperone that acts as a client adaptor to link Hsp90 to Skp1p. J Biol Chem. 2006 Nov 3;281(44):33739-48. doi: 10.1074/jbc.M603847200. Epub 2006 Aug 31. PMID: 16945921.

Chen B, Zhong D, Monteiro A. Comparative genomics and evolution of the HSP90 family of genes across all kingdoms of organisms. BMC Genomics. 2006 Jun 17;7:156. doi: 10.1186/1471-2164-7-156. PMID: 16780600; PMCID: PMC1525184.

Chin JW, Martin AB, King DS, Wang L, Schultz PG. Addition of a photocrosslinking amino acid to the genetic code of Escherichiacoli. Proc Natl Acad Sci U S A. 2002 Aug 20;99(17):11020-4. doi: 10.1073/pnas.172226299. Epub 2002 Aug 1. PMID: 12154230; PMCID: PMC123203.

Collins MO, Yu L, Campuzano I, Grant SG, Choudhary JS. Phosphoproteomic analysis of the mouse brain cytosol reveals a predominance of protein phosphorylation in regions of intrinsic sequence disorder. Mol Cell Proteomics. 2008 Jul;7(7):1331-48. doi: 10.1074/mcp.M700564-MCP200. Epub 2008 Apr 3. PMID: 18388127.

Courtneidge SA, Bishop JM. Transit of pp60v-src to the plasma membrane. Proc Natl Acad Sci U S A. 1982 Dec;79(23):7117-21. doi: 10.1073/pnas.79.23.7117. PMID: 6296817; PMCID: PMC347289.

Cuéllar J, Ludlam WG, Tensmeyer NC, Aoba T, Dhavale M, Santiago C, Bueno-Carrasco MT, Mann MJ, Plimpton RL, Makaju A, Franklin S, Willardson BM, Valpuesta JM. Structural and functional analysis of the role of the chaperonin CCT in mTOR complex assembly. Nat Commun. 2019 Jun 28;10(1):2865. doi: 10.1038/s41467-019-10781-1. PMID: 31253771; PMCID: PMC6599039.

Cunningham CN, Krukenberg KA, Agard DA. Intra- and intermonomer interactions are required to synergistically facilitate ATP hydrolysis in Hsp90. J Biol Chem. 2008 Jul 25;283(30):21170-8. doi: 10.1074/jbc.M800046200. Epub 2008 May 20. PMID: 18492664; PMCID: PMC2475720.

Czar MJ, Galigniana MD, Silverstein AM, Pratt WB. Geldanamycin, a heat shock protein 90-binding benzoquinone ansamycin, inhibits steroid-dependent translocation of the glucocorticoid receptor from the cytoplasm to the nucleus. Biochemistry. 1997 Jun 24;36(25):7776-85. doi: 10.1021/bi970648x. PMID: 9201920.

Daturpalli S, Waudby CA, Meehan S, Jackson SE. Hsp90 inhibits α-synuclein aggregation by interacting with soluble oligomers. J Mol Biol. 2013 Nov 15;425(22):4614-28. doi: 10.1016/j.jmb.2013.08.006. Epub 2013 Aug 13. PMID: 23948507.

DeZwaan DC, Toogun OA, Echtenkamp FJ, Freeman BC. The Hsp82 molecular chaperone promotes a switch between unextendable and extendable telomere states. Nat Struct Mol Biol. 2009 Jul;16(7):711-6. doi: 10.1038/nsmb.1616. Epub 2009 Jun 14. PMID: 19525972; PMCID: PMC2744139.

Dollins DE, Warren JJ, Immormino RM, Gewirth DT. Structures of GRP94-nucleotide complexes reveal mechanistic differences between the hsp90 chaperones. Mol Cell. 2007 Oct 12;28(1):41-56. doi: 10.1016/j.molcel.2007.08.024. PMID: 17936703; PMCID: PMC2094010.

Dormán G, Prestwich GD. Benzophenone photophores in biochemistry. Biochemistry. 1994 May 17;33(19):5661-73. doi: 10.1021/bi00185a001. PMID: 8180191.

Dyson HJ, Wright PE. Intrinsically unstructured proteins and their functions. Nat Rev Mol Cell Biol. 2005 Mar;6(3):197-208. doi: 10.1038/nrm1589. PMID: 15738986.

Echtenkamp FJ, Gvozdenov Z, Adkins NL, Zhang Y, Lynch-Day M, Watanabe S, Peterson CL, Freeman BC. Hsp90 and p23 Molecular Chaperones Control Chromatin Architecture by Maintaining the Functional Pool of the RSC Chromatin Remodeler. Mol Cell. 2016 Dec 1;64(5):888-899. doi: 10.1016/j.molcel.2016.09.040. Epub 2016 Nov 3. PMID: 27818141; PMCID: PMC7774989.

Evans CG, Wisén S, Gestwicki JE. Heat shock proteins 70 and 90 inhibit early stages of amyloid beta-(1-42) aggregation in vitro. J Biol Chem. 2006 Nov 3;281(44):33182-91. doi: 10.1074/jbc.M606192200. Epub 2006 Sep 14. PMID: 16973602.

Falsone SF, Gesslbauer B, Tirk F, Piccinini AM, Kungl AJ. A proteomic snapshot of the human heat shock protein 90 interactome. FEBS Lett. 2005 Nov 21;579(28):6350-4. doi: 10.1016/j.febslet.2005.10.020. Epub 2005 Oct 24. PMID: 16263121.

Falsone SF, Kungl AJ, Rek A, Cappai R, Zangger K. The molecular chaperone Hsp90 modulates intermediate steps of amyloid assembly of the Parkinson-related protein alpha-synuclein. J Biol Chem. 2009 Nov 6;284(45):31190-9. doi: 10.1074/jbc.M109.057240. Epub 2009 Sep 15. PMID: 19759002; PMCID: PMC2781518.

Flaherty KM, DeLuca-Flaherty C, McKay DB. Three-dimensional structure of the ATPase fragment of a 70K heat-shock cognate protein. Nature. 1990 Aug 16;346(6285):623-8. doi: 10.1038/346623a0. PMID: 2143562.

Freeman BC, Yamamoto KR. Disassembly of transcriptional regulatory complexes by molecular chaperones. Science. 2002 Jun 21;296(5576):2232-5. doi: 10.1126/science.1073051. PMID: 12077419.

Frydman J, Nimmesgern E, Ohtsuka K, Hartl FU. Folding of nascent polypeptide chains in a high molecular mass assembly with molecular chaperones. Nature. 1994 Jul 14;370(6485):111-7. doi: 10.1038/370111a0. PMID: 8022479.

Gestaut D, Roh SH, Ma B, Pintilie G, Joachimiak LA, Leitner A, Walzthoeni T, Aebersold R, Chiu W, Frydman J. The Chaperonin TRiC/CCT Associates with Prefoldin through a Conserved

Electrostatic Interface Essential for Cellular Proteostasis. Cell. 2019 Apr 18;177(3):751-765.e15. doi: 10.1016/j.cell.2019.03.012. Epub 2019 Apr 4. PMID: 30955883; PMCID: PMC6629582.

Girstmair H, Tippel F, Lopez A, Tych K, Stein F, Haberkant P, Schmid PWN, Helm D, Rief M, Sattler M, Buchner J. The Hsp90 isoforms from S. cerevisiae differ in structure, function and client range. Nat Commun. 2019 Aug 9;10(1):3626. doi: 10.1038/s41467-019-11518-w. PMID: 31399574; PMCID: PMC6689086.

Götze M, Pettelkau J, Fritzsche R, Ihling CH, Schäfer M, Sinz A. Automated assignment of MS/MS cleavable cross-links in protein 3D-structure analysis. J Am Soc Mass Spectrom. 2015 Jan;26(1):83-97. doi: 10.1007/s13361-014-1001-1. Epub 2014 Sep 27. PMID: 25261217.

Guenther UP, Weinberg DE, Zubradt MM, Tedeschi FA, Stawicki BN, Zagore LL, Brar GA, Licatalosi DD, Bartel DP, Weissman JS, Jankowsky E. The helicase Ded1p controls use of near-cognate translation initiation codons in 5' UTRs. Nature. 2018 Jul;559(7712):130-134. doi: 10.1038/s41586-018-0258-0. Epub 2018 Jun 27. PMID: 29950728; PMCID: PMC6226265.

Hainzl O, Lapina MC, Buchner J, Richter K. The charged linker region is an important regulator of Hsp90 function. J Biol Chem. 2009 Aug 21;284(34):22559-67. doi: 10.1074/jbc.M109.031658. Epub 2009 Jun 24. PMID: 19553666; PMCID: PMC2755663.

Harris SF, Shiau AK, Agard DA. The crystal structure of the carboxy-terminal dimerization domain of htpG, the Escherichia coli Hsp90, reveals a potential substrate binding site. Structure. 2004 Jun;12(6):1087-97. doi: 10.1016/j.str.2004.03.020. PMID: 15274928.

Hellenkamp B, Wortmann P, Kandzia F, Zacharias M, Hugel T. Multidomain structure and correlated dynamics determined by self-consistent FRET networks. Nat Methods. 2017 Feb;14(2):174-180. doi: 10.1038/nmeth.4081. Epub 2016 Dec 5. PMID: 27918541; PMCID: PMC5289555.

Hershey JW, Sonenberg N, Mathews MB. Principles of translational control: an overview. Cold Spring Harb Perspect Biol. 2012 Dec 1;4(12):a011528. doi: 10.1101/cshperspect.a011528. PMID: 23209153; PMCID: PMC3504442.

Iakoucheva LM, Radivojac P, Brown CJ, O'Connor TR, Sikes JG, Obradovic Z, Dunker AK. The importance of intrinsic disorder for protein phosphorylation. Nucleic Acids Res. 2004 Feb 11;32(3):1037-49. doi: 10.1093/nar/gkh253. PMID: 14960716; PMCID: PMC373391.

Iserman C, Desroches Altamirano C, Jegers C, Friedrich U, Zarin T, Fritsch AW, Mittasch M, Domingues A, Hersemann L, Jahnel M, Richter D, Guenther UP, Hentze MW, Moses AM, Hyman AA, Kramer G, Kreysing M, Franzmann TM, Alberti S. Condensation of Ded1p Promotes a Translational Switch from Housekeeping to Stress Protein Production. Cell. 2020 May 14;181(4):818-831.e19. doi: 10.1016/j.cell.2020.04.009. Epub 2020 Apr 30. PMID: 32359423; PMCID: PMC7237889.

Jahn M, Rehn A, Pelz B, Hellenkamp B, Richter K, Rief M, Buchner J, Hugel T. The charged linker of the molecular chaperone Hsp90 modulates domain contacts and biological function.

Proc Natl Acad Sci U S A. 2014 Dec 16;111(50):17881-6. doi: 10.1073/pnas.1414073111. Epub 2014 Dec 2. PMID: 25468961; PMCID: PMC4273377.

Jarosz DF, Lindquist S. Hsp90 and environmental stress transform the adaptive value of natural genetic variation. Science. 2010 Dec 24;330(6012):1820-4. doi: 10.1126/science.1195487. PMID: 21205668; PMCID: PMC3260023.

Jayaraj GG, Hipp MS, Hartl FU. Functional Modules of the Proteostasis Network. Cold Spring Harb Perspect Biol. 2020 Jan 2;12(1):a033951. doi: 10.1101/cshperspect.a033951. PMID: 30833457; PMCID: PMC6942124.

Joab I, Radanyi C, Renoir M, Buchou T, Catelli MG, Binart N, Mester J, Baulieu EE. Common non-hormone binding component in non-transformed chick oviduct receptors of four steroid hormones. Nature. 1984 Apr 26-May 2;308(5962):850-3. doi: 10.1038/308850a0. PMID: 6201744.

Joachimiak LA, Walzthoeni T, Liu CW, Aebersold R, Frydman J. The structural basis of substrate recognition by the eukaryotic chaperonin TRiC/CCT. Cell. 2014 Nov 20;159(5):1042-1055. doi: 10.1016/j.cell.2014.10.042. PMID: 25416944; PMCID: PMC4298165.

Johnson BD, Schumacher RJ, Ross ED, Toft DO. Hop modulates Hsp70/Hsp90 interactions in protein folding. J Biol Chem. 1998 Feb 6;273(6):3679-86. doi: 10.1074/jbc.273.6.3679. PMID: 9452498.

Johnson JL, Toft DO. A novel chaperone complex for steroid receptors involving heat shock proteins, immunophilins, and p23. J Biol Chem. 1994 Oct 7;269(40):24989-93. PMID: 7929183.

Jumper J, Evans R, Pritzel A, Green T, Figurnov M, Ronneberger O, Tunyasuvunakool K, Bates R, Žídek A, Potapenko A, Bridgland A, Meyer C, Kohl SAA, Ballard AJ, Cowie A, Romera-Paredes B, Nikolov S, Jain R, Adler J, Back T, Petersen S, Reiman D, Clancy E, Zielinski M, Steinegger M, Pacholska M, Berghammer T, Bodenstein S, Silver D, Vinyals O, Senior AW, Kavukcuoglu K, Kohli P, Hassabis D. Highly accurate protein structure prediction with AlphaFold. Nature. 2021 Aug;596(7873):583-589. doi: 10.1038/s41586-021-03819-2. Epub 2021 Jul 15. PMID: 34265844; PMCID: PMC8371605.

Koulov AV, LaPointe P, Lu B, Razvi A, Coppinger J, Dong MQ, Matteson J, Laister R, Arrowsmith C, Yates JR 3rd, Balch WE. Biological and structural basis for Aha1 regulation of Hsp90 ATPase activity in maintaining proteostasis in the human disease cystic fibrosis. Mol Biol Cell. 2010 Mar 15;21(6):871-84. doi: 10.1091/mbc.e09-12-1017. Epub 2010 Jan 20. PMID: 20089831; PMCID: PMC2836968.

Krishnamurthy M, Dugan A, Nwokoye A, Fung YH, Lancia JK, Majmudar CY, Mapp AK. Caught in the act: covalent cross-linking captures activator-coactivator interactions in vivo. ACS Chem Biol. 2011 Dec 16;6(12):1321-6. doi: 10.1021/cb200308e. Epub 2011 Nov 14. PMID: 21977905; PMCID: PMC3245988.

Kriwacki RW, Hengst L, Tennant L, Reed SI, Wright PE. Structural studies of p21Waf1/Cip1/Sdi1 in the free and Cdk2-bound state: conformational disorder mediates binding

diversity. Proc Natl Acad Sci U S A. 1996 Oct 15;93(21):11504-9. doi: 10.1073/pnas.93.21.11504. PMID: 8876165; PMCID: PMC38087.

Labbadia J, Morimoto RI. The biology of proteostasis in aging and disease. Annu Rev Biochem. 2015;84:435-64. doi: 10.1146/annurev-biochem-060614-033955. Epub 2015 Mar 12. PMID: 25784053; PMCID: PMC4539002.

Lackie RE, Maciejewski A, Ostapchenko VG, Marques-Lopes J, Choy WY, Duennwald ML, Prado VF, Prado MAM. The Hsp70/Hsp90 Chaperone Machinery in Neurodegenerative Diseases. Front Neurosci. 2017 May 16;11:254. doi: 10.3389/fnins.2017.00254. PMID: 28559789; PMCID: PMC5433227.

Langer T, Pfeifer G, Martin J, Baumeister W, Hartl FU. Chaperonin-mediated protein folding: GroES binds to one end of the GroEL cylinder, which accommodates the protein substrate within its central cavity. EMBO J. 1992 Dec;11(13):4757-65. doi: 10.1002/j.1460-2075.1992.tb05581.x. PMID: 1361169; PMCID: PMC556951.

Laskowski RA, Thornton JM. Understanding the molecular machinery of genetics through 3D structures. Nat Rev Genet. 2008 Feb;9(2):141-51. doi: 10.1038/nrg2273. PMID: 18160966.

Lauria F, Tebaldi T, Bernabò P, Groen EJN, Gillingwater TH, Viero G. riboWaltz: Optimization of ribosome P-site positioning in ribosome profiling data. PLoS Comput Biol. 2018 Aug 13;14(8):e1006169. doi: 10.1371/journal.pcbi.1006169. PMID: 30102689; PMCID: PMC6112680.

Lee K, Ziegelhoffer T, Delewski W, Berger SE, Sabat G, Craig EA. Pathway of Hsp70 interactions at the ribosome. Nat Commun. 2021 Sep 27;12(1):5666. doi: 10.1038/s41467-021-25930-8. PMID: 34580293; PMCID: PMC8476630.

Li B, Fields S. Identification of mutations in p53 that affect its binding to SV40 large T antigen by using the yeast two-hybrid system. FASEB J. 1993 Jul;7(10):957-63. doi: 10.1096/fasebj.7.10.8344494. PMID: 8344494.

Li J, Richter K, Buchner J. Mixed Hsp90-cochaperone complexes are important for the progression of the reaction cycle. Nat Struct Mol Biol. 2011 Jan;18(1):61-6. doi: 10.1038/nsmb.1965. Epub 2010 Dec 19. PMID: 21170051.

Li J, Richter K, Reinstein J, Buchner J. Integration of the accelerator Aha1 in the Hsp90 co-chaperone cycle. Nat Struct Mol Biol. 2013 Mar;20(3):326-31. doi: 10.1038/nsmb.2502. Epub 2013 Feb 10. PMID: 23396352.

Liu CC, Schultz PG. Adding new chemistries to the genetic code. Annu Rev Biochem. 2010;79:413-44. doi: 10.1146/annurev.biochem.052308.105824. PMID: 20307192.

Lopez T, Dalton K, Frydman J. The Mechanism and Function of Group II Chaperonins. J Mol Biol. 2015 Sep 11;427(18):2919-30. doi: 10.1016/j.jmb.2015.04.013. Epub 2015 Apr 30. PMID: 25936650; PMCID: PMC4706738.

Louvion JF, Warth R, Picard D. Two eukaryote-specific regions of Hsp82 are dispensable for its viability and signal transduction functions in yeast. Proc Natl Acad Sci U S A. 1996 Nov 26;93(24):13937-42. doi: 10.1073/pnas.93.24.13937. PMID: 8943039; PMCID: PMC19473.

Marsh JA, Kalton HM, Gaber RF. Cns1 is an essential protein associated with the hsp90 chaperone complex in Saccharomyces cerevisiae that can restore cyclophilin 40-dependent functions in cpr7Delta cells. Mol Cell Biol. 1998 Dec;18(12):7353-9. doi: 10.1128/MCB.18.12.7353. PMID: 9819422; PMCID: PMC109317.

McClellan AJ, Xia Y, Deutschbauer AM, Davis RW, Gerstein M, Frydman J. Diverse cellular functions of the Hsp90 molecular chaperone uncovered using systems approaches. Cell. 2007 Oct 5;131(1):121-35. doi: 10.1016/j.cell.2007.07.036. PMID: 17923092.

McGlincy NJ, Ingolia NT. Transcriptome-wide measurement of translation by ribosome profiling. Methods. 2017 Aug 15;126:112-129. doi: 10.1016/j.ymeth.2017.05.028. Epub 2017 Jun 1. PMID: 28579404; PMCID: PMC5582988.

McLaughlin SH, Smith HW, Jackson SE. Stimulation of the weak ATPase activity of human hsp90 by a client protein. J Mol Biol. 2002 Jan 25;315(4):787-98. doi: 10.1006/jmbi.2001.5245. PMID: 11812147.

Mercier R, LaPointe P. The role of cellular proteostasis in antitumor immunity. J Biol Chem. 2022 May;298(5):101930. doi: 10.1016/j.jbc.2022.101930. Epub 2022 Apr 11. PMID: 35421375; PMCID: PMC9108985.

Meyer P, Prodromou C, Hu B, Vaughan C, Roe SM, Panaretou B, Piper PW, Pearl LH. Structural and functional analysis of the middle segment of hsp90: implications for ATP hydrolysis and client protein and cochaperone interactions. Mol Cell. 2003 Mar;11(3):647-58. doi: 10.1016/s1097-2765(03)00065-0. PMID: 12667448.

Meyer P, Prodromou C, Liao C, Hu B, Mark Roe S, Vaughan CK, Vlasic I, Panaretou B, Piper PW, Pearl LH. Structural basis for recruitment of the ATPase activator Aha1 to the Hsp90 chaperone machinery. EMBO J. 2004 Feb 11;23(3):511-9. doi: 10.1038/sj.emboj.7600060. Epub 2004 Jan 22. Erratum in: EMBO J. 2004 Mar 24;23(6):1402. Corrected and republished in: EMBO J. 2004 Mar 24;23(6):1402-10. PMID: 14739935; PMCID: PMC1271799.

Michel AM, Mullan JP, Velayudhan V, O'Connor PB, Donohue CA, Baranov PV. RiboGalaxy: A browser based platform for the alignment, analysis and visualization of ribosome profiling data. RNA Biol. 2016;13(3):316-9. doi: 10.1080/15476286.2016.1141862. Epub 2016 Jan 29. PMID: 26821742; PMCID: PMC4829337.

Millson SH, Truman AW, King V, Prodromou C, Pearl LH, Piper PW. A two-hybrid screen of the yeast proteome for Hsp90 interactors uncovers a novel Hsp90 chaperone requirement in the activity of a stress-activated mitogen-activated protein kinase, Slt2p (Mpk1p). Eukaryot Cell. 2005 May;4(5):849-60. doi: 10.1128/EC.4.5.849-860.2005. PMID: 15879519; PMCID: PMC1140089.

Millson SH, Truman AW, Wolfram F, King V, Panaretou B, Prodromou C, Pearl LH, Piper PW. Investigating the protein-protein interactions of the yeast Hsp90 chaperone system by two-hybrid analysis: potential uses and limitations of this approach. Cell Stress Chaperones. 2004 Winter;9(4):359-68. doi: 10.1379/csc-29r1.1. PMID: 15633294; PMCID: PMC1065275.

Minet E, Mottet D, Michel G, Roland I, Raes M, Remacle J, Michiels C. Hypoxia-induced activation of HIF-1: role of HIF-1alpha-Hsp90 interaction. FEBS Lett. 1999 Oct 29;460(2):251-6. doi: 10.1016/s0014-5793(99)01359-9. PMID: 10544245.

Mishra P, Bolon DN. Designed Hsp90 heterodimers reveal an asymmetric ATPase-driven mechanism in vivo. Mol Cell. 2014 Jan 23;53(2):344-50. doi: 10.1016/j.molcel.2013.12.024. PMID: 24462207; PMCID: PMC3923517.

Miyata Y, Nakamoto H, Neckers L. The therapeutic target Hsp90 and cancer hallmarks. Curr Pharm Des. 2013;19(3):347-65. doi: 10.2174/138161213804143725. PMID: 22920906; PMCID: PMC7553218.

Mollapour M, Tsutsumi S, Neckers L. Hsp90 phosphorylation, Wee1 and the cell cycle. Cell Cycle. 2010 Jun 15;9(12):2310-6. doi: 10.4161/cc.9.12.12054. Epub 2010 Jun 15. PMID: 20519952; PMCID: PMC7316391.

Murzin AG, Brenner SE, Hubbard T, Chothia C. SCOP: a structural classification of proteins database for the investigation of sequences and structures. J Mol Biol. 1995 Apr 7;247(4):536-40. doi: 10.1006/jmbi.1995.0159. PMID: 7723011.

Nathan DF, Lindquist S. Mutational analysis of Hsp90 function: interactions with a steroid receptor and a protein kinase. Mol Cell Biol. 1995 Jul;15(7):3917-25. doi: 10.1128/MCB.15.7.3917. PMID: 7791797; PMCID: PMC230631.

Neckers L, Workman P. Hsp90 molecular chaperone inhibitors: are we there yet? Clin Cancer Res. 2012 Jan 1;18(1):64-76. doi: 10.1158/1078-0432.CCR-11-1000. PMID: 22215907; PMCID: PMC3252205.

Oates ME, Romero P, Ishida T, Ghalwash M, Mizianty MJ, Xue B, Dosztányi Z, Uversky VN, Obradovic Z, Kurgan L, Dunker AK, Gough J. D²P²: database of disordered protein predictions. Nucleic Acids Res. 2013 Jan;41(Database issue):D508-16. doi: 10.1093/nar/gks1226. Epub 2012 Nov 29. PMID: 23203878; PMCID: PMC3531159.

Obermann WM, Sondermann H, Russo AA, Pavletich NP, Hartl FU. In vivo function of Hsp90 is dependent on ATP binding and ATP hydrolysis. J Cell Biol. 1998 Nov 16;143(4):901-10. doi: 10.1083/jcb.143.4.901. PMID: 9817749; PMCID: PMC2132952.

Oppermann H, Levinson W, Bishop JM. A cellular protein that associates with the transforming protein of Rous sarcoma virus is also a heat-shock protein. Proc Natl Acad Sci U S A. 1981 Feb;78(2):1067-71. doi: 10.1073/pnas.78.2.1067. PMID: 6262754; PMCID: PMC319947.

Panaretou B, Prodromou C, Roe SM, O'Brien R, Ladbury JE, Piper PW, Pearl LH. ATP binding and hydrolysis are essential to the function of the Hsp90 molecular chaperone in vivo. EMBO J.

1998 Aug 17;17(16):4829-36. doi: 10.1093/emboj/17.16.4829. PMID: 9707442; PMCID: PMC1170812.

Panaretou B, Siligardi G, Meyer P, Maloney A, Sullivan JK, Singh S, Millson SH, Clarke PA, Naaby-Hansen S, Stein R, Cramer R, Mollapour M, Workman P, Piper PW, Pearl LH, Prodromou C. Activation of the ATPase activity of hsp90 by the stress-regulated cochaperone aha1. Mol Cell. 2002 Dec;10(6):1307-18. doi: 10.1016/s1097-2765(02)00785-2. PMID: 12504007.

Parsell DA, Kowal AS, Singer MA, Lindquist S. Protein disaggregation mediated by heat-shock protein Hsp104. Nature. 1994 Dec 1;372(6505):475-8. doi: 10.1038/372475a0. PMID: 7984243.

Picard D, Khursheed B, Garabedian MJ, Fortin MG, Lindquist S, Yamamoto KR. Reduced levels of hsp90 compromise steroid receptor action in vivo. Nature. 1990 Nov 8;348(6297):166-8. doi: 10.1038/348166a0. PMID: 2234079.

Powers ET, Morimoto RI, Dillin A, Kelly JW, Balch WE. Biological and chemical approaches to diseases of proteostasis deficiency. Annu Rev Biochem. 2009;78:959-91. doi: 10.1146/annurev.biochem.052308.114844. PMID: 19298183.

Pratt WB, Toft DO. Steroid receptor interactions with heat shock protein and immunophilin chaperones. Endocr Rev. 1997 Jun;18(3):306-60. doi: 10.1210/edrv.18.3.0303. PMID: 9183567.

Prodromou C, Roe SM, O'Brien R, Ladbury JE, Piper PW, Pearl LH. Identification and structural characterization of the ATP/ADP-binding site in the Hsp90 molecular chaperone. Cell. 1997 Jul 11;90(1):65-75. doi: 10.1016/s0092-8674(00)80314-1. PMID: 9230303.

Prodromou C, Siligardi G, O'Brien R, Woolfson DN, Regan L, Panaretou B, Ladbury JE, Piper PW, Pearl LH. Regulation of Hsp90 ATPase activity by tetratricopeptide repeat (TPR)-domain co-chaperones. EMBO J. 1999 Feb 1;18(3):754-62. doi: 10.1093/emboj/18.3.754. PMID: 9927435; PMCID: PMC1171168.

Protter DSW, Parker R. Principles and Properties of Stress Granules. Trends Cell Biol. 2016 Sep;26(9):668-679. doi: 10.1016/j.tcb.2016.05.004. Epub 2016 Jun 9. PMID: 27289443; PMCID: PMC4993645.

Putcha P, Danzer KM, Kranich LR, Scott A, Silinski M, Mabbett S, Hicks CD, Veal JM, Steed PM, Hyman BT, McLean PJ. Brain-permeable small-molecule inhibitors of Hsp90 prevent alpha-synuclein oligomer formation and rescue alpha-synuclein-induced toxicity. J Pharmacol Exp Ther. 2010 Mar;332(3):849-57. doi: 10.1124/jpet.109.158436. Epub 2009 Nov 24. PMID: 19934398; PMCID: PMC2835433.

Queitsch C, Sangster TA, Lindquist S. Hsp90 as a capacitor of phenotypic variation. Nature. 2002 Jun 6;417(6889):618-24. doi: 10.1038/nature749. Epub 2002 May 12. PMID: 12050657.

Richter K, Muschler P, Hainzl O, Reinstein J, Buchner J. Sti1 is a non-competitive inhibitor of the Hsp90 ATPase. Binding prevents the N-terminal dimerization reaction during the atpase

cycle. J Biol Chem. 2003 Mar 21;278(12):10328-33. doi: 10.1074/jbc.M213094200. Epub 2003 Jan 13. PMID: 12525481.

Richter K, Walter S, Buchner J. The Co-chaperone Sba1 connects the ATPase reaction of Hsp90 to the progression of the chaperone cycle. J Mol Biol. 2004 Oct 1;342(5):1403-13. doi: 10.1016/j.jmb.2004.07.064. PMID: 15364569.

Ritossa F. Discovery of the heat shock response. Cell Stress Chaperones. 1996 Jun;1(2):97-8. doi: 10.1379/1466-1268(1996)001<0097:dothsr>2.3.co;2. PMID: 9222594; PMCID: PMC248460.

Roe SM, Ali MM, Meyer P, Vaughan CK, Panaretou B, Piper PW, Prodromou C, Pearl LH. The Mechanism of Hsp90 regulation by the protein kinase-specific cochaperone p50(cdc37). Cell. 2004 Jan 9;116(1):87-98. doi: 10.1016/s0092-8674(03)01027-4. PMID: 14718169.

Rohner N, Jarosz DF, Kowalko JE, Yoshizawa M, Jeffery WR, Borowsky RL, Lindquist S, Tabin CJ. Cryptic variation in morphological evolution: HSP90 as a capacitor for loss of eyes in cavefish. Science. 2013 Dec 13;342(6164):1372-5. doi: 10.1126/science.1240276. PMID: 24337296; PMCID: PMC4004346.

Rommelaere H, Van Troys M, Gao Y, Melki R, Cowan NJ, Vandekerckhove J, Ampe C. Eukaryotic cytosolic chaperonin contains t-complex polypeptide 1 and seven related subunits. Proc Natl Acad Sci U S A. 1993 Dec 15;90(24):11975-9. doi: 10.1073/pnas.90.24.11975. PMID: 7903455; PMCID: PMC48108.

Rosenzweig R, Nillegoda NB, Mayer MP, Bukau B. The Hsp70 chaperone network. Nat Rev Mol Cell Biol. 2019 Nov;20(11):665-680. doi: 10.1038/s41580-019-0133-3. PMID: 31253954.

Rouillon A, Surdin-Kerjan Y, Thomas D. Transport of sulfonium compounds. Characterization of the s-adenosylmethionine and s-methylmethionine permeases from the yeast Saccharomyces cerevisiae. J Biol Chem. 1999 Oct 1;274(40):28096-105. doi: 10.1074/jbc.274.40.28096. Erratum in: J Biol Chem 1999 Nov 19;274(47):33825. PMID: 10497160.

Rudiger S, Freund SM, Veprintsev DB, Fersht AR. CRINEPT-TROSY NMR reveals p53 core domain bound in an unfolded form to the chaperone Hsp90. Proc Natl Acad Sci U S A. 2002 Aug 20;99(17):11085-90. doi: 10.1073/pnas.132393699. Epub 2002 Aug 5. PMID: 12163643; PMCID: PMC123214.

Rutherford SL, Lindquist S. Hsp90 as a capacitor for morphological evolution. Nature. 1998 Nov 26;396(6709):336-42. doi: 10.1038/24550. PMID: 9845070.

Rutherford SL, Lindquist S. Hsp90 as a capacitor for morphological evolution. Nature. 1998 Nov 26;396(6709):336-42. doi: 10.1038/24550. PMID: 9845070.

Sanchez ER, Toft DO, Schlesinger MJ, Pratt WB. Evidence that the 90-kDa phosphoprotein associated with the untransformed L-cell glucocorticoid receptor is a murine heat shock protein. J Biol Chem. 1985 Oct 15;260(23):12398-401. PMID: 3900074.

Scheibel T, Neuhofen S, Weikl T, Mayr C, Reinstein J, Vogel PD, Buchner J. ATP-binding properties of human Hsp90. J Biol Chem. 1997 Jul 25;272(30):18608-13. doi: 10.1074/jbc.272.30.18608. PMID: 9228028.

Schopf FH, Biebl MM, Buchner J. The HSP90 chaperone machinery. Nat Rev Mol Cell Biol. 2017 Jun;18(6):345-360. doi: 10.1038/nrm.2017.20. Epub 2017 Apr 21. PMID: 28429788.

Schopf FH, Huber EM, Dodt C, Lopez A, Biebl MM, Rutz DA, Mühlhofer M, Richter G, Madl T, Sattler M, Groll M, Buchner J. The Co-chaperone Cns1 and the Recruiter Protein Hgh1 Link Hsp90 to Translation Elongation via Chaperoning Elongation Factor 2. Mol Cell. 2019 Apr 4;74(1):73-87.e8. doi: 10.1016/j.molcel.2019.02.011. Epub 2019 Mar 12. PMID: 30876805.

Shen Y, Liu J, Wang X, Cheng X, Wang Y, Wu N. Essential role of the first intron in the transcription of hsp90beta gene. FEBS Lett. 1997 Aug 11;413(1):92-8. doi: 10.1016/s0014-5793(97)00883-1. PMID: 9287123.

Shiau AK, Harris SF, Southworth DR, Agard DA. Structural Analysis of E. coli hsp90 reveals dramatic nucleotide-dependent conformational rearrangements. Cell. 2006 Oct 20;127(2):329-40. doi: 10.1016/j.cell.2006.09.027. PMID: 17055434.

Shimamura T, Lowell AM, Engelman JA, Shapiro GI. Epidermal growth factor receptors harboring kinase domain mutations associate with the heat shock protein 90 chaperone and are destabilized following exposure to geldanamycins. Cancer Res. 2005 Jul 15;65(14):6401-8. doi: 10.1158/0008-5472.CAN-05-0933. PMID: 16024644.

Siligardi G, Panaretou B, Meyer P, Singh S, Woolfson DN, Piper PW, Pearl LH, Prodromou C. Regulation of Hsp90 ATPase activity by the co-chaperone Cdc37p/p50cdc37. J Biol Chem. 2002 Jun 7;277(23):20151-9. doi: 10.1074/jbc.M201287200. Epub 2002 Mar 26. PMID: 11916974.

Sillitoe I, Cuff AL, Dessailly BH, Dawson NL, Furnham N, Lee D, Lees JG, Lewis TE, Studer RA, Rentzsch R, Yeats C, Thornton JM, Orengo CA. New functional families (FunFams) in CATH to improve the mapping of conserved functional sites to 3D structures. Nucleic Acids Res. 2013 Jan;41(Database issue):D490-8. doi: 10.1093/nar/gks1211. Epub 2012 Nov 29. PMID: 23203873; PMCID: PMC3531114.

Sittler A, Lurz R, Lueder G, Priller J, Lehrach H, Hayer-Hartl MK, Hartl FU, Wanker EE. Geldanamycin activates a heat shock response and inhibits huntingtin aggregation in a cell culture model of Huntington's disease. Hum Mol Genet. 2001 Jun 1;10(12):1307-15. doi: 10.1093/hmg/10.12.1307. Erratum in: Hum Mol Genet 2001 Aug 1;10(16):1719. PMID: 11406612.

Soroka J, Wandinger SK, Mäusbacher N, Schreiber T, Richter K, Daub H, Buchner J. Conformational switching of the molecular chaperone Hsp90 via regulated phosphorylation. Mol Cell. 2012 Feb 24;45(4):517-28. doi: 10.1016/j.molcel.2011.12.031. PMID: 22365831.

Spiess C, Miller EJ, McClellan AJ, Frydman J. Identification of the TRiC/CCT substrate binding sites uncovers the function of subunit diversity in eukaryotic chaperonins. Mol Cell. 2006 Oct 6;24(1):25-37. doi: 10.1016/j.molcel.2006.09.003. PMID: 17018290; PMCID: PMC3339573.

Taipale M, Jarosz DF, Lindquist S. HSP90 at the hub of protein homeostasis: emerging mechanistic insights. Nat Rev Mol Cell Biol. 2010 Jul;11(7):515-28. doi: 10.1038/nrm2918. Epub 2010 Jun 9. PMID: 20531426.

Taipale M, Krykbaeva I, Koeva M, Kayatekin C, Westover KD, Karras GI, Lindquist S. Quantitative analysis of HSP90-client interactions reveals principles of substrate recognition. Cell. 2012 Aug 31;150(5):987-1001. doi: 10.1016/j.cell.2012.06.047. PMID: 22939624; PMCID: PMC3894786.

Takacs JE, Neary TB, Ingolia NT, Saini AK, Martin-Marcos P, Pelletier J, Hinnebusch AG, Lorsch JR. Identification of compounds that decrease the fidelity of start codon recognition by the eukaryotic translational machinery. RNA. 2011 Mar;17(3):439-52. doi: 10.1261/rna.2475211. Epub 2011 Jan 10. PMID: 21220547; PMCID: PMC3039144.

Ting SY, Yan NL, Schilke BA, Craig EA. Dual interaction of scaffold protein Tim44 of mitochondrial import motor with channel-forming translocase subunit Tim23. Elife. 2017 Apr 25;6:e23609. doi: 10.7554/eLife.23609. PMID: 28440746; PMCID: PMC5422074.

Tissières A, Mitchell HK, Tracy UM. Protein synthesis in salivary glands of Drosophila melanogaster: relation to chromosome puffs. J Mol Biol. 1974 Apr 15;84(3):389-98. doi: 10.1016/0022-2836(74)90447-1. PMID: 4219221.

Toogun OA, Dezwaan DC, Freeman BC. The hsp90 molecular chaperone modulates multiple telomerase activities. Mol Cell Biol. 2008 Jan;28(1):457-67. doi: 10.1128/MCB.01417-07. Epub 2007 Oct 22. PMID: 17954556; PMCID: PMC2223280.

Tsaytler PA, Krijgsveld J, Goerdayal SS, Rüdiger S, Egmond MR. Novel Hsp90 partners discovered using complementary proteomic approaches. Cell Stress Chaperones. 2009 Nov;14(6):629-38. doi: 10.1007/s12192-009-0115-z. Epub 2009 Apr 26. PMID: 19396626; PMCID: PMC2866955.

van der Lee R, Buljan M, Lang B, Weatheritt RJ, Daughdrill GW, Dunker AK, Fuxreiter M, Gough J, Gsponer J, Jones DT, Kim PM, Kriwacki RW, Oldfield CJ, Pappu RV, Tompa P, Uversky VN, Wright PE, Babu MM. Classification of intrinsically disordered regions and proteins. Chem Rev. 2014 Jul 9;114(13):6589-631. doi: 10.1021/cr400525m. Epub 2014 Apr 29. PMID: 24773235; PMCID: PMC4095912.

Vaughan CK, Mollapour M, Smith JR, Truman A, Hu B, Good VM, Panaretou B, Neckers L, Clarke PA, Workman P, Piper PW, Prodromou C, Pearl LH. Hsp90-dependent activation of protein kinases is regulated by chaperone-targeted dephosphorylation of Cdc37. Mol Cell. 2008 Sep 26;31(6):886-95. doi: 10.1016/j.molcel.2008.07.021. PMID: 18922470; PMCID: PMC2568865.

Verba KA, Wang RY, Arakawa A, Liu Y, Shirouzu M, Yokoyama S, Agard DA. Atomic structure of Hsp90-Cdc37-Cdk4 reveals that Hsp90 traps and stabilizes an unfolded kinase. Science. 2016 Jun 24;352(6293):1542-7. doi: 10.1126/science.aaf5023. PMID: 27339980; PMCID: PMC5373496.

Wandinger SK, Suhre MH, Wegele H, Buchner J. The phosphatase Ppt1 is a dedicated regulator of the molecular chaperone Hsp90. EMBO J. 2006 Jan 25;25(2):367-76. doi: 10.1038/sj.emboj.7600930. Epub 2006 Jan 12. PMID: 16407978; PMCID: PMC1383513.

Wang A, Kolhe JA, Gioacchini N, Baade I, Brieher WM, Peterson CL, Freeman BC. Mechanism of Long-Range Chromosome Motion Triggered by Gene Activation. Dev Cell. 2020 Feb 10;52(3):309-320.e5. doi: 10.1016/j.devcel.2019.12.007. Epub 2020 Jan 2. PMID: 31902656; PMCID: PMC7108666.

Wayne N, Bolon DN. Dimerization of Hsp90 is required for in vivo function. Design and analysis of monomers and dimers. J Biol Chem. 2007 Nov 30;282(48):35386-95. doi: 10.1074/jbc.M703844200. Epub 2007 Oct 1. PMID: 17908693.

Wegele H, Wandinger SK, Schmid AB, Reinstein J, Buchner J. Substrate transfer from the chaperone Hsp70 to Hsp90. J Mol Biol. 2006 Feb 24;356(3):802-11. doi: 10.1016/j.jmb.2005.12.008. Epub 2005 Dec 20. PMID: 16403523.

Whitesell L, Bagatell R, Falsey R. The stress response: implications for the clinical development of hsp90 inhibitors. Curr Cancer Drug Targets. 2003 Oct;3(5):349-58. doi: 10.2174/1568009033481787. PMID: 14529386.

Whitesell L, Lindquist SL. HSP90 and the chaperoning of cancer. Nat Rev Cancer. 2005 Oct;5(10):761-72. doi: 10.1038/nrc1716. PMID: 16175177.

Wiech H, Buchner J, Zimmermann R, Jakob U. Hsp90 chaperones protein folding in vitro. Nature. 1992 Jul 9;358(6382):169-70. doi: 10.1038/358169a0. PMID: 1614549. Freeman BC, Toft DO, Morimoto RI. Molecular chaperone machines: chaperone activities of the cyclophilin Cyp-40 and the steroid aporeceptor-associated protein p23. Science. 1996 Dec 6;274(5293):1718-20. doi: 10.1126/science.274.5293.1718. PMID: 8939864.

Zhang M, Botër M, Li K, Kadota Y, Panaretou B, Prodromou C, Shirasu K, Pearl LH. Structural and functional coupling of Hsp90- and Sgt1-centred multi-protein complexes. EMBO J. 2008 Oct 22;27(20):2789-98. doi: 10.1038/emboj.2008.190. Epub 2008 Sep 25. PMID: 18818696; PMCID: PMC2556094.

Zhang SL, Yu J, Cheng XK, Ding L, Heng FY, Wu NH, Shen YF. Regulation of human hsp90alpha gene expression. FEBS Lett. 1999 Feb 5;444(1):130-5. doi: 10.1016/s0014-5793(99)00044-7. PMID: 10037161.

Zhao R, Davey M, Hsu YC, Kaplanek P, Tong A, Parsons AB, Krogan N, Cagney G, Mai D, Greenblatt J, Boone C, Emili A, Houry WA. Navigating the chaperone network: an integrative map of physical and genetic interactions mediated by the hsp90 chaperone. Cell. 2005 Mar 11;120(5):715-27. doi: 10.1016/j.cell.2004.12.024. PMID: 15766533.

Zheng S, Shuman S, Schwer B. Sinefungin resistance of Saccharomyces cerevisiae arising from Sam3 mutations that inactivate the AdoMet transporter or from increased expression of AdoMet synthase plus mRNA cap guanine-N7 methyltransferase. Nucleic Acids Res. 2007;35(20):6895-903. doi: 10.1093/nar/gkm817. Epub 2007 Oct 11. PMID: 17932050; PMCID: PMC2175321.

Zhu X, Zhao X, Burkholder WF, Gragerov A, Ogata CM, Gottesman ME, Hendrickson WA. Structural analysis of substrate binding by the molecular chaperone DnaK. Science. 1996 Jun 14;272(5268):1606-14. doi: 10.1126/science.272.5268.1606. PMID: 8658133; PMCID: PMC5629921.

Zierer BK, Rübbelke M, Tippel F, Madl T, Schopf FH, Rutz DA, Richter K, Sattler M, Buchner J. Importance of cycle timing for the function of the molecular chaperone Hsp90. Nat Struct Mol Biol. 2016 Nov;23(11):1020-1028. doi: 10.1038/nsmb.3305. Epub 2016 Oct 10. PMID: 27723736; PMCID: PMC6248305.

Zuehlke AD, Johnson JL. Chaperoning the chaperone: a role for the co-chaperone Cpr7 in modulating Hsp90 function in Saccharomyces cerevisiae. Genetics. 2012 Jul;191(3):805-14. doi: 10.1534/genetics.112.140319. Epub 2012 Apr 13. PMID: 22505624; PMCID: PMC3389976.

Zuehlke AD, Wren N, Tenge V, Johnson JL. Interaction of heat shock protein 90 and the co-chaperone Cpr6 with Ura2, a bifunctional enzyme required for pyrimidine biosynthesis. J Biol Chem. 2013 Sep 20;288(38):27406-27414. doi: 10.1074/jbc.M113.504142. Epub 2013 Aug 7. PMID: 23926110; PMCID: PMC3779735.